PUBLICATIONS OF
THE UNIVERSITY OF EASTERN FINLAND


**Dissertations in Forestry and Natural Sciences**

**RINEZ THAPA**

# Recovery of scandium and uranium with bisphosphonate modified mesoporous silicon

# RECOVERY OF SCANDIUM AND URANIUM WITH BISPHOSPHONATE MODIFIED MESOPOROUS SILICON

UNIVERSITY OF
EASTERN FINLAND

PUBLICATIONS OF THE UNIVERSITY OF EASTERN FINLAND
DISSERTATIONS IN FORESTRY AND NATURAL SCIENCES

N:o 435

*Rinez Thapa*

# RECOVERY OF SCANDIUM AND URANIUM WITH BISPHOSPHONATE MODIFIED MESOPOROUS SILICON

ACADEMIC DISSERTATION

To be presented by permission of the Faculty of Science and Forestry for public examination in the Auditorium SN201 in the Snellmania Building at the University of Eastern Finland, Kuopio, on November 26th, 2021, at 12 o'clock noon.

University of Eastern Finland
Kuopio 2021

PunaMusta Oy
Joensuu, 2021
Editors: Pertti Pasanen, Raine Kortet,
Jukka Tuomela, Matti Tedre
Distribution: University of Eastern Finland / Sales of publications
www.uef.fi/kirjasto
ISBN: 978-952-61-4330-9
ISBN: 978-952-61-4331-6 (PDF)
ISSNL: 1798-5668
ISSN: 1798-5668
ISSN: 1798-5676 (PDF)

Author's address: University of Eastern Finland
Department of Applied Physics
P.O. Box 1627
70211 KUOPIO, FINLAND
rinez.thapa@uef.fi

Supervisors: Senior Researcher Joakim Riikonen, Ph.D.
University of Eastern Finland
Department of Applied Physics
P.O. Box 1627
70211 KUOPIO, FINLAND
joakim.riikonen@uef.fi

Professor Vesa-Pekka Lehto
University of Eastern Finland
Department of Applied Physics
P.O. Box 1627
70211 KUOPIO, FINLAND
vesa-pekka.lehto@uef.fi

Reviewers: Associate Professor Eveliina Repo
Lappeenranta University of Technology
LUT School of Engineering Science
LAPPEENRANTA, FINLAND
eveliina.repo@lut.fi

Principal scientist Rabiul Awual, Ph.D.
Japan Atomic Energy Agency
RENESA, JAPAN
awual75@yahoo.com

Opponent: Professor Ulla Lassi
University of Oulu
Sustainable Chemistry, Faculty of Technology
P.O. Box 8000
90014 OULU, FINLAND
ulla.lassi@oulu.fi

Thapa, Rinez
Title of the thesis. Recovery of scandium and uranium with bisphosphonate modified mesoporous silicon
Kuopio: University of Eastern Finland, 2021
Publications of the University of Eastern Finland
Dissertations in Forestry and Natural Sciences 2021; 435
ISBN: 978-952-61-4330-9 (print)
ISSNL: 1798-5668
ISSN: 1798-5668
ISBN: 978-952-61-4331-6 (PDF)
ISSN: 1798-5676 (PDF)

# ABSTRACT

Metals are essential raw materials which have many applications, in household appliances and from transportation to energy production. Thus, there is a constant need for more and especially rather rare metals in many of the sophisticated devices apparently essential for today's standard of living. In nature, metals are not found as pure elements but are mixed with all kinds of other elements. The increasing demand for metals has led to increasing amounts of ore mining but these are also a source of pollution and wastes e.g., mine tailings. It would be advantageous to recover specific metals from these wastes, because of their high value and toxicity to the environment. Two good examples of these kinds of metals are scandium and uranium, which were studied in this thesis.

Scandium is used in several applications such as in scandium-aluminium alloys and solid oxide fuel cells. However, the availability of scandium is limited because it is rarely found in any appreciable concentrations in ores. Currently, scandium is mainly produced from secondary resources such as the mine-tailings produced from the processing of other metals e.g., aluminium, uranium. In these resources, the concentrations of other metals are much higher than the concentration of scandium, making its extraction and purification very difficult. Therefore, novel methods are needed that could efficiently recover scandium from these tailings to meet the increased need for scandium and to reduce its cost.

Many polymetallic deposits also contain uranium, a compound that is difficult to remove during the production of other metals. The exploitation of uraniferous ores leads to the creation of mine tailings contaminated by uranium that are prone to pollute the environment e.g., they may end up in wells used for drinking water. Since uranium is a toxic radionuclide, its exposure even at trace amounts is harmful to humans e.g., causing kidney failure. Therefore, it is important to remove uranium to prevent it from contaminating the environment and the recovered uranium needs to be stored safely to secure public health.

A major challenge in the recovery of scandium and uranium is associated with their low concentration with respect to other metals present at higher concentrations such as iron, aluminium, and magnesium. Especially when the desired metals exist at a low concentration, conventional metal recovery processes such as precipitation and solvent extraction are not feasible because of their low selectivity towards the metals and the poor ability to recycle the spent reagent/extractant. Adsorption technology can be employed to ameliorate this issue; in this approach, metal ions are adsorbed onto a solid adsorbent from aqueous solutions. However, if it is to be economically viable and truly sustainable, the adsorbent is not only required to be

reusable for several tens or hundreds of adsorption/desorption cycles but also needs to be selective towards the target metal.

The aim of the present work was to develop an adsorbent with good reusability and high selectivity towards scandium and uranium from multi-metal solutions. The adsorbent was made of carbonized mesoporous silicon functionalized with bisphosphonate molecules. The bisphosphonates were mainly responsible for metal adsorption whereas the carbonized mesoporous silicon support maintained the stability of the adsorbent to allow its reutilization.

The mesoporous silicon was prepared using electrochemical etching of silicon wafers and the carbonization was carried out under thermal treatment in presence of acetylene. The developed functionalization was based on the utilization of the radicals present on the carbonized surface of mesoporous silicon which can directly conjugate the bisphosphonate molecules. Due to the stable carbon-carbon and silicon-carbon bonds between the carbonized surfaces and the bisphosphonates, the functionalization was stable for several days in water, hydrochloric acid as well as in sodium hydroxide solutions. Importantly, the adsorbent could be effectively recycled without any significant reduction in its adsorption/desorption performance for up to the 50 cycles examined in a flow-through setup.

The metal adsorption properties of the adsorbent such as the adsorption capacity and its selectivity were studied with artificial metal solutions as well as with processed ore solutions. When using the artificial metal solution, the adsorption was found to be dependent on the pH of the solution. For example, the adsorbed amount of scandium at pH 1 was half than that obtained at pH 3. On the other hand, the selectivity towards scandium was higher at pH 1 than at pH 3 examined using an equimolar metal solution containing scandium, iron, aluminium, copper, and zinc. However, from a processed ore solution the adsorbent was ineffective in extracting trace amounts of scandium due to the presence of other metals at higher concentrations. For example, the concentrations of iron, aluminium and titanium in the solution were about 1000, 300 and 50 times higher than that of scandium. In order to reduce the concentration of these metals, a precipitation method was used that involved the addition of ammonium hydroxide and potassium permanganate to the ore solution. This method decreased the concentration of metals by 99 ± 2 % for iron, 100 ± 14 % for titanium, 35 ± 1 % for aluminium as well as 12 ± 1 % for scandium. After the treatment of the ore solution by precipitation, the adsorbent was capable of adsorbing scandium in higher amounts.

The extraction of uranium with the adsorbent was examined from a tailing solution processed from an ore containing some uranium. Regardless of the fact that the concentration of uranium was 10 times lower in comparison with other metals e.g., iron and magnesium, the adsorbent was effective at selectively adsorbing uranium. For example, the adsorption efficiency for uranium reached up to 100 % whereas the efficiencies for other metals were low e.g., 30 % for aluminium, 10 % for iron and 5 % for magnesium. Crucially, the adsorbed uranium was efficiently desorbed in a small volume where the concentration of uranium was increased by 15 times in comparison to the original solution. The collection of uranium in a small volume is beneficial as it allows the uranium contaminated wastewater to be stored safely.

The results emerging from this thesis can serve as a benchmark to further develop the adsorbent for its potential use in industrial settings. The adsorbent exhibited good reusability as well as good selectivity towards scandium and uranium. In addition, the porous structure of the adsorbent meant that it was water permeable and thus could be used in a column system where metal solutions were continuously passed through the column. The flow-through process is better than traditional batch process in its ability to recover metals in terms of lowering the operating cost, low energy consumption and eliminating the need to store the metal solution in pools or tanks.

*Universal Decimal Classification: 544.723.2, 544.14, 544.6, 669.054, 620.3, 546.28*

*Keywords: scandium, uranium, adsorbent, mesoporous, silicon, bisphosphonates*

# ACKNOWLEDGEMENTS

This study was carried out during the years 2016 – 2021 in Department of Applied Physics at the University of Eastern Finland. I want to express my deepest gratitude to my principal supervisor Senior Researcher Joakim Riikonen for guiding me to plan every single experiment, to insightfully evaluate the results as well as to improve my scientific writing skills. Joakim, I recall your saying, 'if you have already spent several years doing the research, put more effort to bring out the best from it'. Unfortunately, in all those efforts, you had to be involved as well. So, thank you for looking after me. You have always shown the path how to implement the research aims and be enthusiastic in both good and bad results.

I am grateful to my other supervisor Professor Vesa-Pekka Lehto (VP) for the reviews, corrections and correspondences you have made to all of the publications I have been involved in. VP, you have encouraged me to be more independent researcher and I recall your three specific sayings; i) never to be hopeful, be realistic, ii) believing is not making science; it is something else, and the most popular one iii) sweat saves blood. All of these sayings makes so much sense in terms of growing up as a researcher.

It is my pleasure to thank all the co-authors/collaborators for your contributions in the publications used in this thesis. I want to thank Tuomo Nissinen for guiding me during the first year of this project that also included one of the important parts of this thesis; the production of nanoporous silicon. In addition, of course, I thank all my colleagues in Pharmaceutical Physics research group (both past and present members) for your co-operation, weekly discussions and creating friendly atmosphere. For the financial supports, I acknowledge the Foundation for Research of Natural Resources in Finland, The Finnish Cultural Foundation, Academy of Finland, and University of Eastern Finland.

It is a great honor for me to defend my thesis against Professor Ulla Lassi and I thank you for accepting to be my opponent and taking crucial part in my academic career. I am also grateful to the pre-examiners of this thesis, Associate Professor Eveliina Repo and Principal Scientist Rabiul Awual for your comments and feedbacks that clearly improved the thesis. Moreover, my sincere thanks to Ewen MacDonald for correcting the language of this thesis.

Throughout these years, one of the important lessons I have realized is that I have not learned enough and there is so much to learn ahead. I am glad that I can discuss about the learning curve (or work) also with my wife, Sonja, who have often helped solving problems that occurred in laboratory/experiments. Needless to say, Sonja, you also set a limit how long I can discuss about work in order to bring quality family time. I appreciate you for maintaining the balance between work and family. Now, I started smiling when I think about our son, Kanes. I want to set a remark here to Kanes that you are a very funny kid, quite humorous already at this age (2 years old) and often dramatic. I am so happy the way we are and will be as a family.

I am also happy to have my Finnish family, Johanna, Ari, Sami, Sara and Samuli. The moments we share are always cheerful. With high importance, I am glad to have my friends Ananta, Chris, Kalle, Sameer, and Ville, to name a few, for your genuine friendship and involvement in recreational activities that included making music, videos, and playing FIFA.

Finally, I want to thank my family back in Nepal, my mother Sunita, elder sister Rinja, brother-in-law Dil, and my nephew Nidesh for your continuous love, support and motivation.

Kuopio, 2021
Rinez Thapa

# LIST OF ABBREVIATIONS

| | |
|---|---|
| APTES | Amino Propyl Tri-Ethoxy Silane |
| BET | Brunauer Emmett Teller |
| BP | Bisphosphonates |
| BP-TCPSi | Bisphosphonate modified Thermally Carbonized Porous Silicon |
| BJH | Barrett Joyner Halenda |
| CPMAS | Cross Polarization Magic Angle Spinning |
| DEHPA | Di-(2-Ethyl-Hexyl) Phosphoric Acid |
| DETA | Diethylenetriamine |
| DIMS | Dihydroimidazole |
| DNA | Deoxyribonucleic Acid |
| FTIR | Fourier Transform Infrared Spectroscopy |
| HCl | Hydrocholoric acid |
| HTPSi | Hydrogen Terminated Porous Silicon |
| KIT-6 | Korea Advanced Institute of Science and Technology – 6 |
| KT | Knelson Tails |
| LOS | Leached Ore Solution |
| MCM-41 | Mobil Composition of Matter no. 41 |
| MWNT | Multi-Walled carbon Nanotubes functionalized on silica nano powder |
| NF | Nanofibre |
| NMR | Nuclear Magnetic Resonance Spectroscopy |
| PA | Ethyl-Phosphonic Acid |
| PAN | 1-(2-Pyridyl-Azo)-2-Naphthol 3 |
| PE | Polyethylene |
| PPAF | Phosphorus functionalized Porous Aromatic Frameworks |
| PSi | Porous silicon |
| S.A | Surface Area |
| SBA-15 | Santa Barbara Amorphous -15 |
| SEM | Scanning Electron Microscopy |
| Si-$H_x$ | Silicon Hydride |
| TBP | Tri-Butyl-Phosphate |
| TCPSi | Thermally Carbonized Porous Silicon |
| TGA | Thermo Gravimetric Analysis |
| THC | Thermally Hydro Carbonized |
| Ti-P | Titanium Phosphate |
| TOPSi | Thermally Oxidized Porous Silicon |
| TRPO | Trialkyl Phosphine Oxide |
| UnHTPSi | Undecylenic acid grafted on Hydrogen Terminated Porous Silicon |
| UnTCPSi | Undecylenic acid Thermally Ccarbonized Porous Silicon |
| UnTHCPSi | Undecylenic acid on Thermally Hydro-Carbonized Porous Silicon |
| Zr-P | Zirconium Phosphate |

# LIST OF ORIGINAL PUBLICATIONS

This thesis is based on data presented in the following publications, referred to by the Roman numerals I-IV.

I Riikonen A, Nissinen T, Alanne A, Thapa R, Fioux P, Bonne M, Rigolet S, Morlet-Savary F, Aussenac F, Marichal C, Lalevee J, Vepsäläinen J, Lebeau B, Lehto VP. (2019). Stable surface functionalization of carbonized mesoporous silicon. *Inorganic Chemistry Frontiers*, 7 (3): 631-641.

II Thapa R, Nissinen T, Turhanen P, Määttä J, Vepsäläinen J, Lehto VP, Riikonen J. (2020). Bisphosphonate modified mesoporous silicon for scandium adsorption. *Microporous and Mesoporous Materials,* 296: 109980.

III Rahmani A, Thapa R, Aalto JM, Turhanen P, Vepsäläinen J, Lehto VP, Riikonen J. (2021). Functionalized nanoporous silicon adsorbent for extraction of scandium from an ore. *Hydrometallurgy (submitted).*

IV Thapa R, Rahmani A, Turhanen P, Taskinen A, Nissinen T, Neitola R, Vepsäläinen J, Lehto VP, Riikonen J. (2021). Recovery of uranium with bisphosphonate modified mesoporous silicon. *Separation and Purfication Technology,* 272: 118913.

# AUTHOR'S CONTRIBUTION

I) The author contributed to the characterization of the samples and reviewed the manuscript.

II) The author planned the study, prepared and characterized the samples and performed all of the experiments except for the isothermal titration calorimetry. The author was the principal writer of the manuscript.

III) The author cooperated in planning the study, provided technical assistance in the flow-through experiments and ICP-MS measurements. The author reviewed the manuscript.

IV) The author planned the study, prepared and characterized the samples and performed all experiments. The author was the principal writer of the manuscript.

# CONTENTS

1. INTRODUCTION ..... 19
1.1 Scandium recovery ..... 19
1.2 Uranium recovery ..... 20
1.3 Metal recovery techniques ..... 21
1.3.1 Precipitation ..... 21
1.3.2 Solvent extraction ..... 21
1.3.3 Adsorption ..... 22
1.3.3.1 Implementation and characterization of adsorption ..... 23
1.3.3.2 Adsorption isotherm ..... 23
1.3.3.3 Adsorbents ..... 26
1.4 Mesoporous silicon ..... 28
1.4.1 Electrochemical etching ..... 29
1.4.2 Surface modifications of PSi ..... 29
1.5 Bisphosphonates as metal chelators ..... 31
2. AIMS OF THE STUDY ..... 33
3. MATERIALS AND METHODS ..... 35
3.1 Bisphosphonate and metal solution ..... 35
3.2 Preparation of PSi microparticles ..... 35
3.3 Surface modifications of PSi ..... 35
3.4 Characterization of the material ..... 36
3.5 Adsorption studies ..... 36
4. RESULTS AND DISCUSSION ..... 39
4.1 Surface functionalization ..... 39
4.2 Stability of the functionalized surfaces ..... 40
4.3 Characterization of BP-TCPSi ..... 41
4.4 Adsorption isotherms of scandium ..... 43
4.5 Selective adsorption of Sc from an artificial multi-metal solution ..... 47
4.6 Reusability of BP-TCPSi in Sc recovery from artificial solution ..... 49
4.7 Recovery of trace Sc from a leached solution of Kiviniemi Sc-deposit ..... 51
4.8 Recovery of uranium from a tailing solution using BP-TCPSi ..... 56
5. CONCLUSIONS ..... 63
6. FUTURE PERSPECTIVES ..... 65
References ..... 67

# 1.INTRODUCTION

The present work is focused on the development of an adsorbent to recover scandium (Sc) and uranium (U) from solutions containing various metals. This adsorbent combines the metal adsorption features of bisphosphonate (BP) with the robust stability of thermally carbonized mesoporous silicon (TCPSi). The developed material was used as a permeable adsorbent in a column setup where the metal solutions were rapidly passed through.

In the following chapters, the motivation for recovering Sc and U is followed by a discussion about the need of novel adsorbents especially their reusability features are addressed. The latter part is concerned with the preparation of mesoporous silicon and the developments required on the route towards the final product, bisphosphonate modified thermally carbonized mesoporous silicon (BP-TCPSi).

## 1.1 Scandium recovery

Scandium is the 31st most abundant element in the Earth's crust. However, it is categorized as a rare earth element (REE) because it is rarely found in concentrated ore deposits [1, 2]. There are only a few ores (e.g. thortveitite) known to contain considerable concentrations of Sc are in Evje-Iveland, Norway (250000 g/ton $Sc_2O_3$) and Befanamo, Madagascar (420000 g/ton $Sc_2O_3$) [1-3]. Other Sc deposits have also been identified but with low-grades, e.g., in Nyngan, Australia (235 g/ton in geothite), Zhovti Vody, Ukraine (105 g/ton in riebeckite) and in Kiviniemi, Finland (163 g/t in ferrodiorite) [2, 4-6]. There are also ores where Sc co-exists with other metals in minor quantities e.g., in uraninite (U), bauxite (Al) ilmenite (W) and other REEs [2, 7-11].

Scandium is exclusively produced from secondary resources such as mine tailings and by-products from the production of other metals [1, 2, 7, 12, 13]. For example, Sc has been supplied from the Soviet stockpiles that were originally generated from the uranium tailings produced during the Cold War [1, 14]. At present, China is the major supplier of Sc where it is recovered from the mine tailing of the Bayan Obo Nb-REE-Fe deposit. The Sc content in the deposit is 110 g/ton that becomes concentrated up to 163 g/ton in the tailing [10]. The Bayan obo is the largest known REE deposit worldwide and has been broadly exploited, and hence, a sizable tailing of up to 200 million tons has been produced while 3.86 million tons of new tailings are added every year [1, 11, 15]. Another potential source of Sc is the bauxite residue (red mud) generated from Al production. In the red mud, the Sc content is 41 – 254 g/ton [16]. Globally, an estimated 4 billion tons of the red mud has been generated until 2015 but this value is increasing by 150 million tons annually [16-18]. However, it is not easy to efficiently extract Sc from these kinds of secondary resources because of the presence of high levels of other metals Al, Fe, Ti etc. [1, 17, 19].

The wider utilization of Sc is impeded due to the difficulties associated with Sc extraction as well as its limited availability, and high price (134 000 US$/kg) [4]. Although the use of metallic Sc has not been exploited, its usage as an effective dopant is beneficial in a variety of applications; these are attributed to Sc's properties such as its light weight, good electrical conductivity, and high melting point. For example, Sc is effectively used as an alloying element in combination with Al, making the end-product stronger and more resistant to corrosion [20]. These Sc-Al alloys are used in the aerospace industry and in the manufacture of sports equipment.

Another important application of Sc is in solid oxide fuel cells (SOFC). In SOFC, chemical energy is converted into electricity by directly oxidizing a fuel with the solid-oxide material being

used as the electrolyte. However, for high performance, i.e., efficient oxygen ion transfer through the solid electrolyte, the SOFC needs to be operated at extreme temperatures (~1000 °C) that can potentially damage the cell components and elevate the maintenance costs [21]. It has been shown that an electrolyte doped with $Sc_2O_3$ increases the power density of the SOFC, even at a lower operating temperature (~500 °C) [21-23]. Since energy is produced electrochemically in SOFC, rather little or even no green-house gases (e.g., $CO_2$) are emitted, making SOFC an environmentally friendly technology in comparison to conventional combustion engines [24]. Various natural gases from hydrogen to hydrocarbons (e.g., methane) can be used in SOFC as the fuel source [25]. Therefore, to produce energy, SOFC has the potential to reduce the consumption and burning of fossil fuels (e.g., petroleum, coal), which have been responsible for devastating effects such as global warming due to the emission of greenhouse gases.

Similarly, it has been also reported that the addition of Sc in piezoelectric materials (e.g., Sc-Al-N) was able to enhance the piezoelectric response by 400 % [26]. The increase in the piezoelectric response was attributed to the suitable coordination of Sc in the crystalline structure with Al-N, which softened the material and made it more responsive to strain [27]. Since piezoelectricity involves the generation of an electrical charge by mechanical stress or vice-versa, a material with a high piezoelectric response can be used in modern high-technology devices with micro electro-mechanical systems such as touch screens, fingerprint detectors and highly sensitive microphones [28, 29].

## 1.2 Uranium recovery

Uranium is one of the most common elements in nature occurring as three radioactive isotopes U-238 (99.27 %), U-235 (0.72 %) and U-234 (0.005%). The less abundant isotopes, U-235 and U-234 are highly fissile radionuclides, which are the indispensable fuels in nuclear power plants. Currently, U is mainly mined in Australia, Canada, and Kazakhstan to be utilized in the nuclear power plants [30, 31]. Although a nuclear power plant produces less carbon emissions, it generates radioactive wastewaters containing U and at present, there is no facility/method to ecologically store/dispose of these dangerous wastes [32-35].

Apart from the nuclear industries, another source of U contamination into the environment results from the mining of uraniferous ores. Many polymetallic deposits are enriched in U e.g., uraninite, brannerite, torbernite and some REE [17, 31, 36]. The U naturally present in these minerals can be problematic to remove during the processing of the metals leading to the mine tailings being contaminated by U [17, 37]. For example, U is now being recovered from the by-product of the processing of Ni-Zn-Cu-Co deposits in Talvivaara, Finland [31]. Typically, the wastes accumulate in large volumes and if not disposed of safely, it can leach into the local soils, groundwater as well as the drinking water [32, 33, 38, 39].

Uranium contamination in the environment is a serious public health concern because of its toxicity [32, 40]. Although the naturally occurring U is not highly radioactive, its chemical toxicity is nonetheless harmful to humans [41]. The toxicity depends on its exposure route, speciation, and solubility. For example, highly soluble U compounds (e.g., uranyl nitrate, uranyl fluoride) are absorbed through the skin, and the gastrointestinal tract from where they reach the bloodstream [32, 40, 42]. Drinking water from wells contaminated by the soluble uranium compounds has been found to cause kidney damage [41, 43, 44]. The insoluble form of U (e.g., uranium tetrafluoride) can accumulate in the lungs for a longer timespan causing a risk of cancer [40, 45]. It has been also reported that U exposure evoked deoxyribonucleic acid (DNA) damage in workers recruited in U mines and mill sites [46]. Furthermore, animal experiments with mice have also shown that U can induce reproductive and skeletal defects [47-49]. Because of the severe

health hazards associated with U exposure affecting different organs, the World Health Organization and the U.S. Environmental Protection Agency have issued a maximum contaminant level of U in drinking water as low as 0.03 mg/L and with the objective to reduce it to zero [50].

## 1.3 Metal recovery techniques

Immense volumes of mining-associated wastewaters i.e., the mine tailings tend to accumulate. These wastes containing toxic metals like U can potentially pollute the environment through the groundwater and local soils, eventually posing a risk to human health. Therefore, it is crucial to remove U from the wastewater in order to both ensure the public health and guarantee environmental safety. The wastewaters may also contain other valuable metals such as Sc. The extraction of Sc from these secondary resources is beneficial because it involves no new mining or exploitation of natural reserves. The recycling of the wastewaters to produce Sc also fits with the principle of a circular economy. Nevertheless, it is challenging to extract specific metals from these wastes because they tend to be co-extracted with other dissolved metals. As an example, Sc can be recovered from the red mud by extracting (leaching) with an acid, but the leachate contains many other metals at higher concentrations. For example, the concentration of Sc in bauxite residue leachates was 2.2 mg/L while the concentrations of other metals were much higher e.g., 2617 mg/L for Al, 539 mg/L for Ti and 478 mg/L for Fe [18]. The different methods that have been employed to recover metals from wastewater including precipitation, solvent extraction, and adsorption are briefly discussed in the following sections.

### 1.3.1 Precipitation

Precipitation is a common method used in the recovery of dissolved metals where chemical reagents are added to yield insoluble metal complexes. Unfortunately, these reagents are expensive and difficult to reuse. In most cases, high amount of reagents is needed to recover the desired metals at acceptable amounts [51]. The method is not effective when the desired metal is at a low level because of co-precipitation of the other metals present at higher concentrations [1, 7]. Often, precipitation tends to be used as pre-treatment step to remove the major constituents (impurities) from the wastewaters before employing other methods such as solvent extraction and adsorption [18, 52].

### 1.3.2 Solvent extraction

Solvent extraction is an extensively used liquid-liquid separation process where one of the liquids is the aqueous phase containing the dissolved metals and other is the organic phase containing the extractant (organic compounds) [53]. These liquids are immiscible with each other and can be easily partitioned. Upon stirring of these liquids, the metals react chemically with the extractant and migrate into the organic phase [32]. The aqueous phase is separated, and the metals now present in the organic phase are recovered by stripping. Stripping is a back-extraction process to release metals form the organic phase into fresh aqueous phase, usually with an acid [54].

In the organic phase, a specific extractant with relevant properties such as solubility and binding affinity towards the desired metal can be chosen to achieve optimum recovery of the metal [33, 55, 56]. For instance, several extractants bearing various functional groups such as the

organo-phosphorus group, -POOH (e.g., di-(2-ethylhexyl) phosphoric acid, DEHPA, tri-butyl-phosphate, TBP) and carboxylic acid groups, -COOH (e.g., naphthenic acid) have been used to recover Sc and U [7, 30, 56-58]. Although solvent extraction is the most well-established technology in the treatment of wastewater, there are several disadvantages associated with this technique. For example, it requires a large volume of organic solvent and that increases the cost of recycling. In addition, the solvents are usually toxic and harmful to the environment. During the stripping process, there is a frequent loss of solvent when separating it from the aqueous phase. [9, 12, 59]. Moreover, the method is uneconomical when metals are present at low levels (< 0.5 g/L) [53].

### 1.3.3 Adsorption

Adsorption is another widely used technology in the wastewater treatment, which is effective also with low-concentrated metals, even those in the μg/L range [33, 53]. Unlike solvent extraction, adsorption technology does not require the use of the organic solvents meaning that there are no toxic emissions into the environment. Adsorption is a surface phenomenon where metal ions (adsorbates) are attached (adsorbed) on the surface of a solid material (adsorbent) and subsequently released (desorbed) to regenerate the adsorbent for reutilization. There are two mechanisms how an adsorption can occur: physisorption and chemisorption. Physisorption is the unspecific attachment via an electrostatic attraction between the adsorbate and the surface of the adsorbent. Chemisorption is the attachment of the adsorbate via the formation of chemical bonds on specific binding sites present on the adsorbent [60].

In chemisorption, the binding sites are facilitated by the functional groups (e.g., OH, COOH, POOH) present on the surface of the adsorbent. The functional groups, also called ligands, can donate/share electrons with the metal ions resulting formation of metal complexes [61-64]. These complexes can be formed in several ways depending upon the number of binding site that the ligands facilitate [62-64]. The number of the binding sites are referred for example as monodentate (one binding site), bidentate (two binding site) and polydentate (more than two binding site). In fact, a single metal ion can bind on multiple site of one or more ligands in a coordination fashion and the number of bonds associated in the metal complex are represented by coordination numbers [61, 64]. When the coordination number is more than one, the formation of the metal complexes are described as a chelation process (and the product as chelates). The chelates formed with higher coordination numbers are more stable, for instance, a metal chelated with polydentate sites are more stable than the metal bound on a monodentate site [63]. Likewise, stronger complexes are formed when the chelating ligands facilitate highly electronegative donor atoms (e.g., several oxygen atoms) to the positively charged metal ions (or cations) [63]. Furthermore, the angle at which the binding sites are configured (bite angle) also determines the coordination of the metal ion [65-70]. For instance, ligands with larger bite angle favors larger ions and vice-versa [68]. Some researchers report that a metal ion with an appropriate size that can perfectly fit in the coordination environment hosted by the ligands is chelated efficiently [62, 71].

It can be recognized that the adsorption mechanism depends upon the surface chemistry of the adsorbent as well as the chemical forms of the adsorbate (e.g., ionic speciation of the dissolved metals) [63]. In addition, several other factors such as the ratio of the adsorbent-adsorbate pair, concentration of the metal ions and pH of the solution also alter the adsorption process. Accordingly, the adsorption parameters such as the adsorption capacity of the adsorbent and the binding affinities between the adsorbate and the adsorbent are influenced.

#### 1.3.3.1 Implementation and characterization of adsorption

Adsorption can be implemented in two ways: batch setup and flow-through/column setup. In the batch setup, certain volume of metal solution is mixed all at once with a certain amount of adsorbent in a container (e.g., pools, tanks, Eppendorf). The scale at which this setup can be implemented is limited by the size of the container. For example, for the treatment of 1000 L of metal solution, a container with volume capacity of at least 1000 L or alternatively, 5 containers with the capacity of 200 L are required. In the column setup, certain amount of adsorbent is packed (fixed) in a column through which metal solution is flown-through continuously. As this setup does not require storage of metal solution in separate containers, it consumes less energy and is more efficient over batch setup to be operated in large-scale [72]. However, in the column setup, the adsorbent is not dispersed in the metal solution, an equilibrium will not be achieved between the adsorbent bed and the feed solution [73]. In order to characterize the adsorption parameters such as the adsorption capacity of the adsorbent, equilibrium studies are crucial, which can be determined using the batch setup [72].

In the batch setup, when the adsorbate and the adsorbent are in contact for long enough time, an equilibrium is established after which no further adsorption takes place. The equilibrium describes the distribution of the adsorbate between the solid phase and the liquid phase. If the adsorbate-adsorbent system already at equilibrium experiences changes (e.g., concentration, adsorbent mass, temperature), a new equilibrium will be established. The equilibrium data that are obtained experimentally can be mathematically modeled to predict the adsorption parameters. To do so, adsorption isotherm models are widely employed.

#### 1.3.3.2 Adsorption isotherm

Adsorption isotherm is the adsorption equilibrium data measured at a constant temperature. The adsorption isotherm graph correlates the mass of adsorbate adsorbed per unit mass of the adsorbent at equilibrium conditions ($Q_e$) with the residual concentration of the adsorbate in the liquid phase at the equilibrium ($C_e$). The adsorption parameters can be determined by fitting the equations of various isotherm models with the experimental isotherm data to elucidate the adsorption parameters. The isotherm models used in this thesis are listed in Table 1.

Table 1. Different isotherm models and their equations. $Q_e$ represents the amount of the adsorbed metal at equilibrium and $C_e$ refers to the metal concentration in the liquid phase at equilibrium.

| **Isotherm model** | **Equation** |
|---|---|
| Langmuir | $Q_e = \frac{Q_m K_L C_e}{1 + K_L C_e}$ |
| Freundlich | $Q_e = K_f {C_e}^{1/n}$ |
| Sips | $Q_e = \frac{Q_{ms} K_S {C_e}^{n_s}}{1 + K_S {C_e}^{n_s}}$ |

$Q_m$ and $Q_{ms}$ represent the adsorption capacity.
$K_f$ is used as the approximation of the adsorption capacity
$K_L$ and $K_s$, are the constants defining the binding affinity.
n and $n_s$ refer to the degree of surface heterogeneity of adsorbent's binding sites.

***Langmuir isotherm model***

The Langmuir isotherm model assumes that the adsorption occurs via chemisorption on homogeneous (identical) binding sites of the adsorbent with only a monolayer coverage of the attached adsorbate [60, 74]. The equation of this model can be derived as follows [60, 75].

Let's consider an adsorbent have a total number of binding sites as 1 and 'θ' be fraction of occupied sites by the adsorbate, then the unoccupied sites become (1 - θ). Since the rate of adsorption ($r_a$) is directly proportional to the concentration of the adsorbate (C) and the unoccupied sites, it can be written as

$$r_a \alpha\, C\,(1-\theta)$$
$$r_a = k_a C\,(1-\theta) \qquad (1)$$

where $k_a$ is the adsorption rate constant.

Before reaching the equilibrium, the rate of desorption ($r_d$) is directly proportional to the adsorbed amount i.e.,

$$r_d \alpha\, \theta$$
$$r_d = k_d \theta \qquad (2)$$

where $k_d$ is the desorption rate constant.

When the system reaches equilibrium, the occupied binding sites (θ) is equal to the adsorbed amount of the adsorbate ($Q_e$) divided by the total adsorption capacity of the adsorbent ($Q_m$).

$$\theta = \frac{Q_e}{Q_m} \qquad (3)$$

At the equilibrium, the rate of adsorption will be equal to the rate of desorption. Thus, the Eq. (1) is equal to the Eq. (2)

$$r_a = r_d$$
$$K_a C_e\,(1-\theta) = K_d\,\theta \qquad (4)$$

where $C_e$ refers to the equilibrium concentration of the adsorbate.

If K be the equilibrium constant between the adsorption and desorption, $K = k_a/k_d$ then above Eq. (4) can be written as

$$K\,C_e\,(1-\theta) = \theta$$
$$K\,C_e = \theta + K\,C_e\,\theta$$
$$K\,C_e = \theta\,(1 + K\,C_e)$$

$$\theta = \frac{K\,C_e}{1+K\,C_e} \qquad (5)$$

Combining the equations (3) and (5)

$$\frac{Q_e}{Q_m} = \frac{KC_e}{1+KC_e}$$

$$Q_e = \frac{Q_m K_L C_e}{1+K_L C_e} \qquad (6)$$

The Eq. (6) is the Langmuir model equation where equilibrium constant K is replaced by the Langmuir constant ($K_L$) that refers to the binding affinity. By fitting the Langmuir equation in the isotherm graph, its parameters can be determined. For example, by plotting the experimental values, $Q_e$ (μmol/g) in Y-axis and $C_e$ (mg/L) in X-axis, the maximum adsorption capacity of the adsorbent ($Q_m$ in μmol/g) and the Langmuir constant ($K_L$ in L/mg) can be obtained.

It is worthy to note some limitation of the Langmuir model that have been addressed in literature, which are a) the non-uniformity in the use of unit of the Langmuir constant, $K_L$ (L/mg, L/mol, L/g etc.) and b) the role of concentration of the adsorbate in the desorption rate is not considered. To solve these limitations, Azizian et al., presented a modified equation of the Langmuir model [75] as:

$$Q_e = \frac{Q_m K_{ML} C_e}{(C_s - C_e)+K_{ML} C_e} \qquad (7)$$

where $K_{ML}$ (dimensionless) is the modified Langmuir model constant, and $C_s$ is saturation concentration of the adsorbate.

Nonetheless, in this thesis, the modified Langmuir model was not employed because of the unavailability of any reliable solubility data ($C_s$) of Sc and U that simulated the liquid used in the adsorption experiments. Determination of the $C_s$ values experimentally was also not feasible because only dilute solutions of the metals were used. Thus, the traditional Langmuir model (Eq. 6) has been used to interpret the adsorption isotherm results.

### *Freundlich isotherm model*

The Freundlich model represents multi-layer coverage via both chemisorption and physisorption on a heterogenous surface [60]. It assumes that at a low concentration of the adsorbate, adsorbed amount is directly proportional to the equilibrium concentration given by following equation

$$Q_e \alpha\, C_e^{\,1}$$

And, at high concentration, adsorption is independent of concentration as;

$$Q_e \alpha\, C_e^{\,0}$$

At intermediate concentrate, adsorption is proportional to the equilibrium concentration raised to the power 1/n.

$$Q_e \alpha\, C_e^{\frac{1}{n}}$$

$$Q_e = K_f\, C_e^{\frac{1}{n}} \qquad (8)$$

The above Eq (8) is the Freundlich equation. The constants $K_f$ (μmol/g) and 'n' represent the adsorption capacity and heterogeneity factor, respectively [76-78]. The value 1/n below 1 (or n > 1) indicates non-cooperative adsorption, which means that there is no interaction between the adsorbed and unadsorbed species. On the contrary, the value 1/n above 1 indicates cooperative adsorption [74, 76, 77].

It should be realized that the parameters derived from this model are considered as an approximate values for a few reasons [74, 78, 79]. For example, an adsorbent always has a limited adsorption capacity beyond which no further adsorption is possible despite increasing the concentration. However, in the Freundlich equation, when the exponent 1/n is equal to 0, adsorption becomes independent of concentration implying that the model does not limit the adsorption capacity [79, 80]. Furthermore, at very low concentration, when the exponent 1/n = 1, the equation reduces to linear model. The linear model is explained by the Henry's law, which states that the adsorbed amount is linearly proportional to the residual adsorbate concentration. Since the Henry's law is valid at low concentration when the coverage of the adsorbate on adsorption site is low, the adsorbate-adsorbent system should obey the Henry's law [60, 81, 82]. However, it is often issued in the literature that the Freundlich model does not obey the Henry's law at low concentration [76, 81, 83-85].

#### *Sips isotherm model*

Sips model is a suitable model to apply when the isotherm data does not strictly follow the Langmuir and the Freundlich models. Sips model is the combination of the Langmuir and the Freundlich that describes both the homogeneous and heterogeneous surfaces of the adsorbent, given by the following equation.

$$Q_e = \frac{Q_{ms} K_S C_e^{n_s}}{1 + K_S C_e^{n_s}} \qquad (9)$$

where the Sips constants, $Q_{ms}$ (μmol/g) represent the adsorption capacity, $K_s$ (L/mg) represent the binding affinity and the $n_s$ represents the surface heterogeneity of the adsorbent.

The value of $n_s$ lies between 0 and 1. This value is comparable to the Freundlich constant n ($n_s$ = 1/n) [86, 87]. Higher the value of $n_s$, higher is the heterogeneity of the adsorbent [60, 76, 83]. When $n_s$ = 1, the Sips equation becomes exactly same to the Langmuir model equation, and hence, predicts homogeneous and monolayer adsorption [60, 76, 87]. At very low concentration, the Sips model reduces to the Freundlich model, and therefore, it does not obey the Henry's law [60, 81].

### 1.3.3.3 Adsorbents

#### *Natural adsorbents*

Natural adsorbents such as potato skin, eggshell, rice husks, coffee beans, orange peel, and banana peel can be used to extract a variety of metals [88]. A few studies also reported recovery of Sc and U with some natural adsorbents. Mosai et al., demonstrated higher selectivity of natural zeolite (clay mineral composed of Si, Al, and O) towards Sc than other metals present in a multi-metal solution of REEs. However, the adsorption capacity was rather low (0.24 mg/g or 5 μmol/g

for Sc at pH 5.5) [89]. Mahramanlioglu et al., used carbonized coffee residue to adsorb U which had the adsorption capacity up to 170 μmol/g at pH 4. However, the adsorption efficiency for U reduced by half when the U was mixed in a binary solution containing either Ca, Cd or Co [90]. Utilization of natural adsorbents is a sustainable approach in terms of valorizing the biomass and agricultural residue. Nonetheless, a major limitation of employing natural adsorbents in metal recovery application is associated with their poor reusability. In fact, only few studies are available that report the reusability of some natural adsorbents although the adsorption/desorption performance was shown to decrease within a few cycles (≤ 10 cycles) [88, 91-94].

### *Ion-exchange resins*

Ion-exchange resins (e.g., Amberlite, Dowex, Diphonix) are commercialized adsorbents; these are porous matrices formed by cross-linking copolymers containing ion-exchanging functional groups [95, 96]. In the metal uptake phenomena, the exchangeable ions from the functional groups are exchanged with counter-ions (metal ions) in the liquid phase bearing the same charge [32, 95]. Due to the high density of the functional groups, the resins have good capacity to exchange high amount of metal ions. However, during repeated adsorption/desorption processes, the resins suffer from shrinking and swelling of the polymeric structure leading to poor mechanical stability and contamination problems (fouling). The fouling is caused by the inclusion of pollutants such as organic substances and other solids present in the wastewater that hinder the diffusion of metal ions in the resin and downgrade the performance of the ion-exchange process [51, 96-100].

### *Mesoporous silica as hybrid adsorbent*

Hybrid adsorbents are the synthetic adsorbents that are prepared by conjugating organic compounds (containing functional groups/ligands) on the surface of a solid material (support). These adsorbents confer good metal adsorption properties of the functional groups and the solid support provide better stability compared to the resins or the natural adsorbents. Since the adsorption is a surface phenomenon, the solid support with high surface area is beneficial as it makes it possible to graft a large amount of functional molecules. The large surface area is also preferable to allow good interaction with the adsorbate species (metal ions). One of the supports widely used in hybrid adsorbents is mesoporous silica because of its interesting properties such as non-swelling, large surface area (~1000 $m^2/g$) and well defined pore sizes (2-50 nm) [101-104]. In addition, the mesoporous structure of the material enables its effective use as permeable adsorbent in a flow-through setup [12, 52, 69, 101, 105-107].

Although the chemical structure of mesoporous silica is generally written as $SiO_2$, its surfaces are covered with silanol groups (Si-OH). These silanol groups can act as active binding sites, especially when the metal solution is at a high pH. For example, at pH 4, the silanol groups on mesoporous silica, SBA-15 (Santa Barbara Amorphous -15) were attributed to adsorb up to 340 μmol/g U, but the adsorption of U was negligible below pH 4 [108, 109]. At lower pH value (pH 3), Giret et al., reported adsorption of various metals including Sc, lanthanides, Al, and Fe with some commercial mesoporous silica (SBA-15, silica gel). Nonetheless, the adsorption capacity of these materials was inadequate, for instance, the SBA-15 with surface area as high as 934 $m^2/g$ containing 2600 μmol/g silanol groups adsorbed 26 μmol/g Sc, meaning that as much as 100 silanol moieties were needed to adsorb one Sc ion [107]. The low capacity was referred to improper structural arrangement of Si-OH groups to bind high amount of Sc ions [69, 107]. At

even lower pH (<2.5), the adsorption of Sc was negligible because of the surfaces of SBA-15 being positively charged ($OH_2^+$), which repelled the positively charged metal ions. Further, the proton in the Si-OH groups did not dissociate to facilitate a binding site ($Si\text{-}O^-$) for the metal ion [18, 69, 107].

In order to improve the adsorption of metals, various metal binding ligands have been functionalized on the surface of the mesoporous silica by modifying the silanol groups [33, 68, 69, 100, 101, 103-105, 109-114]. A frequently used surface modification method is based on silanization reaction. In this reaction, alkoxysilanes, $R\text{-}Si\text{-}O^-$ (e.g., 3-aminopropyl triethoxysilane, ATPES) are reacted with the Si-OH groups to conjugate the silane molecules on the surface of the mesoporous silica as Si-O-Si-R [103]. Typically, to increase the adsorption of metal ions, the silanized mesoporous silica are further needed to be functionalized with other organic compounds such as with ethylphosphonic acid (PA) [108], 1-(2-pyridylazo) 2-naphthol (PAN) [111, 113] and diglycolamide (DGA) [68, 69]. Particularly with Sc and U recoveries, phosphorus-based compounds such as di-(2-ethylhexyl) phosphoric acid (DEHPA), bisphosphonates (BP) and tri-butyl-phosphate (TBP) have been frequently applied as the functional molecules [9, 108-110, 115-122]. For instance, adsorption of U with SBA-15 modified with ethylphosphonic acid (PA) at pH 4 (914 μmol/g) was 2.7 times higher than the unfunctionalized sample (340 μmol/g) [108].

Despite the adsorption capabilities of functionalized silica are improved, the aqueous stability of the functionalization is inadequate because of the hydrolysis of Si-O- bonds caused due to the nucleophilic attack by hydroxide ions [111, 123, 124]. In addition, the pore walls of mesoporous silica can be extremely thin, dissolution of few nanometers of the surface can lead to total destruction of the material [101, 125, 126]. Because of the poor stability of the chemical bond between the functional molecules and the support, leaching of the functional layer during repeated adsorption/desorption process is often issued in the literature [105, 111-113, 117, 126]. For example, Lebed et al., reported 25 % mass loss of the grafted functional molecules after only five adsorption/desorption cycles. In some cases, the silica support leached up to 28 % during the regeneration process [111]. Subsequently, due to the loss of the functional groups (pH 1-5), only one adsorption/desorption cycle was performed [111, 113].

The hybrid adsorbents have been well developed as advanced materials to recover a variety of metals. However, there remains a gap to improve the stability of the functionalization. Meanwhile, the functionalization techniques are also susceptible to increase the cost of the material. To complement the high cost, the hybrid adsorbents are not only needed to have good adsorption capacity and desired metal selectivity but are also needed to be reusable for several tens to hundreds of adsorption/desorption cycles in order to be truly sustainable and economically feasible.

## 1.4 Mesoporous silicon

Mesoporous silicon (PSi) is an alternative support material that can be developed as a hybrid adsorbent. Unlike mesoporous silica that is composed of silicon and oxygen atoms, PSi is composed of elemental silicon. The mesoporous silicas are synthesized by a bottom-up approach i.e., combining molecules to form the mesostructures [103]. In contrast, PSi is produced by a top-down approach based on the dissolution of bulk silicon.

### 1.4.1 Electrochemical etching

Electrochemical etching is a widely used method for manufacturing PSi; its advantage lies in its ability to tune the material's properties by varying the etching parameters. An etching system requires an anode, a cathode, and an electrolyte solution. In the present study, PSi was etched from p-type crystalline Si wafers as the anode, a platinum wire as the cathode, and a mixture of hydrofluoric acid (HF) and ethanol (EtOH) as the electrolyte solution (Figure 1).

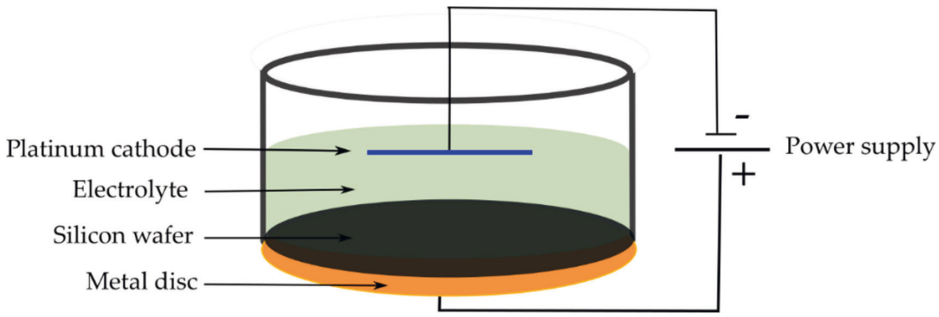


Figure 1. Schematic diagram of electrochemical etching cell used to manufacture porous silicon.

When an electric current is applied through the Si wafer with a current density below the electropolishing region (i.e., the state where Si is completely dissolved at the current density, typically above 100 mA/cm$^2$), HF causes a localized dissolution of Si. This dissolution creates pores first on the surface and subsequently inside the bulk Si. Typically, EtOH is mixed in the electrolyte to reduce the surface tension of HF and in that way it enhances the permeation of HF inside the pores [127-131]. A uniform porous layer can be achieved by applying a constant current density throughout the etching by varying the applied voltage. At the end of the etching, a current density above the electropolishing region can be applied to dissolve the silicon under the porous film and to detach the freshly generated PSi film from the wafer [127-130]. The wafer can be fabricated into PSi microparticles by milling and sieving into the desired particle sizes.

### 1.4.2 Surface modifications of PSi

Freshly etched PSi has a hydrogen terminated surface, (Si-H$_x$, x = 1 – 3) that will gradually oxidize even under ambient conditions [132]. With time, this kind of native oxidation temporarily alters the PSi's structure. In order to stabilize the PSi surface, various methods have been established over the past 30 years.

#### *1.4.2.1 Thermal oxidation*

A straight-forward approach which can be applied to stabilize the PSi surface is to oxidize it with heat treatment. At temperatures ~300 °C, the surface hydrides are released and oxygen diffuses into PSi, resulting in backbond oxidation (Si-O-Si-H$_x$) [133-135]. At temperatures above 400 °C, oxidation of the hydrides will increase forming Si-OH groups, whereas above 800 °C, complete

oxidation into $SiO_2$ can be achieved with sufficient time [136-138]. Nevertheless, the long-term stability of oxidized PSi is poor in aqueous basic media because the Si-O bonds tend to be subjected to a nucleophilic attack (hydrolysis), as described above [123, 124, 139].

#### *1.4.2.2 Hydrosilylation*

In order to achieve a more robust stability than possibly with oxidation, the Si-$H_x$ bonds on the PSi surfaces can be replaced with Si-C bonds by a hydrosilylation reaction where unsaturated organic compounds e.g. alkenes or alkynes, react with Si-$H_x$ [140-142]. The resulting Si-C bonds are more stable in aqueous environments than the Si-O bonds because the Si-C bond is less polar than the Si-O bond making it less susceptible to break down under the nucleophilic attack [140]. However, the hydrosilylated organic molecules (typically with long hydrocarbon chain) do not cover the PSi surface completely, exposing the unreacted Si-$H_x$ to oxidation and their subsequent dissolution in aqueous solutions by hydrolysis [131, 142-145].

#### *1.4.2.3 Thermal hydrocarbonization*

In order to acquire more complete passivation of PSi, gaseous hydrocarbons, typically acetylene ($C_2H_2$) has been fused with PSi [146-148]. Acetylene is flammable and cannot be used continuously above 800 °C because it will graphitize to yield carbon powder [146]. However, at a moderate temperature ~500 °C, acetylene molecules start to dissociate, enabling the carbon atoms to bind with surface silicon atoms. At this temperature, the hydrogen atoms do not completely desorb and bounded to carbon, leading to hydrocarbonized PSi surfaces [146]. The thermally hydrocarbonized porous silicon (THCPSi) have been shown to be further modifiable through hydrosilylation reaction, for instance, by mixing with undecylenic acid (Un) solution for 16 h at 120 °C [144]. A stability study conducted by Jalkanen et al., reported that the Un functionalized THCPSi (Un-THCPSi) had improved stability in 1 M KOH (no dissolution observed after 1 h) in comparison with the hydrosilylated Un-PSi (complete dissolution after 2.5 min). However, after 24 h of immersion, the Un-THCPSi had also dissolved completely [144].

#### *1.4.2.3 Thermal carbonization*

It is possible to produce a durable Si-C-Si structure in the PSi skeleton without the need for graphitization of acetylene. This can be achieved by allowing the adsorption of acetylene molecules on PSi, first at room temperature. Then, the acetylene adsorbed PSi sample is heated above 800 °C where the surface hydrides become completely desorbed from PSi, carbon atoms are disintegrated from the acetylene molecules, and permeate into the PSi skeleton leading to the formation of a non-stoichiometric silicon carbide (Si-C) layer [146-148]. This thermally carbonized porous silicon (TCPSi) has excellent stability even under harsh conditions, such as in the presence of aqueous KOH and HF for several days [143, 148]. The hydrolytic stability of TCPSi in aqueous NaOH has been visually demonstrated to be greater than the oxidized or hydrocarbonized PSi [145]. In addition, the thermal carbonization appears to cause less reduction in the surface area in comparison with thermal oxidation and hydrocarbonization [143]. When one considers the aforementioned properties relating to the stability and high surface area, it does seem that TCPSi is a suitable template which can be employed in demanding applications like metal adsorption.

The native TCPSi surface is slowly passivated in ambient air with an oxide layer making it hydrophilic [149-154]. Despite the presence of the oxide layer, the dissolution of TCPSi even in

HF is prevented by the stable Si-C-Si layer [149, 151]. Instead, HF regenerates surface hydrides, which will oxidize into hydroxyl groups that can be utilized for further functionalization via silanization [149, 155]. Often, if one wishes to intensify the surface density of -OH groups rapidly after the HF treatment, TCPSi requires priming with oxidizing agents such as hydrogen peroxide, $H_2O_2$ [155]. Nonetheless, silanization requires Si-O interface between the TCPSi and the attached moiety, and is therefore, prone to undergo hydrolysis [123, 124].

Although a great amount of research and development has been directed towards stabilization of PSi, the challenge still remains to improve its stability, especially those of the functionalized PSi, even under harsh conditions. Therefore, in the present research project, a new method to directly functionalize a terminal alkene on TCPSi was developed.

## 1.5 Bisphosphonates as metal chelators

Bisphosphonate (BP) are organophosphorus compounds containing two phosphonate groups bonded together with a geminal carbon atom (Figure 2). These are biocompatible compounds clinically used in the treatment of osteoporosis, and have also been shown to be effective in removing U from different organs in mice [156-158]. BP have also the ability to adsorb/desorb a variety of metals from different sources including industrial effluents [61, 66, 70, 110, 159-162].

**a.** **b.**

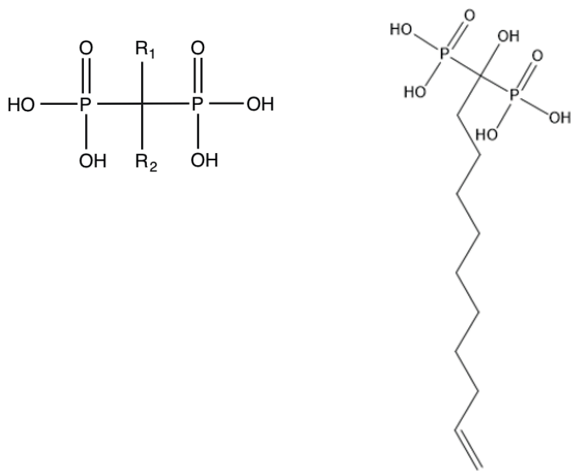


Figure 2. a) General chemical structure of bisphosphonates and b) the structure of the molecule employed in this thesis.

The characteristic P-C-P backbone structure of BP is chemically stable because of its high resistance to hydrolysis [65, 70, 162]. The central carbon can become attached with various sidechains $R_1$ and $R_2$, making it possible to vary the structure and subsequently the properties of the BP [159, 163]. For example, the length of $CH_2$ sidechain in an R group can be altered to tune the hydrophobicity i.e., the longer the chain, the more hydrophobic is the molecule [159, 160, 163].

# 2. AIMS OF THE STUDY

Utilization of adsorbents in metal recovery is a sustainable approach only if the adsorbent can withstand the harsh conditions applied during the adsorption/desorption processes. In addition, when the targeted metal is found at trace levels, the adsorbent needs to be highly selective towards that metal. Keeping these requirements in mind, the present work aims to develop a robust adsorbent that would be capable of capturing scandium and uranium efficiently from aqueous solutions containing mixtures of various metals. The specific aims of the study can be listed as follows.

1. To develop a new functionalization method to conjugate bisphosphonate on carbonized mesoporous silicon (BP-TCPSi).
2. To verify that the hybrid adsorbent and its functionalization would be highly stable even under harsh conditions.
3. To demonstrate the applicability of the material in a flow-through/column setup.
4. To elucidate the adsorption mechanism and selectivity of BP-TCPSi towards scandium.
5. To assess the applicability of BP-TCPSi to extract trace scandium from a real ore solution containing many other metals present at higher concentrations.
6. To efficiently collect uranium from a tailing obtained from the processing of an ore sample using BP-TCPSi

# 3. MATERIALS AND METHODS

## 3.1 Bisphosphonates and metal solution

The synthesis of the bisphosphonate molecule and the preparation of a leached solution of an ore sample (Kiviniemi Sc-deposit, Finland) containing Sc (III) were done in the School of Pharmacy, University of Eastern Finland (UEF). A minewater tailing sample containing U (VI) processed by Knelson concentration method (Knelson tails, KT) was carried out by the Geological Survey of Finland, GTK Mintek, Outokumpu, Finland. Artificial metal solutions were purchased from commercial suppliers (Merck, Finland and AccuStandard, USA).

## 3.2 Preparation of PSi microparticles

Si wafers (p-type, 0.01-0.02 Ωcm) were electrochemically etched using an electrolyte solution of 1:1 mixture of HF (38 – 40%, Merck) and EtOH (99.5 %, Merck) at a current density 30 – 40 mA/cm$^2$ for 40 min. A high current pulse (160 – 255 mA/cm$^2$) was applied to detach the PSi film from the wafers. The dried PSi film (65 °C) were fabricated into microparticles using a planetary ball mill and sieved to the 25 – 75 μm size fraction.

## 3.3 Surface modifications of PSi

The milled microparticles were briefly immersed with the electrolyte solution to produce fresh Si-H$_x$ terminated surfaces. The hydrogen terminated PSi is denoted as HTPSi. Hydrosilylation of HTPSi by undecylenic acid was performed by immersing the HTPSi particles in pure undecylenic acid at 120 °C for 16 h. The undecylenic acid functionalized HTPSi (UnHTPSi) particles were washed using chloroform to remove unbound undecylenic acid, and the sample was dried at 65 °C for 2 h.

With the exception of the hydrosilylation, all other surface modifications were carried out in a tube oven with continuous flow of $N_2$ gas (1 L/min) unless otherwise mentioned. For thermal carbonization, HTPSi microparticles were transferred into a quartz tube and the sample was flushed with $N_2$ for 30 min. Then, acetylene (1 L/min) was added for 15 min at room temperature, followed by heating at 500 °C for 14 min 30 sec. The acetylene flow was then cut off, and the sample was taken out of the oven at 30 s after terminating the acetylene flow. The sample was allowed to cool down to room temperature for 30 min. Then, the acetylene flow was resumed for 9 min 40 s. After 20 s at room temperature without any acetylene flow, the sample was heated at 820 °C for 10 min. The synthesized thermally carbonized porous silicon (TCPSi) particles were cooled down to room temperature.

In the functionalization of TCPSi, pure undecylenic acid or the BP in a mesitylene solution was mixed in the quartz tube under nitrogen flow. The nitrogen flow was then terminated, and the tube was closed. The sample was heated at 120 °C for 16 h or 19 h. To ensure that unbound molecules were eliminated, the undecylenic acid functionalized TCPSi (UnTCPSi) was washed with chloroform, EtOH, sodium hydroxide (NaOH), water ($H_2O$) and hydrochloric acid (HCl) whereas the BP functionalized TCPSi (BP-TCPSi) was washed with chloroform and methanol (MeOH). The characteristics of the functionalized and unfunctionalized samples such as surface area, pore diameter, pore volume and amount of functionalized bisphosphonates were thoroughly characterized using various techniques.

## 3.4 Characterization of the material

The surface chemistry of the prepared samples was examined with several techniques i.e., Electron Paramagnetic Resonance (EPR), Fourier-transform Infrared (FTIR) and Nuclear Magnetic Resonance (NMR) spectroscopy.

The changes in the paramagnetic species during functionalization were measured using an EPR device (Bruker EMX-plus Biospin). The TCPSi samples were transferred under an inert atmosphere into a glove box and put into glass tubes and sealed. The tube was put inside the spectrometer and measured. The undecylenic acid was injected through the cap in the tube and the measurements were repeated.

The surface compositions were analysed with FTIR (ThermoScientific Nicolet mode 8700) measurements in the transmission mode using freestanding PSi films. The molecular structures of the samples were measured with NMR (Bruker Avance II 300 spectrometer) to obtain the $^{1}H$-$^{29}Si$ cross polarization magic angle spinning (CPMAS) spectrum.

The surface area, pore diameter, and pore volume were determined from $N_2$ adsorption/desorption measurements (Micromertics Tristar II 3020). The surface area was calculated using the Brunauer-Emmett-Teller (BET) equation [164]. The pore volume and pore size distribution were evaluated using the Barrett-Joyner-Halenda (BJH) equation [165]. The amount of grafted molecules in the functional layer was estimated based on thermogravimetric analysis (TGA, Q50 TA instruments or NETZSCH 209 *F1 Libra*) by first heating the sample at 80 °C for 30 min to remove any adsorbed water (moisture) and then increasing the temperature at 20 °C/min up to 700 °C under an $N_2$ flow (200 mL/min). The morphology of the PSi samples (prepared on an aluminum stub with conducting carbon adhesive) was visualized with a scanning electron microscope (SEM, Zeiss Sigma).

## 3.5 Adsorption studies

Before the adsorption experiments, the microparticles were primed with HCl to confirm that the phosphonate moieties were fully protonated. Adsorption experiments were done either in a batch setup or in a flow-through setup. In the batch setup, 15 mL Eppendorf tubes were used where the desired amount of adsorbent and metal solutions at pre-determined concentrations were agitated in an orbital shaker (80 rpm) for 24 h at room temperature. Selectivity and reusability experiments were conducted in a flow-through setup where the adsorbent was packed in a glass column, and the metal solutions were passed through the adsorbent bed using a syringe pump (Figure 3). The concentrations of the metals were measured using inductively coupled plasma mass spectrometer (ICP-MS, NexION 350D, PerkinElmer).

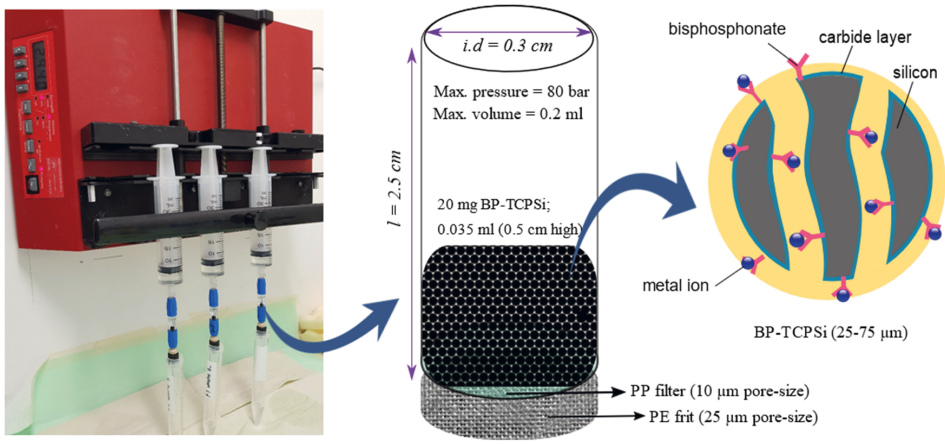


Figure 3. Schematic representation of the flow-through setup consisting of a syringe pump (left), a column filter (middle) and the BP-TCPSi (right). Inside the column, adsorbent was packed on top of polypropylene filter (PP) supported onto a polyethylene (PE) frit.

# 4. RESULTS AND DISCUSSION

## 4.1 Surface functionalization

Publication I focuses on the development of the functionalization method of TCPSi. The entire surface modification of PSi, i.e., the stabilization with thermal carbonization (TCPSi) followed by the conjugation of the functional molecules was made congruently under an inert atmosphere. When the freshly prepared TCPSi was abruptly exposed to air, a bright light was produced. This is because of the presence of highly reactive radicals on the TCPSi's surface [153].

According to the EPR measurements at room temperature, there were $3.4 \times 10^{18}$/g radicals on the TCPSi sample that were not exposed to air after carbonization. With the TCPSi sample that was exposed to air, the number of radicals were lower ($7.2 \times 10^{14}$/g). As long as the material resided in an inert atmosphere, those radicals on the TCPSi surface remained highly reactive. When the particles were mixed with an alkene, a radical addition reaction occurred resulting in direct functionalization of the TCPSi's surface. Functionalized materials prepared by the radical addition method and the conventional hydrosilylation method were compared by using undecylenic acid as the model molecule (Figure 4). The comparisons were done in terms of the amount of conjugated molecules, surface chemistry and stability.

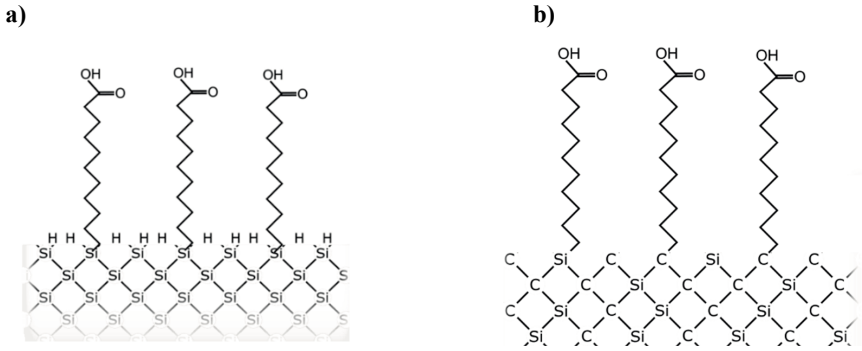


Figure 4. Schematic representation of undecylenic acid functionalized PSi samples by two separate methods a) hydrosilylation of HTPSi's surfaces (UnHTPSi) and b) radical addition onto the surface of the TCPSi (UnTCPSi).

Based on the mass loss (-wt %) during TG measurements of the samples, the amounts of conjugated molecules on the UnTCPSi and UnHTPSi were calculated by comparing their mass losses with the corresponding reference samples, TCPSi and HTPSi. The mass losses associated with the decomposition of the functional layer were comparable between UnHTPSi (2.7 ± 0.8 % w/w) and UnTCPSi (2.3 ± 0.3 % w/w) regardless of the different methods applied. This confirmed that the functionalization of the undecylenic acid molecules by both methods was successful. In addition, in the FTIR spectra, the intensity of the $CH_x$ and C=O peaks associated with the undecylenic acid were higher in UnTCPSi and UnHTPSi samples in comparison to the unfunctionalized TCPSi and HTPSi samples respectively (Figure 5A). With the HTPSi and the UnHTPSi samples, distinct peaks associated with Si-$H_x$ were observed but these were not evident with the carbonized samples. This means that the TCPSi sample was principally hydride-free,

and the functionalization occurred on the carbonized surface. In the NMR analysis, there were also higher signals of carbons from the $CH_2$ and COOH groups in the UnTCPSi sample than in the TCPSi sample (Figure 5B).

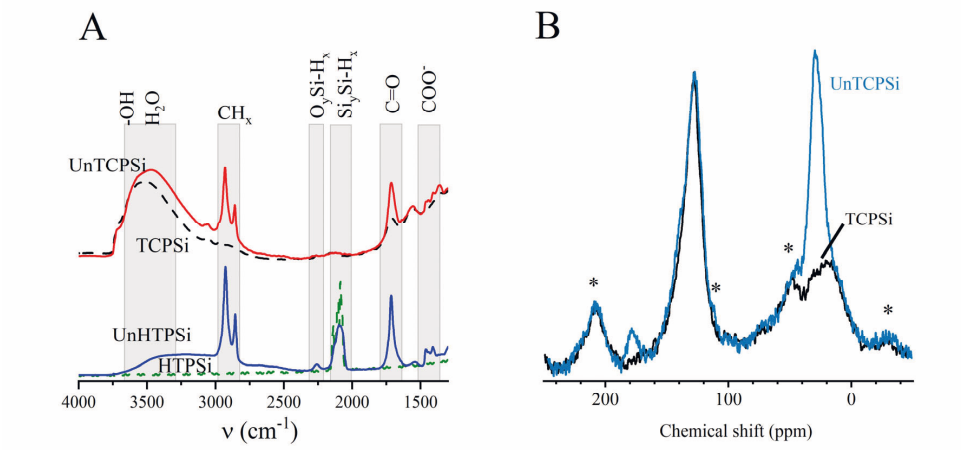


Figure 5. Surface chemistry of functionalized and unfunctionalized samples studied with (A) FTIR spectra and (B) $^{1}$H-29Si CP-MAS spectrum.

## 4.2 Stability of the functionalized surfaces

The stabilities of the UnHTPSi and the UnTCPSi samples were studied separately in deionized water, 1 M HCl, and 1 M NaOH at 30 °C. At pre-determined time-points (1, 3, 6, and 20 days), small aliquots of the microparticles were taken while the liquid was replaced with a fresh liquid. The microparticles at each time points were washed copiously with water and EtOH. After drying at 65 °C, TG measurements were carried out to calculate the remaining functionalization (%) on the samples in comparison to the original mass losses.

In water and HCl, 70 – 80 % of the functionalization was intact on the UnTCPSi sample, even after 20 days whereas only 25 – 40 % of the functionalization remained present on the UnHTPSi sample (Figure 6). In NaOH, the UnHTPSi sample dissolved within a few minutes, but no degradation was observed with UnTCPSi for up to 6 days. Nevertheless, the present functionalization (UnTCPSi sample) exhibited good stability under the harsh conditions in comparison to that encountered with the commonly used hydrosilylation technique (UnHTPSi).

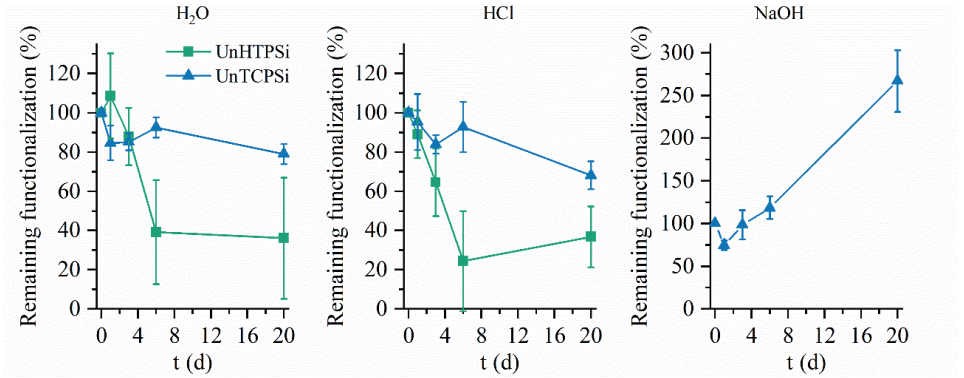


Figure 6. Stability of UnTCPSi in comparison with UnHTPSi in deionized water, 1M HCl and 1 M NaOH. Remaining functionalization (%) in the sample was calculated based on the difference in TG mass losses at time point 0 h and at pre-determined time points. The error bars represent the mean ± σ (n = 3).

## 4.3 Characterization of BP-TCPSi

In order to utilize the PSi as efficient adsorbents with good stability and selective metal adsorption properties, the developed functionalization method (by radical addition) was employed to functionalize the TCPSi with the bisphosphonate molecules. The BP-TCPSi was characterized with SEM, gas adsorption and TGA. The SEM images of BP-TCPSi show the pore openings on the irregular and rough surface of the microparticles (Figure 7). In comparison with the unfunctionalized TCPSi, the surface area, pore size and pore volume were reduced after the functionalization (Table 2). However, the pores were not completely blocked by the functional layer and the BP-TCPSi retained a mesoporous structure with a pore diameter of approx. 10 nm and a large surface area of approx. 220 $m^2/g$. The mass losses associated with the decomposition of BP varied between the studies (1 – 3 wt %) (Table 2).

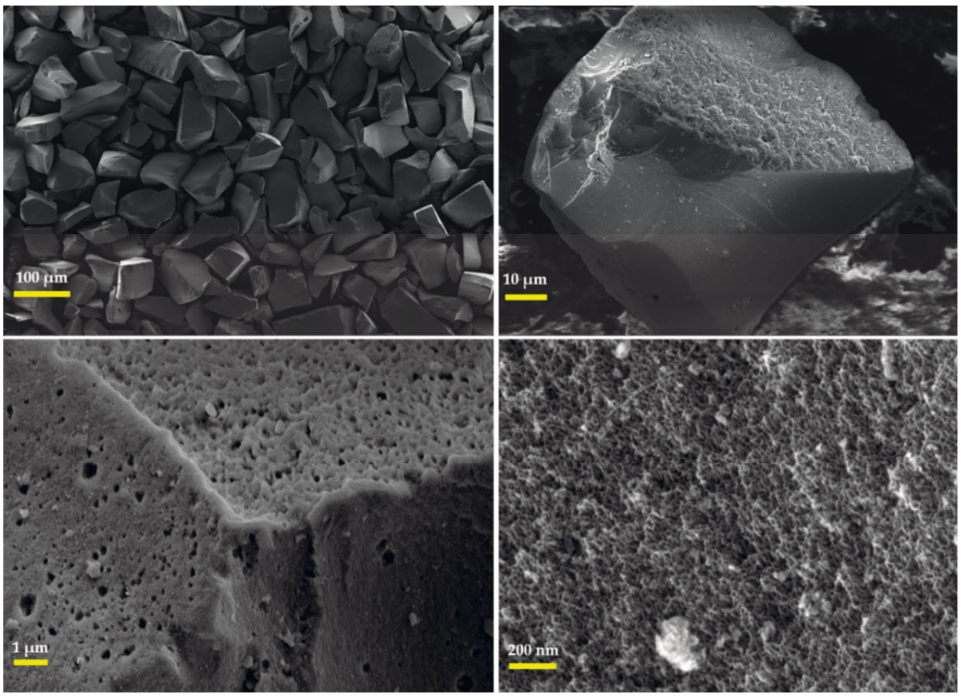


Figure 7. SEM images at various scale showing the morphology of BP-TCPSi.

Table 2. Characterization of the materials based on gas adsorption and TG measurements (mean ± σ, n = 3).

| Publications | Material | Surface area ($m^2/g$) [a] | Pore volume ($cm^3/g$) [b] | Pore diameter (nm) [c] | BP content wt % [d] | BP content µmol/g |
|---|---|---|---|---|---|---|
| I | TCPSi | 240 ± 5 | 0.98 ± 0.02 | 15.8 ± 0.1 | – | – |
| | BP-TCPSi | 224 ± 2 | 0.87 ± 0.01 | 14.5 ± 0.6 | 2.9 ± 0.5 | 88 ± 15 |
| II | TCPSi | 250 ± 3 | 0.6 ± 0.1 | 10.5 ± 0.1 | – | – |
| | BP-TCPSi | 220 ± 2 | 0.5 ± 0.01 | 10.1 ± 0.1 | 1.98 ± 0.04 | 60 ± 1 |
| III | TCPSi | | | | – | – |
| | BP-TCPSi | 212 ± 1 | 0.6 ± 0.1 | 10.1 ± 0.1 | 1.19 ± 0.03 | 36 ± 4 |
| IV | TCPSi | 238 ± 1 | 0.8 ± 0.1 | 12.3 ± 0.2 | – | – |
| | BP-TCPSi | 221 ± 1 | 0.7 ± 0.1 | 10.5 ± 0.1 | 1.71 ± 0.03 | 52 ± 1 |

[a] BET surface area calculated from the isotherm.
[b] Specific pore volume calculated from the desorption isotherm at $p/p_0 = 0.9$.
[c] Average pore diameter calculated by the BJH theory using the desorption branch of the isotherm.
[d] Mass loss of BP divided by total mass of the sample as determined by TG.

## 4.4 Adsorption isotherms of scandium

The predominant oxidation state of Sc (III) exists in a soluble form only in acidic pH as $Sc^{3+}$ [166]. Above pH 4, Sc starts to precipitate and becomes insoluble above pH 7 (e.g., as $Sc(OH)_3$ and $Sc(OH)_4^-$) [12, 71, 107, 166]. Thus, adsorption of Sc was studied at pH 1 and pH 3.

Adsorption isotherms were conducted at room temperature and the experimental equilibrium data were fitted with various isotherm models . The parameters derived from the non-linear fittings (Figure 8) are given in Table 3. Note that only the Langmuir model was employed in the original publication II.

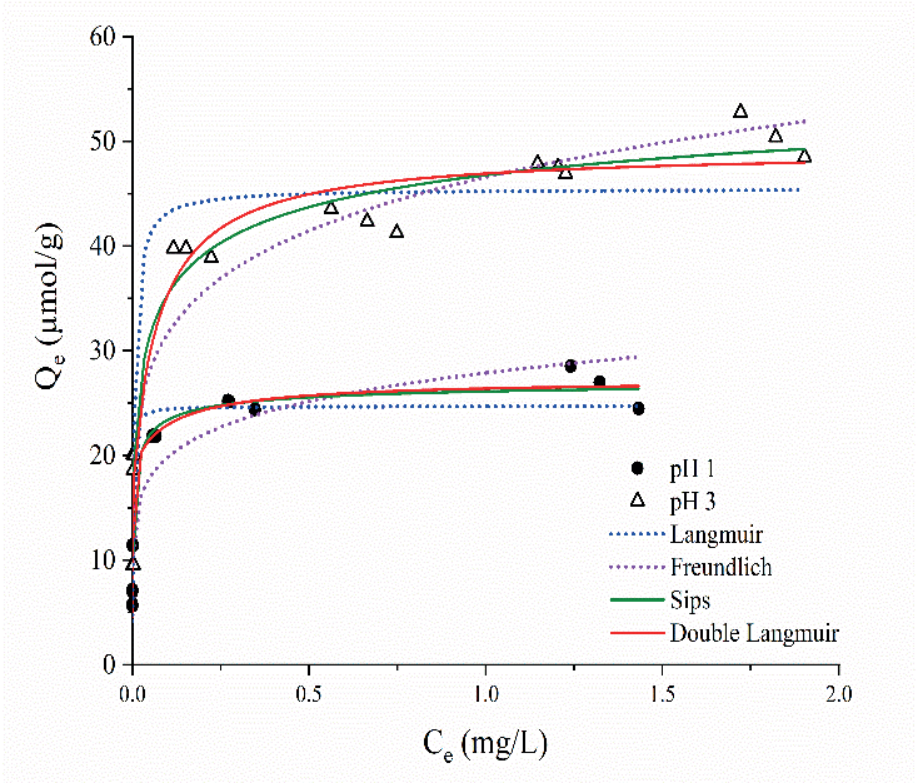


Figure 8. Adsorption isotherms of Sc with BP-TCPSi at room temperature. Experimental conditions: BP-TCPSi (10 – 100 mg) was in contact with 10 mL of Sc solution at concentrations of 2.5 mg/L (pH 1) and 4 mg/L (pH 3) for 24 h (Publication II).

Table 3. Adsorption isotherm results of Sc with BP-TCPSi.

| | **Langmuir** | | | **Double Langmuir** | | | | |
|---|---|---|---|---|---|---|---|---|
| | $R^2$ | $Q_m$ (μmol/g) | $K_L$ (L/mg) | $R^2$ | $Q_{m1}$ (μmol/g) | $Q_{m2}$ (μmol/g) | $K_{L1}$ (L/mg) | $K_{L2}$ (L/mg) |
| **pH 1** | 0.95 | 25 ± 1 | 780 ± 90 | 0.98 | 20 ± 3 | 8 ± 2 | 1000 ± 300 | 10 ± 10 |
| **pH 3** | 0.89 | 46 ± 2 | 190 ± 50 | 0.95 | 32 ± 5 | 18 ± 5 | 2000* | 13 ± 7 |
| | **Freundlich** | | | **Sips** | | | | |
| | $R^2$ | $K_f$ (μmol/g) | n (L/mg) | $R^2$ | $Q_{ms}$ (μmol/g) | $K_S$ (L/mg) | $n_s$ | |
| **pH 1** | 0.91 | 28 ± 1 | 8 ±1 | 0.98 | 28 ± 1 | 20 ± 10 | 0.5 ± 0.1 | |
| **pH 3** | 0.93 | 47 ± 1 | 6 ± 1 | 0.95 | 60 ± 10 | 3 ± 2 | 0.4 ± 0.1 | |

*Unreliable standard error

With the unfunctionalized TCPSi, the adsorption of Sc was negligible at both pH values (2 – 5 μmol/g, publication II) because of the absence of active binding sites for Sc. In the case with BP-TCPSi, adsorption of Sc at pH 3 (50 ± 2 μmol/g,) was two-times greater than at pH 1 (26 ± 2 μmol/g,). These are the experimental values corresponding to the adsorbed amount of Sc at the highest concentration of Sc used in the isotherm, which are represented by equilibrium concentrations, $C_e$ at 1.8 mg/L (pH 1) and 1.2 mg/L (pH 3) (Figure 8). The total amount of the BP grafted on the BP-TCPSi sample employed in this adsorption isotherm was 60 ± 1 μmol/g (publication II).

One observation that can be made is that one BP molecule was sufficient to adsorb one Sc ion at pH 3, whereas at pH 1, at least two BP molecule were required to participate in the adsorption of one Sc ion. In other words, the binding ratio of BP:Sc were 2:1 (pH 1) and 1:1 (pH 3). The pH dependent adsorption mechanism can be explained by the degree of deprotonations from the BP molecule. There are four -OH groups on the phosphonate moieties, each of them have different pKa values. The first pKa is < 1, the second pKa is around 2.5, whereas the remaining pKa values are above 6 [160, 163, 167]. This implies that the binding sites could be monodentate at pH 1 and bidentate at pH 3, explaining the pH dependent adsorption. After the deprotonations have occurred in relation to the solution pH, the anionic oxygen atoms function as the ligands for metal cations that facilitated a suitable coordination environment to form the chelates [70, 168]. Additionally, the oxygen in P=O group is also postulated to participate in the chelate formation via a coordination bond [118, 161, 169-171]. Thus, there appears to be several ways with which the chemisorption can occur; by virtue of deprotonation or by coordination with P=O, or by a combination of both mechanisms. It is noteworthy that the alcoholic -OH group of BP does not deprotonate below pH 13 and its role in metal complexation is unclear [70, 168].

When the experimental data were fitted with the Langmuir model, the coefficient of the fitting at pH 3 ($R^2$ = 0.89) was not as good as at pH 1 ($R^2$ = 0.95) (Figure 8 and Table 3). Since the Langmuir model assumes that the adsorption occurs on identical binding sites with monolayer coverage, its poor fitting especially at pH 3 indicated that the binding sites were not identical. In cases where the monolayer coverage is assumed to take place at two active but energetically non-identical binding sites, the double Langmuir model can be used given by following equation [86, 172, 173]

$$Q_e = \frac{Q_{m1}K_{L1}C_e}{1+K_{L1}C_e} + \frac{Q_{m2}K_{L2}C_e}{1+K_{L2}C_e} \qquad (10)$$

Where $Q_{m1}$, and $Q_{m2}$ represent the adsorption capacity whereas, $K_{L1,}$ and $K_{L2}$ are the constants representing the binding affinity.

With the double Langmuir model, the data fitted better both at pH 3 ($R^2$ = 0.95) and at pH 1 ($R^2$ =0.98), indicative of the presence of two non-identical (heterogeneous) binding sites. The binding affinities of one of these sites ($K_{L1}$ = ca. 1000 L/mg) was substantially higher than the other ($K_{L2}$ = ca. 10 L/mg). The total capacities of BP-TCPSi obtained with this model ($Q_{m1}$+ $Q_{m2}$), 50 ± 7 μmol/g at pH 3 and 28 ± 4 μmol/g at pH 1 were also comparable to the above-mentioned experimental values at pH 1 (50 ± 2 μmol/g) and at pH 3 (26 ± 2 μmol/g).

The isotherm data were also fitted with the Freundlich and the Sips models, both of which provided good coefficient values at pH 3 with $R^2$ of 0.95 and 0.93, respectively indicating heterogeneous adsorption sites (non-identical) on the surface of BP-TCPSi. This further supported the assumption used in the double Langmuir model that the adsorption sites are heterogeneous. With the Freundlich model, the heterogeneity factor, n was > 1 at both pH values that represents non-cooperative adsorption, implying that there was no interaction between the adsorbed and unadsorbed Sc ions [74]. Also with the Sips model, the heterogeneity factor, $n_s$ was < 1, implying that the adsorption sites were heterogeneous [60, 76]. The adsorption capacity values obtained with the Freundlich model ($K_f$) was comparable to the Langmuir model. The adsorption capacities ($Q_{ms}$) based on the Sips model at pH 1 (28 ± 1 μmol/g) and pH 3 (60 ± 10 μmol/g) were slightly higher than those obtained with the double Langmuir model.

It is evident that the adsorption was pH dependent such that the adsorption of Sc at pH 3 was twice as higher than at pH 1. Also in publication III, the experimental equilibrium data revealed that the adsorption of Sc at pH 3 (61 ± 1 μmol/g) was two times higher than at pH 1 (33 ± 1 μmol/g). Surprisingly, the binding ratios of BP:Sc were not in agreement between the BP-TCPSi samples used in publication II and publication III. In publication III, the BP content determined from the TG measurements was 36 ± 4 μmol/g (Table 2). Based on this amount of the grafted BP, the ratios of BP:Sc were 1:1 (pH 1) and 1:2 (pH 3). While the same binding ratios were opposite in publication II i.e., 2:1 (pH 1) and 1:1 (pH 3). Because of this discrepancy, the exact binding mechanism in terms of the formation of metal complexes and the coordination number between the BP ligands and Sc still remain to be explored further.

The adsorption capacity of BP-TCPSi was also compared with a commercial ion-exchange resin, Dowex50WX8, frequently used in the literature [8, 174-180]. The Dowex is a strong cation exchange resin containing sulfonic acid functional groups with exchangeable $Na^+$ ions (Figure 9).

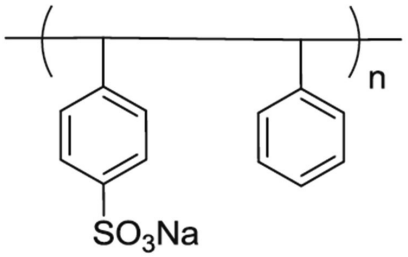


Figure 9. Chemical structure of Dowex resin.

Based on the Langmuir model fitted on the adsorption isotherm datasets (Publication II), the adsorption capacity of Dowex50WX8 for Sc was 830 ± 30 μmol/g (pH 1) and 940 ± 40 μmol/g (pH 3). In comparison to the developed BP-TCPSi, the capacity of Dowex was 30 and 20 times higher at pH 1 and pH 3, respectively. The low capacity with BP-TCPSi can be attributed to fewer number of functional groups (60 ± 1 μmol/g). By contrast, the theoretical ion-exchange capacity of the Dowex is 1.7 mEq/ml, corresponding to 708 μmol/g for $Sc^{3+}$ ions. For a brief comparison, the adsorption capacity of some of the hybrid adsorbents (with or without functionalization) used in literature for Sc recovery is listed in Table 4.

Table 4. Characteristics of some adsorbents in terms of their surface area (S.A), adsorption capacity ($Q_m$) and the number of adsorption/desorption cycles (reusability) reported in literature for recovery of Sc.

| **Adsorbents** | **$Q_m$, μmol/g** | **S.A $m^2/g$** | **pH** | **Reusability** | **Reference** |
|---|---|---|---|---|---|
| SBA-15 | 25 | 934 | 3 | – [a] | [107] |
| KIT-6 | 23 | 850 | 3 | 10 | [107] |
| Silica gel | 11 | 378 | 3 | – [a] | [107] |
| PAN-APTES-silica | 1700 | 128 | 4 | 1 | [113] |
| PAN-APTES-MWNT-silica | 730 | 107 | 4 | 5 | [114] |
| TRPO/SiO2-P | 295 | 53 | – [a] | – [a] | [120] |
| SG-MTPB | 600 | – [a] | 3 | – [a] | [181] |
| Zr-P | 830 | – [a] | 1.5 | 3 | [182] |
| Ti-P | 540 | – [a] | 2 | 5 | [71] |
| BP-TCPSi | 28 | 220 | 1 | 50 | This study |
| BP-TCPSi | 50 | 220 | 3 | – [a] | This study |

[a] not measured.

Illustrations of the adsorbent's abbreviations:

- SBA-15 (Santa Barbara Amorphous batch no. 15 mesoporous silica)
- KIT-6 (Kores Institute of Institute of Science and Technology -6 mesoporous silica)
- PAN-APTES-silica (1-(2-pyridylazo)-2-naphthol – 3-aminopropyl-triethoxy silane modified on silica gel)
- PAN-APTES-MWNT-silica (PAN-APTES- multi-walled carbon nanotubes functionalized on silica nano powder)
- TRPO/$SiO_2$-P (trialkyl phosphine oxide extractant functionalized with styrene-divinylbenzene copolymer in porous silica)
- Zr-P (zirconium functionalized with phosphate)
- Ti-P (Titanium functionalized with phosphate)

## 4.5 Selective adsorption of Sc from an artificial multi-metal solution

The selectivity of BP-TCPSi towards Sc was tested at pH 1 and pH 3 and compared to the selectivity of Dowex50WX8 towards Sc from an equimolar multi-metal solution. The experiment was conducted in the flow-through setup where 5 mL of the equimolar multi-metal solution containing Sc, Al, Fe, Cu and Zn was flown-through 20 mg of either BP-TCPSi or Dowex50WX8. The initial concentrations of the metals were adjusted such that the molar amount of each metal was at the same level as the adsorption capacities of the adsorbents, as determined by the isotherm results.

When the BP-TCPSi was used as the adsorbent, the initial amount of each metal was adjusted to 25 μmol/g and 50 μmol/g at pH 1 and pH 3, respectively. The corresponding molar concentrations of each metal was 110 μM and 220 μM. In the case when the Dowex50WX8 was used as the adsorbent, the initial amount of each metal was 700 μmol/g at pH 1, corresponding to the molar concentration of 3100 μM. The result with Dowex50WX8 at pH 3 was unreliable due to the precipitation of Fe (34 %) at high concentration (3500 μM Fe).

The selectivity results were interpreted by using a distribution coefficient ($K_d$ values, Eq 11) that defines the ratio of the concentration of metals between the solid phase and the liquid phase.

$$K_d = \frac{(C_i - C_f)}{C_f} \times \frac{V}{m} \qquad (11)$$

Where, $C_i$ and $C_f$ are the metal concentrations in the liquid phase before and after the adsorption, respectively, *m* is the mass of adsorbent and *V* is the volume of metal solution.

The $K_d$ is frequently used parameter to elucidate the adsorption performance such that higher the $K_d$ value of a metal, the higher is the adsorption of the metal [62, 69, 71, 100]. Furthermore, the $K_d$ values can be used to calculate a separation factor between a given set of two metals. The separation factor (β) can be computed using following equation

$$\beta = \frac{K_d(M1)}{K_d(M2)} \qquad (12)$$

Where, $K_d$ ($M_1$) is the distribution coefficients of a metal (in the present study, either Sc or U) and $K_d$ ($M_2$) is the distribution coefficient for another metal either Fe or Al and so on.

At pH 1, the $K_d$ values with BP-TCPSi for Sc was higher (ca. 1200 mL/g ) in comparison to other metals ($K_d$ < 20 mL/g) (Figure 10). Also, with Dowex50WX8, the $K_d$ values for Sc was higher (ca. 200 mL/g) than for other metals (< 70 mL/g). Since the experiment was conducted in an equimolar metal mixture, higher $K_d$ value of Sc in comparison to other metals indicate that both adsorbents were selective towards Sc at pH 1. Especially with BP-TCPSi at pH 1, Sc was selectively adsorbed with a β values as high as 100 for Al, 200 for Cu, 150 for Zn and 30 for Fe (Table 5). By contrast, the β values with Dowex50WX8 for Sc were below 30 with respect to every other metals. The result affirmed BP-TCPSi to be superior to Dowex50WX8 in terms of the selective adsorption of Sc from the examined multimetal solution.

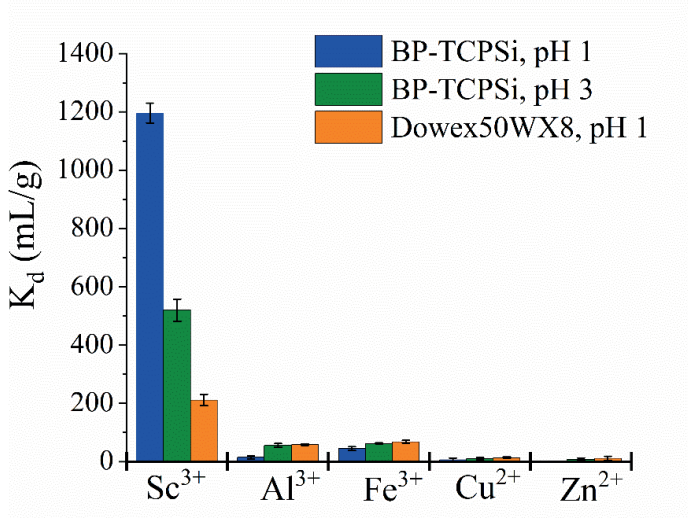


Figure 10. Distribution coefficients of BP-TCPSi towards Sc from an equimolar multi-metal solution at pH 1 and pH 3 in comparison with the ion-exchange resin, Dowex50WX8 at pH 1. Error bars represent the standard deviation (n = 3).

Table 5. Separation factor of either BP-TCPSi or Dowex50WX8 for Sc with respect to other metals (mean ± σ, n = 3).

| **Adsorbent, pH** | **β (Sc/Al)** | **β (Sc/Fe)** | **β (Sc/Cu)** | **β (Sc/Zn)** |
|---|---|---|---|---|
| BP-TCPSi, pH 1 | 90 ± 10 | 30 ± 10 | 200 ± 10 | 150 ± 10 |
| BP-TCPSi, pH 3 | 10 ± 2 | 10 ± 1 | 50 ± 20 | 60 ± 30 |
| Dowex50WX8, pH 1 | 4 ± 1 | 3 ± 1 | 15 ± 3 | 20 ± 10 |

The $K_d$ values of Sc with BP-TCPSi at pH 3 (ca. 500 mL/g) was at-least one half smaller than at pH 1 (1200 mL/g). Subsequently, the β values of Sc with BP-TCPSi at pH 3 were reduced in comparison to pH 1. At pH 1, the concentration of protons is comparatively higher that at pH 3. In the sense that more positively charged surfaces at pH 1 enhances the electrostatic repulsion against the metal ions, the affinity between the metal ion and the ligand needs to be greater than the electrostatic force of repulsion for it to occupy a binding site. Based on the affinity constant values ($K_L$) generated by fitting the Langmuir model in the isotherm data (Table 3), the affinity of Sc at pH 1 (780 ± 90 L/mg) was superior to pH 3 (190 ± 50 L/mg) suggesting Sc to be more strongly bonded with the BP moiety at pH 1. Furthermore, in publication III, the $K_L$ values obtained from the Langmuir model fittings of individual isotherms of Sc, Al and Fe at pH 1 were 32 ± 6, L/mg, 5 ± 1 L/mg and 8 ±4 L/mg respectively. These $K_L$ values also corresponded to the $K_d$ values, which were in the following order, Sc > Fe > Al (Figure 10).

The selectivity of the functional ligands towards specific metal also depends on various other factors such as the ionic charge of the metal ion (speciation), the radii of the ion, and the

electronic configurations of the atom. Generally, in multi-metal solutions, the metal with a higher ionic charge is more likely to occupy the binding site because it exerts stronger electrostatic attractive forces than a metal with a smaller ionic charge. This phenomenon can also be explained by the β values of Sc, which were greater to the divalent ions $Cu^{2+}$ (200 ± 10) and $Zn^{2+}$ (150 ± 10) in comparison to the trivalent ions, $Al^{3+}$ (90 ± 10) and $Fe^{3+}$ (30 ± 10).

Despite the equal ionic charge and the comparable concentration between the Sc, Al and Fe, the $K_d$ value of Sc was higher than that of Fe and Al. The higher adsorption of Sc than Fe and Al may be explained based on the hydration enthalpies of these metal ions. When the metals are first dissolved in an aqueous solution, they undergo hydration where water molecules surround the metal ion (forming a hydration shell). The energy released during this process is the hydration enthalpy. Upon addition of the adsorbent into the system, the hydrated metal ions has to release the water molecules before it can bind with the functional ligands on the adsorbent. Thus, a metal ion with low hydration enthalpy requires a low energy to dehydrate and hence, can be more favorably bound onto the binding sites [18, 182-186]. In accordance with this hypothesis, Sc which has a lower hydration enthalpy (-3897 kJ/mol) than Fe (-4430 kJ/mol) and Al (-4665 kJ/mol) was more selectively adsorbed with BP-TCPSi [184, 187].

## 4.6 Reusability of BP-TCPSi in Sc recovery from artificial solution

The reusability is crucial feature of an adsorbent in terms of the sustainability and economical point of view. Although a great number of hybrid adsorbents have been developed, their reusability is inadequate because of the poor stability of the material or the degradation of the functional layer [105, 111, 113, 117, 188-190]. Moreover, the reusability of the adsorbents are rarely reported for more than 10 adsorption/desorption cycles [52, 68, 100, 105, 118, 171, 191].

In the present work, the reusability of BP-TCPSi was studied up to 50 adsorption/desorption cycles of Sc in the flow-through setup. In order to expose BP-TCPSi at its full potential, adsorption was conducted at the maximum capacity i.e., 25 μmol/g at pH 1 so that the actual loss of the adsorption capacity or the leaching of functional layer can be examined. The pH 1 was chosen because the adsorbent depicted higher selectivity towards Sc than at pH 3, as described above.

In the 1st cycle, the adsorption reached 88 ± 3 % of the adsorption capacity (Figure 11). This incomplete adsorption can be attributed to shorter contact time between the adsorbent bed and the Sc ions (filtration time, 20 min), while the maximum capacity was determined at longer time (contact time, 24 h). The desorption of Sc from the 1st cycle was not complete. It is possible that the fraction of Sc ions that remained on the BP-TCPSi (21 ± 4 %) were chelated with higher coordination number. For instance, both P=O and the $PO_3^-$ groups were involved to bind the Sc ions (binding affinity, $K_L$ = 1000 ± 300 mL/g, Table 3) while only either of the binding sites was involved in binding the fraction of Sc ions that were desorbed ($K_L$ = 10 ± 10 mL/g). However, from the 2nd to the 50th cycle, BP-TCPSi exhibited good stability without essential reduction in the performance with the average of 60 ± 4 % adsorption efficiency and 98 ± 4 % desorption efficiency. To investigate the possible leaching of the functional layer, TG measurements of the BP-TCPSi sample was made after the 50th cycle has been completed. The difference in the mass losses of BP-TCPSi before (1.98 ± 0.04 wt%) and after the 50 cycles (2.3 ± 0.6 wt%) was not statistically significant ($p > 0.5$) implying that the BP ligands remained intact on the material (Figure 12).

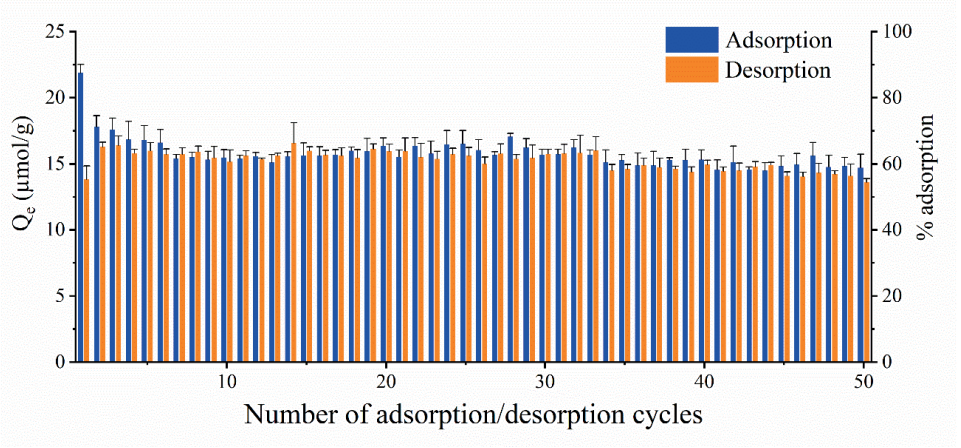


Figure 11. Adsorption/desorption cycles of Sc with BP-TCPSi examined in a flow-through setup. Adsorption step; 10 mL of 5 mg/L Sc at pH 1, flowrate 0.25 mL/min. Desorption step; 15 mL of 1 M HNO3, flowrate 1.25 mL/min. Error bars represent the standard deviation (n=4).

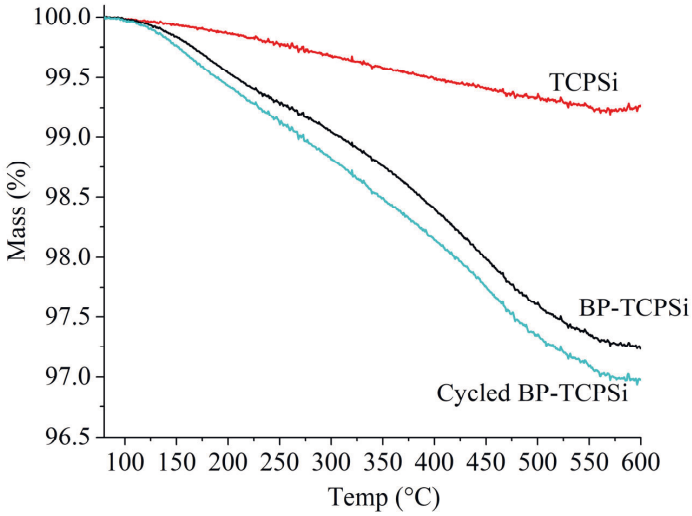


Figure 12. TGA curves of TCPSi, BP-TCPSi and cycled BP-TCPSi (50 adsorption/desorption of scandium).

## 4.7 Recovery of trace Sc from a leached solution of Kiviniemi Sc-deposit

Publication III focuses on the extraction of Sc from an ore solution using BP-TCPSi. The pH of the leached ore solution (LOS) was 0.7. The concentration of Sc in the solution was relatively low (3 mg/L, 65 μM) in comparison to the other metals such as Fe (80000 μM) and Al (21000 μM). Despite BP-TCPSi depicted good selectivity towards Sc in an equimolar metal mixtures as discussed in section 4.5, only negligible (< 1 μmol/g) Sc was adsorbed from the ore solution at pH 1 (adjusted using 1M NaOH) (Figure 13). The adsorbed amounts of other metals were exceptionally high (e.g., above 100 μmol/g Al) than the total BP content in the sample (36 ± 4 μmol/g, Table 2). The high adsorption can be attributed to physisorption phenomena involving co-operative adsorption such that the interaction between the adsorbed and unadsorbed metal ions existed. In order to employ BP-TCPSi to extract the trace Sc, pre-treatment steps (precipitation) were carried to remove/diminish the major constituents from the LOS solution.

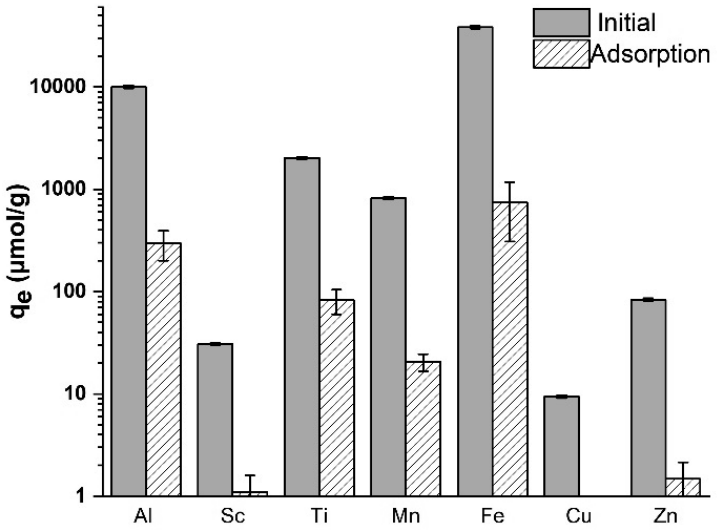


Figure 13. Amounts of metals in the leached ore solution, LOS (initial) and after adsorption with BP-TCPSi examined in the flow-through setup. Error bars represent standard deviation (n=3). Experimental conditions: 15 mg BP-TCPSi, 10 mL LOS (pH 1), flowrate 1 mL/min.

### *4.7.1 Pre-treatment of the ore solution by precipitation*

Since Sc precipitates above pH 4, the precipitation experiments were conducted at pH 4. Two separate reagents were tested: a) sodium hydroxide (NaOH) or b) combination of ammonium hydroxide and potassium permanganate ($NH_4OH/KMnO_4$). With NaOH, the pH of the LOS solution (20 mL) was first adjusted from 0.7 to 4, stirred at 90 °C for 2 h to accelerate the hydrolysis reaction, and the obtained solid residues (precipitates) were discarded by filtration. The final volume after the filtration was adjusted to 100 mL. The efficiency of the precipitation was calculated from the molar amounts of the metals in the LOS, before (20 mL) and after (100 mL)

the treatment. As shown in Table 6, the concentration of Ti was reduced effectively by 99 ± 37 %. At the same time 7.5 ± 0.2 % Sc was also precipitated. However, in comparison to the concentration of Sc in the treated solution (12 ± 0.1 μM), the concentrations of Al (1740 ± 62 μM), Mn (355 ± 11 μM) and Fe (4826 ± 51 μM) still remained higher.

Table 6. Concentration and amounts of metals in the leached ore solution (LOS), before and after the oxidative precipitation (mean ± σ, n = 3).

| Precipitation | Unit | Al | Sc | Ti | Mn | Fe | Cu | Zn |
|---|---|---|---|---|---|---|---|---|
| Original, 20 mL | C (μM) | 21000 | 65 | 4000 | 2000 | 80000 | 25 | 200 |
| | $n_i$ (μmol) | 413 | 1.3 | 77 | 36 | 1600 | 0.5 | 3 |
| NaOH, 100 mL | C (μM) | 1740 ± 62 | 12.1 ± 0.1 | 8 ± 3 | 355 ± 11 | 4826 ± 51 | 4 ± 1 | 34 ± 1 |
| | $n_f$ (μmol) | 174 ± 6 | 1.21 ± 0.01 | 0.8 ± 0.3 | 35.5 ± 1.1 | 483 ± 5 | 0.4 ± 0.1 | 3.4 ± 0.01 |
| | %[a] | 58 ± 2 | 7.5 ± 0.2 | 99 ± 37 | 2.5 ± 0.1 | 70 ± 2 | 18 ± 1 | 2.5 ± 0.1 |
| $NH_4OH/KMnO_4$, 100 mL | C (μM) | 2700 ± 30 | 11 ± 1 | 2.1 ± 0.3 | 88 ± 1 | 84 ± 1 | 5 ± 1 | 31 ± 1 |
| | $n_f$ (μmol) | 270 ± 3 | 1.15 ± 0.05 | 0.21 ± 0.03 | 8.8 ± 0.1 | 8.4 ± 0.1 | 0.5 ± 0.1 | 3.1 ± 0.1 |
| | %[a] | 35 ± 1 | 12 ± 1 | 100 ± 14 | 76 ± 2 | 99 ± 2 | 2 ± 1 | 10 ± 1 |

[a] Precipitation efficiency calculate based on the difference in molar amounts of metals, before and after the treatment, $(n_i-n_f)/n_i$.

In order to improve the precipitation efficiency of the metals than by NaOH, an oxidative precipitation using $NH_4OH$ and $KMnO_4$ was employed. First, 2.5 mL of $NH_4OH$ (7 wt%) was added to 20 mL of LOS until the pH increased from 0.7 to 4. Secondly, 2.5 mL of $KMnO_4$ (1 wt %) was added, and the solution was agitated for 30 min at 60 °C. Finally, the solution was filtered to remove the precipitates, the pH was adjusted to 1 by adding 1 M $HNO_3$ and the total volume was adjusted to 100 mL.

Since $KMnO_4$ is a strong oxidizing agent that can oxidize $Fe^{2+}$ to $Fe^{3+}$ and $Mn^{2+}$ to $Mn^{4+}$, as much as 76 ± 2 % Mn and 99 ± 2 % Fe was precipitated out from the ore solution as $Fe(OH)_3$ and $MnO_2$. The precipitation reaction can be illustrated as follows [192, 193].

$$MnO_4^- + 5Fe^{2+} + 8H^+ \rightarrow 5Fe^{3+} + Mn^{2+} + 4H_2O$$
$$Fe^{3+} + 3OH^- \rightarrow Fe(OH)_3\,(s)$$
$$3Mn^{2+} + 2KMnO_4 + 2H_2O \rightarrow 5MnO_2\,(s) + 2K^+ + 4H^+$$

Even though the Mn and Fe were effectively reduced with the oxidative precipitation, the precipitation efficiency of Al (35 ± 1 %) was not as good as the one obtained using NaOH (58 ± 2 %). Nevertheless, oxidative precipitation effectively reduced Mn, Fe as well as Al, which were adsorbed on the BP-TCPSi in major amounts (Figure 13). Hence, oxidative precipitation was exploited to pre-treat the ore solution before using it with BP-TCPSi.

### *4.7.2 Adsorption of metals using BP-TCPSi from the pre-treated ore solution*

The performance of BP-TCPSi to selectively adsorb Sc from the pre-treated solution (oxidative precipitation) was studied in the flow-through setup. Adsorption of the metals was evaluated based on the breakthrough curve, which describes how the outlet metal concentration ($C_f$) varies with the inlet concentration ($C_i$) as function of filtration volume. The breakthrough graph was plotted with the relative concentration of metal ions ($C_f/C_i$) in Y-axis and the filtrated volume in X-axis. The better the metal was retained by the column, the slower the metal permeated out of the column. As the metal solution passed through and out of the column, the concentration in the outlet gradually increased. When the column did not adsorb a given metal ion anymore, the outlet concentration of the metal ion was equivalent to its inlet concentration i.e., $C_f/C_i = 1$ (100 % permeation/breakthrough).

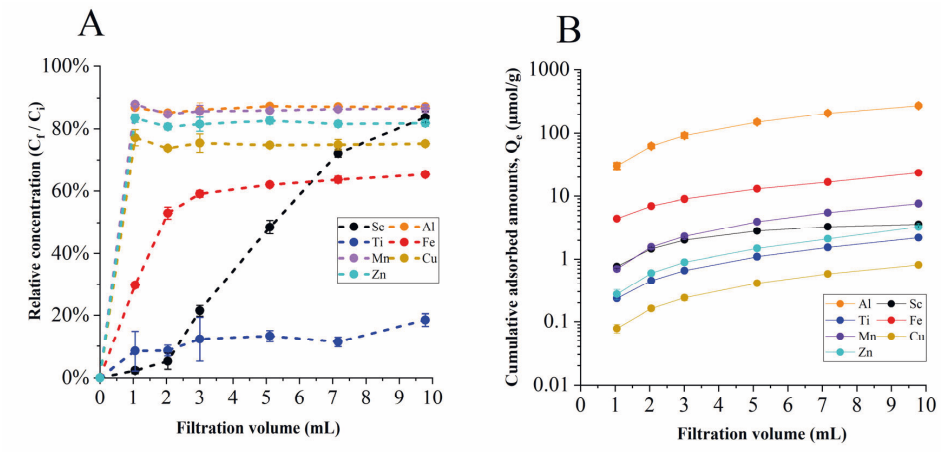


Figure 14. Adsorption of metals with BP-TCPSi from pre-treated ore solution (pH 1) in the flow-through setup. **A)** Breakthrough curves of the metals with BP-TCPSi as function of filtration volume and **B)** Cumulative adsorbed amounts of the metals as function of the filtrated volumes. Error bars represent standard deviation (mean ± σ, n = 3). Experimental condition: 15 mg BP-TCPSi, flowrate; 1 mL/min.

Based on the breakthrough curves of the metal ions, the retention time of the metals were in the order of Ti > Sc > Fe > Al ≈ Cu ≈ Zn ≈ Mg (Figure 14A). With the exception of Ti, Sc was retained longer than other metals. For example, when 3 mL of the solution has passed through, about 20 % Sc eluted out of the column while as much as 60 % Fe and 75-90 % Al, Cu, Mn an Zn were eluted. This means that adsorption efficiency of Sc was 80 %. However, the adsorbed amount of Sc was very low (2.1 ± 0.1 μmol/g) compared to Al (90 ± 10 μmol/g) and Fe (10 ± 1 μmol/g) (Figure 14 B). Although meagerly, the adsorption of Sc increased at 5, 7 and 10 mL with the cumulative adsorbed amount being 2.8 ± 0.1 μmol/g, 3.3 ± 0.1 μmol/g and 3.6 ± 0.1 μmol/g, respectively. Nevertheless, the adsorption of Sc seem to reach a plateau after the 5 mL had passed through. Therefore, 5 mL of the ore solution was utilized to examine the reusability of BP-TCPSi.

### *4.7.3 Reusability of BP-TCPSi to recover Sc from the pre-treated leached ore solution*

With the information obtained from section 4.6 (Figure 11) that the nitric acid (1 M $HNO_3$) was not effective to desorb Sc completely from the BP-TCPSi, several acids and acid mixtures were tested to desorb the Sc completely (Figure 15A). As expected, the desorption of Sc with 1 M $HNO_3$ was not complete (10 %). Also, with hydrochloric acid (1 M HCl) and sulfuric acid (1 M $H_2SO_4$), the desorption was inadequate, the efficiencies being 5 and 50 %, respectively. However, with phosphoric acid (1 M $H_3PO_4$), up to 90 % Sc was desorbed. Importantly, complete desorption (100 %) was achieved using the mixture of the 1 M $H_3PO_4$ either with 1 M $HNO_3$, 1 M HCl, or 1 M $H_2SO_4$. The effective desorption with the phosphoric acid can be attributed to a high affinity of Sc with $PO_4^{3-}$ ions [67, 194]. In particular, with the phosphonate-based adsorbents, acid mixtures containing phosphoric acid has often been often applied to efficiently desorb Sc [71, 182]. Zhang et al., used mixture of phosphoric acid and nitric acid to desorb Sc from titanium phosphonate in a selective manner. In brief, a pre-desorption step with nitric acid was used that desorbed majority of other metals such as Fe, Al, Na, La and Ca whereas only the mixture of phosphoric acid and nitric acid was able to desorb the Sc completely [71].

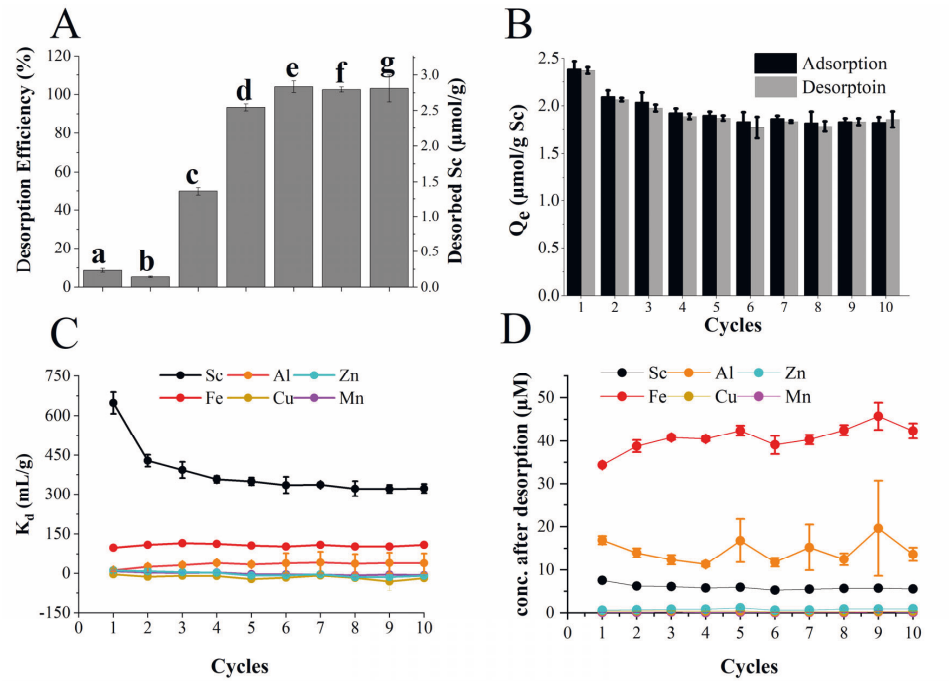


Figure 15. Results of Sc recovery from the pre-treated ore solution using BP-TCPSi in the flow-through setup. **A)** Desorption of Sc examined in a) 1 M $HNO_3$ b) 1 M HCl c) 1 M $H_2SO_4$ d) 1 M $H_3PO_4$ e) 1 M $H_3PO_4$ + 1 M $H_2SO_4$ f) 1 M $H_3PO_4$ + 1 M $HNO_3$ and g) 1 M $HNO_3$ + 1 M HCl, **B)** Reusability of BP-TCPSi to recover Sc (desorption with 1 M $H_3PO_4$ + 1 M $H_2SO_4$), **C)** distribution coefficient ($K_d$ values, Eq 11) of the metals calculated from the adsorption data and **D)** concentration of the metals (µM) after desorption step. Error bars represent standard deviation (n=3). Adsorption conditions: 15 mg BP-TCPSi, 5 mL pre-treated ore solution (pH 1), flowrate: 1 mL/min. Desorption conditions: 5 mL, flowrate:0.5 mL/min.

Since the sulfuric acid and phosphoric acid yielded higher desorption than other single component acid, mixture of these acids i.e., 1M $H_2SO_4$ + 1M $H_3PO_4$ was utilized in the reusability experiment. It should be noted that the results for Ti was unreliable because of its contamination (about 1.5 mg/L Ti, 30 μM) in the phosphoric acid. Therefore, the results of Ti are not included in the present results. In total, 10 adsorption/desorption cycles were completed.

Although the desorption of Sc was complete (99 ± 4 %) in the first cycle, adsorption was reduced by 12 % in the 2nd cycles and further by 23 % until the 5th cycles (Figure 15B). Nevertheless, in the remaining cycles, the performance was stable. Accordingly, the $K_d$ values of Sc also dropped from 650 mL/g to 350 mL/g until the 5th cycle and remained steady in the remaining cycles (Figure 15C). Despite the low concentration of Sc in the ore solution, BP-TCPSi was capable to adsorb Sc efficiently from the ore solution. Especially at the 1st cycle, Sc was adsorbed with a high separation factor of 80 ± 30 for Mn, 60 ± 40 for Zn, 50 ± 30 for Al, 7 ± 1 for Fe and 3 ± 3 for Ti (Table 7). As the $K_d$ values decreased in the subsequent cycles, the separation factor also decreased. However, the separation factor from several samples could not be reliably calculated because of the very low amount adsorbed amounts ($C_f > C_i$).

Table 7. Separation factor of BP-TCPSi for Sc with respect to other metals (M) present in the ore solution during the reusability studies (mean ± σ, n = 3).

| Cycle | β (Sc/Al) | β (Sc/Fe) | β (Sc/Ti) | β (Sc/Mn) | β (Sc/Zn) | β (Sc/Cu) |
|---|---|---|---|---|---|---|
| Cycle 1 | 50 ± 30 | 7 ± 1 | 3 ± 3 | 80 ± 30 | 60 ± 40 | –[a] |
| Cycle 2 | 20 ± 2 | 4 ± 1 | –[a] | 100 ± 10 | 50 ± 50 | –[a] |
| Cycle 3 | 10 ± 2 | 4 ± 1 | 3 ± 1 | –[a] | 90 ± 40 | –[a] |
| Cycle 4 | 10 ± 1 | 4 ± 1 | 2 ± 2 | 100 ± 50 | 130 ± 110 | –[a] |
| Cycle 5 | 10 ± 1 | 4 ± 1 | –[a] | –[a] | –[a] | –[a] |
| Cycle 6 | 10 ± 10 | 4 ± 1 | 1 ± 1 | –[a] | –[a] | –[a] |
| Cycle 7 | 10 ± 10 | 4 ± 1 | 4 ± 1 | –[a] | –[a] | –[a] |
| Cycle 8 | 10 ± 10 | 4 ± 1 | 2 ± 1 | –[a] | –[a] | –[a] |
| Cycle 9 | 10 ± 10 | 4 ± 1 | 4 ± 3 | –[a] | –[a] | –[a] |
| Cycle 10 | 10 ± 10 | 3 ± 1 | 3 ± 1 | –[a] | –[a] | –[a] |

[a] β values could not be reliably determined because of very low adsorbed amounts.

In the final filtrate after the desorption (Figure 15D), the average concentration of the metals were in the decreasing order as follows: Fe (41 ± 3 μM) > Al (14 ± 3 μM) > Sc (6 ± 1 μM) > Zn (0.8 ± 0.2 μM) > Mn (0.11 ± 0.05 μM) > Cu (0.3 ± 0.1 μM). In comparison with the pretreated ore solution (oxidative precipitation, Table 6), the concentrations of the metals after adsorption/desorption with BP-TCPSi were reduced to 50 ± 10 % for Fe, 100 ± 20 % for Al, 50 ± 10 % for Sc, 100 ± 20 % for Zn, 100 ± 50 % for Mn, and 90 ± 30 % for Cu. Although Sc was not totally purified by BP-TCPSi from the ore solution, the major components were significantly

reduced in the final filtrate. After the 10th cycle, TG measurements were carried to examine the degradation of the functional layer. The mass loss associated to BP molecule before (1.19 ± 0.03 %) and after the 10th cycle (1.17 ± 0.03 %) was not statistically significant ($p > 0.5$) indicating that the functionalization was stable during the regenerations.

## 4.8 Recovery of uranium from a tailing solution using BP-TCPSi

Publication IV focuses on the recovery of U from the tailing solution (Knelson tails, KT) using BP-TCPSi. The concentration of U in the KT sample was 9 mg/L (38 μM). The concentration of other metals were Mg 452 μM, Fe 368 μM, Al 40 μM, Mn 17 μM, Cu 13 μM. In aqueous media below pH 5, only U (VI) is stable and exists as uranyl ion $[UO_2]^{2+}$. Hence, the oxidation state of U is expected to be U (VI) in the KT sample since the pH of the solution was 3.3 [32, 118, 195]. The adsorption isotherm of U at room temperature was studied at pH 3 using standard U solution.

### 4.8.1 Adsorption isotherm of U

The experimental isotherm datasets of U were fitted with the different isotherm models listed in Table 1. The fitted curves of the isotherm models are shown in Figure 16, and the obtained parameters are given in Table 8.

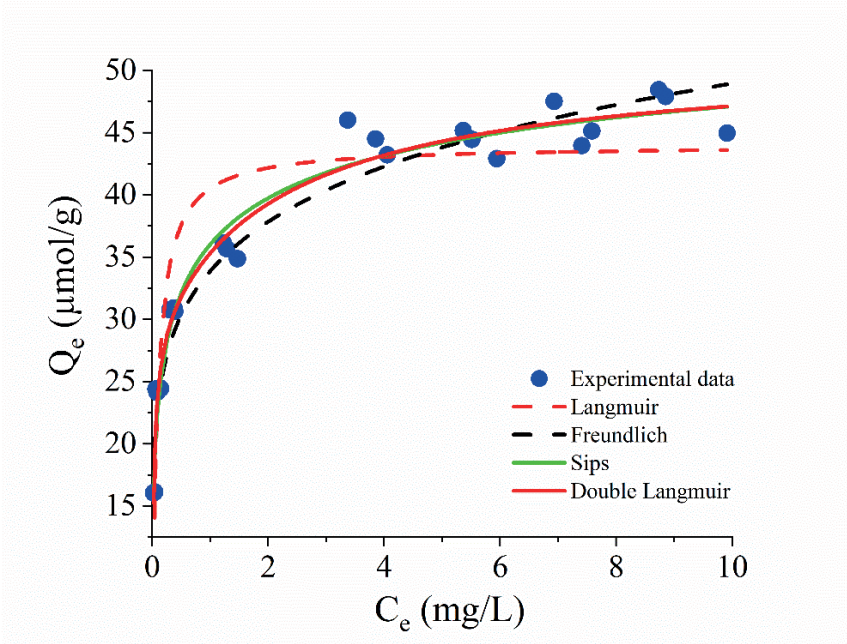


Figure 16. Adsorption isotherm of U with BP-TCPSi at pH 3. Experimental conditions: BP-TCPSi (10 mg) was in contact with 10 mL of U solution (4 – 20 mg/L U) at pH 3 for 24 h (Publication IV).

Table 8. Adsorption isotherm results of U with BP-TCPSi at pH 3.

| Langmuir | | | Double Langmuir | | | | |
|---|---|---|---|---|---|---|---|
| $R^2$ | $Q_m$ (μmol/g) | $K_L$ (L/mg) | $R^2$ | $Q_{m1}$ (μmol/g) | $Q_{m2}$ (μmol/g) | $K_{L1}$ (L/mg) | $K_{L2}$ (L/mg) |
| 0.88 | 45 ± 2 | 9 ± 3 | 0.97 | 30 ± 2 | 22 ± 2 | 40 ± 10 | 0.5 ± 0.2 |
| **Freundlich** | | | **Sips** | | | | |
| $R^2$ | $K_f$ (μmol/g) | n (L/mg) | $R^2$ | $Q_{ms}$ (μmol/g) | $K_S$ (L/mg) | $n_s$ | |
| 0.95 | 34 ± 1 | 6 ± 1 | 0.97 | 60 ± 7 | 2 ± 1 | 0.4 ± 0.1 | |

The total amount of BP grafted on the BP-TCPSi sample (publication IV) was 52 ± 1 μmol/g (Table 2). The Langmuir isotherm model did not fit the isotherm data well ($R^2$ = 0.88). It should be noticed that the Langmuir model did not fit well also with the Sc isotherm data at pH 3 as described above ($R^2$ = 0.89, Table 3). However, the fit of the double Langmuir to the isotherm data of U was good ($R^2$ = 0.97) yielding a value for the total adsorption capacity from the two non-identical binding sites ($Q_{m1} + Q_{m2}$) as 52 ± 3 μmol/g.

The Freundlich and the Sips model, both fitted the data well with $R^2$ values of 0.95 and 0.97, respectively suggesting the presence of heterogeneous adsorption sites on the BP-TCPSi. It is noteworthy that the Freundlich constant values with U isotherm data (n = 6 ± 1, Table 8) and with the Sc isotherm data (n = 6 ± 1, Table 3) were identical. Similarly, the Sips constant values with U isotherm data ($n_s$ = 0.4 ± 0.1, Table 8) and with Sc isotherm data ($n_s$ = 0.4 ± 0.1, Table 3) were also identical. Since these values indicate that there are heterogeneous adsorption sites on the surface of the adsorbent with n > 1 and $n_s$ < 1, it is apparent that the BP-TCPSi possessed non-identical binding sites at pH 3, which was concluded by the double Langmuir model as described above. Nonetheless, the adsorption capacity values obtained from the Sips model for U (60 ± 7 μmol/g) were slightly higher than the total BP amount (52 ± 1 μmol/g) grafted onto the adsorbent. For a brief comparison, adsorption capacity of other adsorbents reported in literature for U recovery is listed in Table 9.

Table 9. Characteristics of some adsorbents in terms of their surface area ($m^2$/g), adsorption capacity ($Q_m$) and the number of adsorption/desorption cycles (reusability) used for recovery of U.

| **Adsorbents** | **$Q_m$, μmol/g** | **S.A $m^2$/g** | **pH** | **Reusability** | **Reference** |
|---|---|---|---|---|---|
| SBA-15 | 339 | 815 | 4 | –[a] | [108] |
| SBA-15-PA | 914 | 495 | 4 | 6 | [108] |
| SBA-15-P | 189 | 601 | 4 | –[a] | [105] |
| KIT-6-P | 235 | 540 | 4 | 5 | [105] |
| P-Fe-CMK-3 | 630 | 187 | 4 | 5 | [118] |
| Diphos-NF silica | 540 | 123 | 7.5 | 4 | [110] |

| | | | | | |
|---|---|---|---|---|---|
| $PO_4$/PE | 730 | –[a] | 8.2 | 8 | [189] |
| SBA-15-DIMS | 1126 | –[a] | 5 | 1 | [122] |
| PPAF | 87 | 238 | 1 | 5 | [171] |
| DETA-magnetic chitosan | 747 | –[a] | 3.6 | 6 | [190] |
| BP-TCPSi | 52 | 220 | 3 | 10 | This study |

[a] not measured.

Illustrations of the adsorbent's abbreviations:

- SBA-15-PA (SBA-15 mesoporous silica functionalized with ethylphosphonic acid)
- SBA-15-DIMS (SBA-15 mesoporous silica functionalized with dihydroimidazole)
- KIT-6-P (KIT-6 mesoporous silica functionalized with phosphonate)
- Diphos-NF-silica (bisphosphonate functionalized on nanofibre silica)
- P-Fe-CMK-3 (phosphonate functionalized with iron embedded mesoporous carbon)
- $PO_4$/PE (phosphonate functionalized on polyethylene),
- PPAF (phosphorus functionalized porous aromatic frameworks)
- DETA-magnetic chitosan (Diethylenetriamine functionalized magnetic chitosan nanoparticles)

### 4.8.2 Adsorption performance of BP-TCPSi from the tailing solution

The adsorption performance of BP-TCPSi for the metal ions present in the Knelson Tails (KT) sample was experimented in the flow-through setup. From the breakthrough curves (Figure 17A), it is evident that the BP-TCPSi retained U for a longer time than other metals despite the fact that the concentration of U was relatively smaller (38 μM) than, for example, Mg (452 μM) and Fe (362 μM). The majority of the metals were adsorbed during the first 5 mL (Figure 17B), where the adsorption efficiency of U was 100 % (adsorbed amount; 9 ± 1 μmol/g) and did not elute out of the column (0 % breakthrough). Meanwhile, the adsorption efficiency and the adsorbed amounts of other metals were 60 ± 10 % for Al (7 ± 1 μmol/g), 20 ± 10 % for Cu (0.7 ± 0.2 μmol/g), 10 ± 3 % Fe (14 ± 4 μmol/g), 5 ± 3 % for Mn (0.1 ± 0.1 μmol/g), and 3 ± 1 % for Mg (5 ± 1 μmol/g) (Figure 17 B). Combining all the adsorbed amounts, the total amount of metals in the BP-TCPSi was 35 ± 1 μmol/g, meaning that ~70 % of the total capacity (52 ± 3 μmol/g, determined by double Langmuir) has been saturated at the 5 mL filtrated volume.

When further passing the metal solution, at 10 mL, only Al (14 ± 8 %, 3 ± 1 μmol/g) and U (96 ± 4 %, 8 ± 1 μmol/g) were adsorbed while other metals reached 100 % breakthrough. At this point, the total amount of all the metals adsorbed in the BP-TCPSi was 47 ± 1 μmol/g, which was slightly lower than the total capacity i.e., 52 ± 3 μmol/g as mentioned above. Nevertheless, at the subsequent filtration volumes i.e., 20, 30 and 40 mL, only U was adsorbed with adsorption efficiencies of 51 ± 3 % (5 ± 1 μmol/g), 43 ± 7 % (4 ± 1 μmol/g) and 2 ± 1 % (0.2 ± 0.1 μmol/g) respectively (Figure 17B).

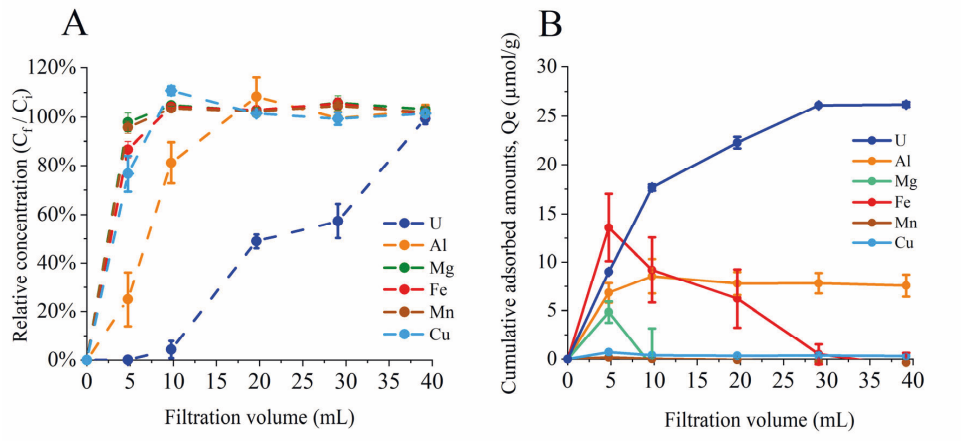


Figure 17. Adsorption of metals in BP-TCPSi from Knelson tails (pH 3.3) in flow through setup. **A)** Breakthrough curves of the metals with BP-TCPSi as function of filtration volume (up to 40 mL) and **B)** Cumulative adsorbed amounts of the metals as function of filtration volume. Experimental condition: 20 mg BP-TCPSi, flowrate 0.25 mL/min.

At the end of the experiment, i.e., at 40 mL, the total amount of all adsorbed metals on the BP-TCPSi was 55 ± 1 μmol/g, which is comparable with the total capacity of the adsorbent (52 ± 3 μmol/g), meaning that the binding sites has been fully saturated. At this saturation stage, the total amount of adsorbed U was 26 ± 1 μmol/g i.e., 50 % of all the binding sites were consumed by the U ions. Since the adsorption of U was predominant over other metals despite its low concentration, BP-TCPSi was more selective towards U than other metals. The good selectivity of BP-TCPSI towards U can be attributed to its lower hydration enthalpy (- 70.2 kJ/mol) than Al (- 4665 kJ/mol), Fe (- 4430 kJ/mol), Mg (-1921 kJ/mol), Mn (- 1841 kJ/mol), and Ca (- 1577 kJ/mol) [187, 196]. Because of the lower hydration enthalpy of U than other metals, it required lesser energy to dehydrate and occupied the binding sites on BP-TCPSi rapidly.

### 4.8.3 Reusability of BP-TCPSi to recover U from the tailing solution

With the aim to reduce the U concentration in the final filtrate, reusability of BP-TCPSi was examined using 10 mL of KT because at this volume, the total adsorption efficiency of U was as much as 96 ± 4 % (16 ± 1 μmol/g). The adsorbent was effectively regenerated to recover U with average adsorption and desorption efficiencies of 91 ± 6 % and 97 ± 9 %, respectively (Figure 18 A).

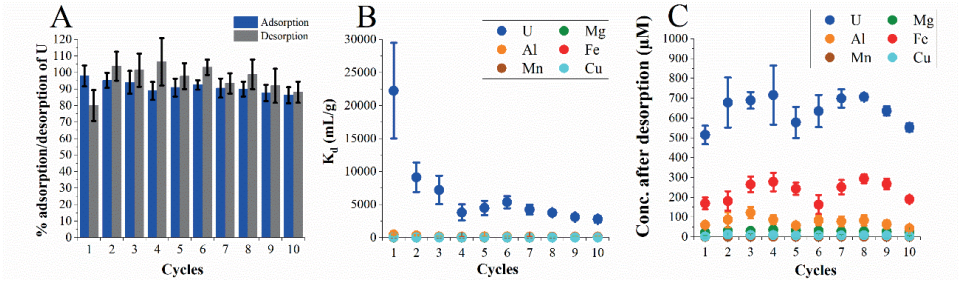


Figure 18. Results from the flow-through setup **A)** reusability of the adsorbent for 10 adsorption/desorption cycles of U, **B)** distribution coefficient ($K_d$) of the metals present in the KT sample and **C)** concentration of the metals after the desorption steps. Error bars represent the standard deviation (n = 4). Experimental conditions: 20 mg BP-TCPSi, adsorption: 10 mL of Knelson tails (pH 3.3), flowrate 0.25 mL/min, desorption: 0.5 mL of 1 M $H_2SO_4$, flowrate 1.25 mL/min.

Because of the good selectivity of BP-TCPSi for U, the $K_d$ value of U was as high as 22000 mL/g (cycle 1, Figure 18 B) with the adsorption efficiency close to 100 %. Whereas the $K_d$ values for other metals were substantially low; 500 mL/g for Al (adsorption efficiency 50 %) or below 100 mL/g for Fe, Mg, Cu, and Mn (adsorption efficiencies < 20 %). The separation factor of BP-TCPSi for U to every metal was > 20 in all cycles (Table 10). However, after the 1st cycle, the $K_d$ values of U decreased largely. This decreasing trend can be attributed to the small volume of acid used for desorption. Small volume in desorption was utilized to fulfill the aim of the study to safely dispose the collected U. Due to the small volume in the desorption step, 0.5 mL of 1 M $H_2SO_4$, the adsorbed U did not release completely at the 1st cycle (desorption efficiency, 80 ± 7 %). This incomplete desorption caused the $K_d$ value to decrease in the following cycles because the concentration of U in the filtrate increased ($C_f$ = 0.2 – 1.2 mg/L). Since the $K_d$ is inversely related to the concentration in the filtrate (Eq 11), it decreased in the subsequent cycles. Nonetheless, the values remained steady at about 5000 mL/g after the 4th cycles and was still greater than the $K_d$ of other metals. Consequently, in the final filtrate after the desorption (Figure 18 C), the concentrations of other metals were smaller than that of U due to lower adsorption of the metals than U, as described above. The average concentration of these metals in the final filtrate from the 10 cycles were 230 ± 50 μM for Fe, 80 ± 20 μM for Al, 30 ± 4 μM for Mg, 7 ± 3 μM for Cu and < 1 μM for Mn. In contrast, the concentration of U in the final filtrate was increased by at-least 15 times (640 ± 70 μM) in comparison to the original solution (38 μM).

Table 10. Separation factor (β) of BP-TCPSi for U with respect to other metals (M) present in the Knelson tails during the reusability studies (mean ± σ, n = 4).

| Cycle | β (U/Mg) | β (U/Fe) | β (U/Al) | β (U/Mn) | β (U/Cu) |
|---|---|---|---|---|---|
| Cycle 1 | 700 ± 300 | 300 ± 100 | 50 ± 20 | 900 ± 400 | 300 ± 100 |
| Cycle 2 | 500 ± 300 | 200 ± 50 | 30 ± 10 | 600 ± 200 | –[a] |
| Cycle 3 | 400 ± 100 | 100 ± 50 | 40 ± 10 | 400 ± 100 | 200 ± 100 |

| | | | | | |
|---|---|---|---|---|---|
| Cycle 4 | –[a] | 100 ± 50 | 30 ± 10 | –[a] | 100 ± 50 |
| Cycle 5 | 200 ± 50 | 60 ± 20 | 20 ± 10 | 200 ± 50 | 80 ± 20 |
| Cycle 6 | –[a] | 100 ± 50 | 30 ± 10 | –[a] | 100 ± 50 |
| Cycle 7 | 200 ± 100 | 100 ± 50 | 30 ± 20 | –[a] | 90 ± 20 |
| Cycle 8 | 200 ± 50 | 60 ± 10 | 30 ± 10 | 200 ± 30 | 70 ± 10 |
| Cycle 9 | 100 ± 20 | 50 ± 10 | 20 ± 10 | 100 ± 50 | 60 ± 10 |
| Cycle 10 | 90 ± 20 | 50 ± 10 | 20 ± 10 | 90 ± 30 | 50 ± 10 |

[a] β values could not be reliably determined because of very low adsorbed amounts.

# 5. CONCLUSIONS

A new functionalization method to directly conjugate terminal alkenes on the carbonized mesoporous silicon was developed successfully. The adsorbent was stable under harsh conditions such as in the presence of water, hydrochloric acid, and sodium hydroxide solutions for several days. The adsorbent demonstrated good stability also during 50 adsorption/desorption cycles without any evidence of a significant reduction in its performance.

Adsorption was found to be pH dependent process such that the adsorption capacity was twice greater at pH 3 than at pH 1. Especially at pH 3, the adsorption isotherm studies reveal that the binding sites on BP-TCPSi were heterogeneous because the Langmuir isotherm model did not adequately fit the experimental datasets. The heterogeneous binding surface was further confirmed with the double Langmuir, Freundlich and Sips isotherm models, which fitted the experimental datasets adequately.

In terms of selectivity, BP-TCPSi was more selective towards Sc at pH 1 ($K_d$ = 1200 mL/g) than at pH 3 ($K_d$ = 500 mL/g) examined in an equimolar multi-metal solution containing Sc, Al, Fe, Cu and Zn. At pH 1, the selectivity of BP-TCPSi towards Sc was found to be higher in comparison with a commercial ion exchange resin, Dowex50WX8 ($K_d$ 200 mL/g). Despite the good selectivity towards Sc from the equimolar multi-metal solutions, BP-TCPSi was incapable of adsorbing trace amounts of Sc from a leached ore solution because of the presence of other metals at high concentrations. However, after reducing the major constituents effectively by undertaking a precipitation step using $NH_4OH$ and $KMnO_4$, the BP-TCPSi was capable to selectively adsorb Sc in comparison with other trivalent metals with a separation factor of 50 ± 30 for Al and 7 ± 1 for Fe.

When the BP-TCPSi was employed to recover U from a tailing solution, it adsorbed U efficiently with a substantial $K_d$ value (22000 mL/g) regardless of the high concentrations of other metals dissolved in the solution. More importantly, the adsorbed U could be collected in a small volume where its concentration was increased by 15 times compared to the original solution. The ability to utilize a low volume to collect U is beneficial in situations when one needs to dispose of uranium contaminated wastewaters.

# 6. FUTURE PERSPECTIVES

The developed adsorbent has been shown to be effectively reusable through numerous adsorption/desorption cycles. However, it requires some improvements in several aspects before it can be considered to be used in a large-scale operation. For example, the cost of the adsorbent needs to be reduced. The silicon wafers used as the raw material to produce the mesoporous silicon are expensive and only commercially available. A real step forward would be the identification of an alternative raw material that would be cheap and widely available and more economic raw material to produce in large quantities than the mesoporous silicon.

Currently, our research group is focusing on the syntheses of nanostructured silicon carbide (SiC) from silica-rich plant-based residues such as tabasheer [197] and barley husk [198]. The syntheses involves the purification of silica from the residues followed by the conversion of the silica into porous silicon carbide (SiC) using a magnesiothermic reduction reaction in presence of carbon precursors ($SiO_2 + 2\ Mg + C \rightarrow SiC + 2\ MgO$). The SiC functionalized with BP have been shown to be reusable (examined up to 5 adsorption/desorption cycles of Mn), even when the adsorption was carried out under harsh condition (pH 8) [198]. Nonetheless, the surface area (~140 $m^2/g$), the BP content (2.6 wt %) and the adsorption capacity (89 μmol/g for Mn) were comparable to the present study and still needs improvement.

It is evident that commercial ion exchange resins as well as other hybrid adsorbents reported for Sc and U recoveries have substantial capacity than the adsorbents we have developed. The adsorption capacity is an important factor that needs to be improved significantly with porous silicon-based adsorbents. Since the adsorption capacity relied upon the functional molecules grafted onto the material, there are several possibilities to improve the density of the functional molecules. Few of them include optimization of laboratory apparatus, experimental conditions and even the structure of the functional molecules. Some studies demonstrated that smaller functional molecule (e.g., shorter alkyl chain length) can be grafted in higher amounts on the adsorbent than the molecules with bigger size [109]. Accordingly, adsorbent with a high functional groups were more efficient to recover high amount of metals. Therefore, it would be interesting to investigate the functionalization and adsorption capabilities of bisphosphonate molecules containing shorter alkyl chain length than the one used in the present study (chain length = 9). Moreover, the carbonized silicon support with a very high surface can also implemented to increase the degree of the functionalization and subsequently the adsorption performances.

# REFERENCES


1. W. Wang, Y. Pranolo, C.Y. Cheng, Metallurgical processes for scandium recovery from various resources: A review, Hydrometallurgy 108 (2011) 100-108.
2. Z. Wang, M. Li, Z. Liu, M. Zhou, Scandium: Ore deposits, the pivotal role of magmatic enrichment and future exploration, Ore geology reviews 128 (2021) 103906.
3. E.J. Pruvot, Extraction of scandium from its ores, Patent, (1959)
4. J. Gambogi, U.S. Geological Surve. Mineral commodity summaries: Scandium 2021.
5. M. Ochsenkühn-Petropoulou, K.S. Hatzilyberis, L.N. Mendrinos, C.E. Salmas, Pilot-Plant Investigation of the Leaching Process for the Recovery of Scandium from Red Mud, Industrial & engineering chemistry research 41 (2002) 5794-5801.
6. T. Halkoaho, M. Ahven, O.T. Rämö, J. Hokka, H. Huhma, Petrography, geochemistry, and geochronology of the Sc-enriched Kiviniemi ferrodiorite intrusion, eastern Finland, Mineralium deposita 55 (2020) 1561.
7. W. Wang, C.Y. Cheng, Separation and purification of scandium by solvent extraction and related technologies: a review, Journal of chemical technology and biotechnology (1986) 86 (2011) 1237-1246.
8. M. Ochsenkuhn-Petropolu, T. Lyberopulu, G. Parissakis, Direct determination of lanthanides, yttrium and scandium in bauxites and red mud from alumina production, Analytica Chemica Acta (1994) 05-313.
9. Alexey L. Smirnov, Svetlana M. Titova, Vladimir N. Rychkov, Grigory M. Bunkov, Vladimir S. Semenishchev, Eugeny V. Kirillov, Nikolay N. Poponin, Ilya A. Svirsky, Study of scandium and thorium sorption from uranium leach liquors, Journal of Radioanalytical and Nuclear Chemistry 312 (2017) 277-283.
10. K. Yasukawa, J. Ohta, K. Mimura, E. Tanaka, Y. Takaya, Y. Usui, K. Fujinaga, S. Machida, T. Nozaki, K. Iijima, K. Nakamura, Y. Kato, A new and prospective resource for scandium: Evidence from the geochemistry of deep-sea sediment in the western North Pacific Ocean, Ore geology reviews 102 (2018) 260-267.
11. H. Shimazaki, Z. Yang, R. Miyawaki, M. Shigeoka, Scandium-Bearing Minerals in the Bayan Obo Nb-REE-Fe Deposit, Inner Mongolia, China, Resource geology 58 (2008) 80-86.
12. K. Pyrzyńska, K. Kilian, M. Pęgier, Separation and purification of scandium: From industry to medicine, Separation & Purification Reviews 48 (2018) 65.
13. L. Wang, P. Wang, W. Chen, Q. Wang, H. Lu, Environmental impacts of scandium oxide production from rare earths tailings of Bayan Obo Mine, Journal of cleaner production 270 (2020) 122464.
14. P.C.K. Vesborg, T.F. Jaramillo, Addressing the terawatt challenge: scalability in the supply of chemical elements for renewable energy, RSC advances 2 (2012) 7933-7947.
15. F. Klimpel, M. Bau, T. Graupner, Potential of garnet sand as an unconventional resource of the critical high-technology metals scandium and rare earth elements, Scientific reports 11 (2021) 5306.
16. J. Vind, A. Malfliet, C. Bonomi, P. Paiste, I.E. Sajó, B. Blanpain, A.H. Tkaczyk, V. Vassiliadou, D. Panias, Modes of occurrences of scandium in Greek bauxite and bauxite residue, Minerals engineering 123 (2018) 35-48.
17. K. Evans, The History, Challenges, and New Developments in the Management and Use of Bauxite Residue, J. Sustain. Metall 2 (2016) 316-331.
18. D. Avdibegović, K. Binnemans, Separation of Scandium from Hydrochloric Acid–Ethanol Leachate of Bauxite Residue by a Supported Ionic Liquid Phase, Industrial & engineering chemistry research 59 (2020) 15332-15342.

19. C.R. Borra, Y. Pontikes, K. Binnemans, T. Van Gerven, Leaching of rare earths from bauxite residue (red mud), Minerals engineering 76 (2015) 20-27.
20. Z. Ahmad, The properties and application of scandium-reinforced aluminum, JOM 55 (2003) 35-39.
21. S. Badwal, F. Ciacchi, Oxygen-ion conducting electrolyte materials for solid oxide fuel cells, Ionics 6 (2000) 1-21.
22. S. Badwal, F. Ciacchi, D. Milosevic, Scandia–zirconia electrolytes for intermediate temperature solid oxide fuel cell operation, Solid state ionics 136 (2000) 91-99.
23. D. Jeong, J. Kim, O. Kwon, C. Lim, S. Sengodan, J. Shin, G. Kim, Scandium Doping Effect on a Layered Perovskite Cathode for Low-Temperature Solid Oxide Fuel Cells (LT-SOFCs), Applied sciences 8 (2018) 2217.
24. N. Laosiripojana, W. Wiyaratn, W. Kiatkittipong, A. Arpornwichanop, A. Soottitantawat, S. Assabumrungrat, Reviews on solid oxide fuel cell technology, Engineering Journal 13 (2009) 65-84.
25. A.B. Stambouli, E. Traversa, Solid oxide fuel cells (SOFCs): a review of an environmentally clean and efficient source of energy, Renewable & sustainable energy reviews 6 (2002) 433-455.
26. M. Akiyama, T. Kamohara, K. Kano, A. Teshigahara, Y. Takeuchi, N. Kawahara, Enhancement of Piezoelectric Response in Scandium Aluminum Nitride Alloy Thin Films Prepared by Dual Reactive Cosputtering, Advanced materials (Weinheim) 21 (2009) 593-596.
27. F. Tasnádi, B. Alling, C. Höglund, G. Wingqvist, J. Birch, L. Hultman, I.A. Abrikosov, Origin of the Anomalous Piezoelectric Response in WurtziteScxAl1−xNAlloys, Phys. Rev. Lett. 104 (2009).
28. S. Mertin, B. Heinz, O. Rattunde, G. Christmann, M.A. Dubois, S. Nicolay, P. Muralt, Piezoelectric and structural properties of c-axis textured aluminium scandium nitride thin films up to high scandium content 343 (2018) 2.
29. M. Uehara, T. Mizuno, Y. Aida, H. Yamada, K. Umeda, M. Akiyama, Increase in the piezoelectric response of scandium-doped gallium nitride thin films sputtered using a metal interlayer for piezo MEMS, Appl. Phys. Lett 114 (2019).
30. J.R. Kumar, J. Kim, J. Lee, H. Yoon, A Brief Review on Solvent Extraction of Uranium from Acidic Solutions, Separation and purification reviews 40 (2011) 77-125.
31. Uranium resources, production, and demand. A joint report by the Nuclear Energy Agency and the International Atomic Energy Agency. 2020.
32. M.M. Aly, M.F. Hamza, A Review: Studies on Uranium Removal Using Different Techniques. Overview, Journal of Dispersion Science and Technology 34 (2013) 182-213.
33. 33. J. Wang, S. Zhuang, Extraction and adsorption of U(VI) from aqueous solution using affinity ligand-based technologies: an overview, Rev Environ Sci Biotechnol 18 (2019) 437-452.
34. F. Li, W. Cui, W. Jiang, C. Zhang, R. Liang, J. Qiu, Stable sp carbon-conjugated covalent organic framework for detection and efficient adsorption of uranium from radioactive wastewater, Journal of hazardous materials 392 (2020) 122333.
35. N. Chapman, A. Hooper, The disposal of radioactive wastes underground, Proceedings of the Geologists' Association 123 (2012) 46-63.
36. J. Mercadier, M. Cuney, P. Lach, M. Boiron, J. Bonhoure, A. Richard, M. Leisen, P. Kister, Origin of uranium deposits revealed by their rare earth element signature, Terra nova (Oxford, England) 23 (2011) 264-269.
37. C.R. Edwards, A.J. Oliver. Uranium processing: A review of current methodology and technology. JOM 52 (2000) 12-20.

38. R. Selvakumar, G. Ramadoss, Mridula P. Menon, K. Rajendran, P. Thavamani, Ravi Naidu, M. Megharaj, Challenges and complexities in remediation of uranium contaminated soils: A review, Journal of environmental radioactivity 192 (2018) 592-603.
39. M.L. Zamora, B.L. Tracy, J.M. Zielinski, D.P. Meyerhof, M.A. Moss, Chronic ingestion of uranium in drinking water: a study of kidney bioeffects in humans, Toxicological sciences 43 (1998) 68-77.
40. D. Brugge, J.L. deLemos, B. Oldmixon, Exposure Pathways and Health Effects Associated with Chemical and Radiological Toxicity of Natural Uranium: A Review, Reviews on environmental health 20 (2005) 177-194.
41. M.L. Zamora, B.L. Tracy, J.M. Zielinski, D.P. Meyerhof, M.A. Moss, Chronic Ingestion of Uranium in Drinking Water: A Study of Kidney Bioeffects in Humans, Toxicological sciences 43 (1998) 68-77.
42. R. Konietzka, Gastrointestinal absorption of uranium compounds – A review, Regulatory toxicology and pharmacology 71 (2015) 125-133.
43. 43. U.S. Department of health and human services. Toxicological profile for uranium. 2013.
44. P. Kurttio, A. Auvinen, L. Salonen, H. Saha, J. Pekkanen, I. Mäkeläinen, S.B. Väisänen, I.M. Penttilä, H. Komulainen, Renal Effects of Uranium in Drinking Water, Environmental Health Perspectives 110 (2002) 337-342.
45. K.B. Mulloy, D.S. James, K. Mohs, M. Kornfeld, Lung Cancer in a Nonsmoking Underground Uranium Miner, Environmental health perspectives 109 (2001) 305-309.
46. P.A. Prabhavathi, P. Padmavathi, P.P. Reddy, Chromosomal Aberrations in the Leucocytes of Men Occupationally Exposed to Uranyl Compounds, Bull. Environ. Contam. Toxicol 70 (2003) 0322-0327.
47. P.L.D. Sylvester, R. Lopez, A.M. Ubios, R.L. Cabrini, Exposure to Subcutaneously Implanted Uranium Dioxide Impairs Bone Formation, Archives of Environmental Health: An International Journal 57 (2010) 320.
48. J.L. Domingo, A. Ortega, J.L. Paternain, J. Corbella, Evaluation of the Perinatal and Postnatal Effects of Uranium in Mice upon Oral Administration, Archives of environmental health 44 (1989) 395-398.
49. S. Raymond-Whish, L.P. Mayer, T. O'Neal, A. Martinez, M.A. Sellers, P.J. Christian, S.L. Marion, C. Begay, C.R. Propper, P.B. Hoyer, C.A. Dyer, Drinking Water with Uranium below the U.S. EPA Water Standard Causes Estrogen Receptor-Dependent Responses in Female Mice, Environmental health perspectives 115 (2007) 1711-1716.
50. Uranium Fact Sheet. Water Quality Association. US
51. M.A. Barakat, New trends in removing heavy metals from industrial wastewater, Arabian journal of chemistry 4 (2011) 361-377.
52. J. Roosen, S. Roosendael, C.R. Borra, T Gerven, S Mullens, K. Binnemans. Recovery of scandium from leachates of Greek bauxite residue by adsorption on functionalized chitosan-silica hybrid materials. Green chemistry 18 (2016) 2005-2013.
53. S.E. Kentish, G.W. Stevens, Innovations in separations technology for the recycling and re-use of liquid waste streams, Chemical Engineering Journal 84 (2001) 149-159.
54. D. Beltrami, G. Cote, H. Mokhtari, B. Courtaud, B.A. Moyer, A. Chagnes, Recovery of Uranium from Wet Phosphoric Acid by Solvent Extraction Processes, Chemical Reviews 114 (2014) 12002-12023.
55. F. Xie, T.A. Zhang, D. Dreisinger, F. Doyle, A critical review on solvent extraction of rare earths from aqueous solutions, Minerals Engineering 56 (2014) 10-28.
56. J. Veliscek-Carolan, Separation of actinides from spent nuclear fuel: A review, Journal of hazardous materials 318 (2016) 266-281.

57. R. Chiarizia, D.R. McAlister, A.W. Herlinger, SOLVENT EXTRACTION BY DIALKYL-SUBSTITUTED DIPHOSPHONIC ACIDS IN A DEPOLYMERIZING DILUENT. II. Fe(III) AND ACTINIDE IONS, Solvent extraction and ion exchange 19 (2001) 415-440.
58. I. Mohanty, J. Murlidhar, V. Chakravortty, Synergistic solvent extraction studies of uranium(VI) using a combination of naphthenic acid and various neutral donors into benzene, J Radioanal Nucl Chem 227 (1998) 111-116.
59. N. Van Nguyen, A. Iizuka, E. Shibata, T. Nakamura, Study of adsorption behavior of a new synthesized resin containing glycol amic acid group for separation of scandium from aqueous solutions, Hydrometallurgy 165 (2016) 51-56.
60. J. Wang, X. Guo, Adsorption isotherm models: Classification, physical meaning, application and solving method, Chemosphere (Oxford) 258 (2020) 127279.
61. A. Clearfield, Coordination chemistry of phosphonic acids with special relevance to rare earths, Journal of alloys and compounds 418 (2006) 128-138.
62. G.A. Seisenbaeva, I.V. Melnyk, N. Hedin, Y. Chen, P. Eriksson, E. Trzop, Y.L. Zub, V.G. Kessler, Molecular insight into the mode-of-action of phosphonate monolayers as active functions of hybrid metal oxide adsorbents. Case study in sequestration of rare earth elements, RSC advances 5 (2015) 24575-24585.
63. T. Moeller, D.F. Martin, C. Thompson, R. Ferros, G.R. Feistel, W.J. Randall, The coordination chemistry of yttrium and the rare earth metal ions. Chemical reviews. 65 (1965)
64. H. Pesonen, R. Aksela, K. Laasonen, Density Functional Complexation Study of Metal Ions with Cysteine, The journal of physical chemistry. A, Molecules, spectroscopy, kinetics, environment, & general theory 114 (2010) 466-473.
65. Maeda, Metal phosphonate open-framework materials, Microporous and Mesoporous Materials 73 (2004) 47-55.
66. R. Burgada, T. Bailly, T. Prangé, M. Lecouvey, Synthetic strategy of new powerful tris-bisphosphonic ligands for chelation of uranyl, iron, and cobalt cations, Tetrahedron letters 48 (2007) 2315-2319.
67. J.M. Sears, T.J. Boyle, Structural properties of scandium inorganic salts, Coordination Chemistry Reviews 340 (2017) 154-171.
68. J. Florek, A. Mushtaq, D. Larivière, G. Cantin, F. Fontaine, F. Kleitz, Selective recovery of rare earth elements using chelating ligands grafted on mesoporous surfaces, RSC Advances 5 (2015) 103782-103789.
69. J. Florek, D. Larivière, H. Kählig, S.L. Fiorilli, B. Onida, F. Fontaine, F. Kleitz, Understanding Selectivity of Mesoporous Silica-Grafted Diglycolamide-Type Ligands in the Solid-Phase Extraction of Rare Earths, ACS Appl. Mater. Interfaces 12 (2020) 57003.
70. E. Gumienna-Kontecka, R. Silvagni, R. Lipinski, M. Lecouvey, F. Cesare Marincola, G. Crisponi, V.M. Nurchi, Y. Leroux, H. Kozlowski, Bisphosphonate chelating agents: complexation of Fe(III) and Al(III) by 1-phenyl-1-hydroxymethylene bisphosphonate and its analogues, Inorganica Chimica Acta 339 (2002) 111-118.
71. W. Zhang, R. Koivula, E. Wiikinkoski, J. Xu, S. Hietala, J. Lehto, R. Harjula, Efficient and Selective Recovery of Trace Scandium by Inorganic Titanium Phosphate Ion-Exchangers from Leachates of Waste Bauxite Residue, ACS Sustainable Chemistry & Engineering 5 (2017) 3103-3114.
72. N. Sazali, Z. Harun, N. Sazali, A Review on Batch and Column Adsorption of Various Adsorbent Towards the Removal of Heavy Metal, Journal of Advanced Research in Fluid Mechanics and Thermal Sciences Journal homepage 67 (2020) 66.

73. A.B. Dichiara, S.J. Weinstein, R.E. Rogers, On the Choice of Batch or Fixed Bed Adsorption Processes for Wastewater Treatment, Industrial & engineering chemistry research 54 (1900) 8579-8586.
74. A.O Dada, A.P Olalekan, A.M. Olatunya, O. Dada. Langmuir, Freundlich, Temkin and Dubinin–Radushkevich Isotherms studies of equilibrium Sorption of $Zn^{2+}$ unto phosphoric acid modified rice husk, Journal of Applied Chemistry 3 (2012) 38-45.
75. S. Azizian, S. Eris, L.D. Wilson, Re-evaluation of the century-old Langmuir isotherm for modeling adsorption phenomena in solution, Chemical physics 513 (2018) 99-104.
76. K.Y. Foo, B.H. Hameed, Insights into the modeling of adsorption isotherm systems, Chemical engineering journal (Lausanne, Switzerland : 1996) 156 (2010) 2-10.
77. F. Togue Kamga, Modeling adsorption mechanism of paraquat onto Ayous (Triplochiton scleroxylon) wood sawdust, Appl Water Sci 9 (2019) 1-7.
78. M. Belhachemi, F. Addoun, Comparative adsorption isotherms and modeling of methylene blue onto activated carbons, Appl Water Sci 1 (2011) 111.
79. Proctor, A. J.F. Toro-Vazquez, The Freundlich isotherm in studying adsorption in oil processing, Journal of the American Oil Chemists' Society 73 (1996) 1627-1633.
80. M.B. Desta, Batch Sorption Experiments: Langmuir and Freundlich Isotherm Studies for the Adsorption of Textile Metal Ions onto Teff Straw (Eragrostis tef) Agricultural Waste, Journal of thermodynamics 2013 (2013) 1-6.
81. M.A. Al-Ghouti, D.A. Da'ana, Guidelines for the use and interpretation of adsorption isotherm models: A review, Journal of hazardous materials 393 (2020) 122383.
82. T.K. Poddar, K.K. Sirkar, Henry's Law Constant for Selected Volatile Organic Compounds in High-Boiling Oils, Journal of chemical and engineering data 41 (1996) 1329-1332.
83. R. Saadi, Z. Saadi, R. Fazaeli, N. Fard, Monolayer and multilayer adsorption isotherm models for sorption from aqueous media, Korean J. Chem. Eng 32 (2015) 787-799.
84. A. de Sá, A.S. Abreu, I. Moura, A.V. Machado, 8 - Polymeric materials for metal sorption from hydric resources, in: Water Purification, Elsevier Inc, 2017, pp. 289-322.
85. Y. Ho, J. Porter, G. McKay, Equilibrium Isotherm Studies for the Sorption of Divalent Metal Ions onto Peat: Copper, Nickel and Lead Single Component Systems, Water, Air, & Soil Pollution 141 (2002) 1-33.
86. E. Repo, J.K. Warchoł, A. Bhatnagar, M. Sillanpää, Heavy metals adsorption by novel EDTA-modified chitosan–silica hybrid materials, Journal of colloid and interface science 358 (2011) 261-267.
87. Kumara, N. T. R. N, N. Hamdan, M.I. Petra, K.U. Tennakoon, P. Ekanayake, Equilibrium Isotherm Studies of Adsorption of Pigments Extracted from Kuduk-kuduk (Melastoma malabathricumL.) Pulp onto TiO2Nanoparticles, Journal of chemistry 2014 (2014) 1-6.
88. A. Bhatnagar, M. Sillanpää, Utilization of agro-industrial and municipal waste materials as potential adsorbents for water treatment—A review, Chemical engineering journal (Lausanne, Switzerland : 1996) 157 (2010) 277-296.
89. A.K. Mosai, H. Tutu, Simultaneous sorption of rare earth elements (including scandium and yttrium) from aqueous solutions using zeolite clinoptilolite: A column and speciation study, Minerals engineering 161 (2021) 106740.
90. M. Mahramanlioglu, I. Bicer, T. Misirli, A. Kilislioglu, Removal of uranium by the adsorbents produced from coffee residues, J Radioanal Nucl Chem 273 (2007) 621-624.
91. S. Lata, P. Singh, S. Samadder, Regeneration of adsorbents and recovery of heavy metals: a review, Int. J. Environ. Sci. Technol 12 (2015) 1461-1478.
92. S. Gupta, B.V. Babu, Utilization of waste product (tamarind seeds) for the removal of Cr(VI) from aqueous solutions: Equilibrium, kinetics, and regeneration studies, Journal of environmental management 90 (2009) 3013-3022.

93. F. Mashkoor, A. Nasar, Inamuddin, A.M. Asiri, Exploring the Reusability of Synthetically Contaminated Wastewater Containing Crystal Violet Dye using Tectona grandis Sawdust as a Very Low-Cost Adsorbent, Sci Rep 8 (2018).
94. W. Zou, L. Zhao, L. Zhu, Efficient uranium(VI) biosorption on grapefruit peel: kinetic study and thermodynamic parameters, J Radioanal Nucl Chem 292 (2012) 1303-1315.
95. T.J. Tranter, 13 - Solid-phase extraction technology for actinide and lanthanide separations in nuclear fuel reprocessing, in: Advanced separation techniques for nuclear fuel reprocessing and radioactive waste treatment, Elsevier Ltd, 2011, pp. 377-413.
96. P. Barbaro, F. Liguori, Ion Exchange Resins: Catalyst Recovery and Recycle, Chemical reviews 109 (2009) 515-529.
97. X. Hérès, V. Blet, P. Di Natale, A. Ouaattou, H. Mazouz, D. Dhiba, F. Cuer, Selective Extraction of Rare Earth Elements from Phosphoric Acid by Ion Exchange Resins, Metals (Basel ) 8 (2018) 682.
98. A. Chakrabarti, M.M. Sharma, Cationic ion exchange resins as catalyst, Reactive Polymers 20 (1993) 1-45.
99. K.C. Pugh, E.J. York, J.M. Stewart, Effects of resin swelling and substitution on solid phase synthesis. International journal of peptide and protein research 40 (1992) 208-213.
100. 100. J. Florek, F. Chalifour, F. Bilodeau, D. Larivière, F. Kleitz, Nanostructured Hybrid Materials for the Selective Recovery and Enrichment of Rare Earth Elements, Advanced Functional Materials 24 (2014) 2668-2676.
101. 101. J. Florek, S. Giret, E. Juère, D. Larivière, F. Kleitz, Functionalization of mesoporous materials for lanthanide and actinide extraction, Dalton transactions (Cambridge, England : 2003) 45 (2016) 14832-14854.
102. 102. F. Hoffmann, M. Cornelius, J. Morell, M. Fröba, Silica-Based Mesoporous Organic-Inorganic Hybrid Materials, Angewandte Chemie (International ed.) 45 (2006) 3216-3251.
103. 103. V.B. Cashin, D.S. Eldridge, A. Yu, D. Zhao, Surface functionalization and manipulation of mesoporous silica adsorbents for improved removal of pollutants: a review, Environmental science water research & technology 4 (2018) 11-128.
104. 104. P.N.E. Diagboya, E.D. Dikio, Silica-based mesoporous materials; emerging designer adsorbents for aqueous pollutants removal and water treatment, Microporous and mesoporous materials 266 (2018) 252-267.
105. 105. P.J. Lebed, J. Savoie, J. Florek, F. Bilodeau, D. Larivière, F. Kleitz, Large Pore Mesostructured Organosilica-Phosphonate Hybrids as Highly Efficient and Regenerable Sorbents for Uranium Sequestration, Chemistry of materials 24 (2012) 4166-4176.
106. 106. P.J. Lebed, K. de Souza, F. Bilodeau, D. Larivière, F. Kleitz, Phosphonate-functionalized large pore 3-D cubic mesoporous (KIT-6) hybrid as highly efficient actinide extracting agent, Chemical communications (Cambridge, England) 47 (2011) 11525-11527.
107. 107. Simon Giret, Yimu Hu, Nima Masoumifard, Jean-Francois Boulanger, Estelle Juère, Freddy Kleitz, Dominic Larivière, Selective Separation and Pre-Concentration of Scandium with Mesoporous Silica. ACS Applied materials and interfaces 10 (2008) 448-457.
108. 108. Y. Wang, L. Zhu, B. Guo, S. Chen, W. Wu, Mesoporous silica SBA-15 functionalized with phosphonate derivatives for uranium uptake, New journal of chemistry 38 (2014) 3853-3861.
109. 109. W. Zhang, G. Ye, J. Chen, Novel mesoporous silicas bearing phosphine oxide ligands with different alkyl chains for the binding of uranium in strong HNO3 media, J. Mater. Chem. A 1 (2013) 12706-12709.
110. 110. W. Chouyyok, J.W. Pittman, M.G. Warner, K.M. Nell, D.C. Clubb, G.A. Gill, R.S. Addleman, Surface functionalized nanostructured ceramic sorbents for the effective

collection and recovery of uranium from seawater, Dalton transactions : an international journal of inorganic chemistry 45 (2016) 11312-11325.
111. 111. D.L. Ramasamy, E. Repo, V. Srivastava, M. Sillanpää, Chemically immobilized and physically adsorbed PAN/acetylacetone modified mesoporous silica for the recovery of rare earth elements from the wastewater-comparative and optimization study, Water research 114 (2017) 264-276.
112. D.L. Ramasamy, V. Puhakka, E. Repo, M. Sillanpää, Selective separation of scandium from iron, aluminium and gold rich wastewater using various amino and non-amino functionalized silica gels – A comparative study, Journal of cleaner production 170 (2018) 890-901.
113. D.L. Ramasamy, V. Puhakka, E. Repo, S. Ben Hammouda, M. Sillanpää, Two-stage selective recovery process of scandium from the group of rare earth elements in aqueous systems using activated carbon and silica composites: Dual applications by tailoring the ligand grafting approach, Chemical engineering journal (Lausanne, Switzerland : 1996) 341 (2018) 351-360.
114. D.L. Ramasamy, V. Puhakka, B. Doshi, S. Iftekhar, M. Sillanpää, Fabrication of carbon nanotubes reinforced silica composites with improved rare earth elements adsorption performance, Chemical engineering journal (Lausanne, Switzerland : 1996) 365 (2019) 291-304.
115. A. Paiva, P. Malik, Recent advances on the chemistry of solvent extraction applied to the reprocessing of spent nuclear fuels and radioactive wastes, Journal of Radioanalytical and Nuclear Chemistry 261 (2004) 485-496.
116. 116. M. Nazal, M. Albayyari, F. Khalili, E. Asoudani, Synergistic effect of tri-n-butyl phosphate (TBP) or tri-n-octyl phosphine oxide (TOPO) with didodecylphosphoric acid (HDDPA) on extraction of uranium(VI) and thorium(IV) ions, J Radioanal Nucl Chem 312 (2017) 133-139.
117. P. Yang, Q. Liu, J. Liu, R. Chen, R. Li, X. Bai, J. Wang, Highly efficient immobilization of uranium(VI) from aqueous solution by phosphonate-functionalized dendritic fibrous nanosilica (DFNS), Journal of hazardous materials 363 (2019) 248-257.
118. S.M. Husnain, H.J. Kim, W. Um, Y. Chang, Y. Chang, Superparamagnetic Adsorbent Based on Phosphonate Grafted Mesoporous Carbon for Uranium Removal, Industrial & Engineering Chemistry Research 56 (2017) 9821-9830.
119. X. Wang, J. Lan, Y. Zhao, Z. Li, L. Yuan, Y. Wang, Z. Chai, W. Shi, Y. Feng, Y. Liu, Mesoporous silica SBA-15 functionalized with phosphonate and amino groups for uranium uptake, Sci. China Chem 55 (2012) 1705-1711.
120. Q. Yu, S. Ning, W. Zhang, X. Wang, Y. Wei, Recovery of scandium from sulfuric acid solution with a macro porous TRPO/SiO2-P adsorbent, Hydrometallurgy 181 (2018) 74-81.
121. L. Yuan, Y. Liu, W. Shi, Y. Lv, J. Lan, Y. Zhao, Z. Chai, High performance of phosphonate-functionalized mesoporous silica for U(vi) sorption from aqueous solution, Dalton transactions : an international journal of inorganic chemistry 40 (2011) 7446-7453.
122. L. Yuan, Y. Liu, W. Shi, Z. Li, J. Lan, Y. Feng, Y. Zhao, Y. Yuan, Z. Chai, A novel mesoporous material for uranium extraction, dihydroimidazole functionalized SBA-15, Journal of Materials Chemistry 22 (2012) 17019.
123. E.C. Wu, J. Park, J. Park, E. Segal, F. Cunin, M.J. Sailor, Oxidation-Triggered Release of Fluorescent Molecules or Drugs from Mesoporous Si Microparticles, ACS nano 2 (2008) 2401-2409.
124. K. Mun, S.D. Alvarez, W. Choi, M.J. Sailor, A Stable, Label-free Optical Interferometric Biosensor Based on TiO2 Nanotube Arrays, ACS nano 4 (2010) 2070-2076.

125. S. Mourabit, M. Guillot, G. Toquer, J. Cambedouzou, F. Goettmann, A. Grandjean. Stability of mesoporous silica under acidic conditions, RSC Advances 2 (2012) 10916-10924.
126. M.V. Landau, S.P. Varkey, M. Herskowitz, O. Regev, S. Pevzner, T. Sen, Z. Luz, Wetting stability of Si-MCM-41 mesoporous material in neutral, acidic and basic aqueous solutions, Microporous and Mesoporous Materials 33 (1999) 149-163.
127. G. Korotcenkov, B.K. Cho, Silicon Porosification: State of the Art, Critical reviews in solid state and materials sciences 35 (2010) 153-260.
128. G. Bomchil, A. Halimaoui, R. Herino, Porous silicon: The material and its applications in silicon-on-insulator technologies, Applied surface science 41-42 (1990) 604-613.
129. V. Lehmann, U. Gosele, Porous silicon formation: A quantum wire effect, Applied physics letters 58 (1991) 856-858.
130. X.G. Zhang, S.D. Collins, R.L. Smith, Porous Silicon Formation and Electropolishing of Silicon by Anodic Polarization in HF Solution, Journal of the Electrochemical Society 136 (1989) 1561-1565.
131. J. Salonen, V. Lehto, Fabrication and chemical surface modification of mesoporous silicon for biomedical applications, Chemical engineering journal (Lausanne, Switzerland : 1996) 137 (2008) 162-172.
132. J. Salonen, V.P. Lehto, E. Laine, The room temperature oxidation of porous silicon, Applied surface science 120 (1997) 191-198.
133. J. Salonen, V.P. Lehto, E. Laine, Thermal oxidation of free-standing porous silicon films Applied Physics Letters 70 (1997) 637-639.
134. D.B. Mawhinney, J.A. Glass, J.T. Yates, FTIR Study of the Oxidation of Porous Silicon, The journal of physical chemistry. B 101 (1997) 1202-1206.
135. Y.H. Ogata, F. Kato, T. Tsuboi, T. Sakka, SOLID-STATE SCIENCE AND TECHNOLOGY Changes in the Environment of Hydrogen in Porous Silicon with Thermal Annealing, J. Electrochem. Soc 145 (1998) 2439-2444.
136. A.E. Pap, K. Kordás, G. Tóth, J. Levoska, A. Uusimäki, J. Vähäkangas, S. Leppävuori, T.F. George, Thermal oxidation of porous silicon: Study on structure, Appl. Phys. Lett 86 (2005) 041501.
137. E.C. Wu, J.S. Andrew, A. Buyanin, J.M. Kinsella, M.J. Sailor, Suitability of porous silicon microparticles for the long-term delivery of redox-active therapeutics, Chemical communications 47 (2011) 5699-5701.
138. L. Debarge, J.P. Stoquert, A. Slaoui, L. Stalmans, J. Poortmans, Rapid thermal oxidation of porous silicon for surface passivation, Materials science in semiconductor processing 1 (1998) 281-285.
139. A. Janshoff, K.S. Dancil, C. Steinem, D.P. Greiner, V.S.-. Lin, C. Gurtner, K. Motesharei, M.J. Sailor, M.R. Ghadiri, Macroporous p-Type Silicon Fabry−Perot Layers. Fabrication, Characterization, and Applications in Biosensing, Journal of the American Chemical Society 120 (1998) 12108-12116.
140. M.P. Stewart, J.M. Buriak, New Approaches Toward the Formation of Silicon-Carbon Bonds on Porous Silicon, Comments on modern chemistry. Part A, Comments on inorganic chemistry 23 (2002) 179-203.
141. J.M. Buriak, M.P. Stewart, T.W. Geders, M.J. Allen, H.C. Choi, J. Smith, D. Raftery, L.T. Canham, Lewis Acid Mediated Hydrosilylation on Porous Silicon Surfaces, Journal of the American Chemical Society 121 (1999) 11491-11502.
142. T. Böcking, K.A. Kilian, K. Gaus, J.J. Gooding, Modifying Porous Silicon with Self-Assembled Monolayers for Biomedical Applications: The Influence of Surface Coverage on Stability and Biomolecule Coupling, Advanced functional materials 18 (2008) 3827-3833.

143. M. Björkqvist, J. Salonen, E. Laine, L. Niinistö, Comparison of stabilizing treatments on porous silicon for sensor applications, Phys. stat sol. 197 (2003) 374-377.
144. T. Jalkanen, E. Mäkilä, T. Sakka, J. Salonen, Y.H. Ogata, Thermally promoted addition of undecylenic acid on thermally hydrocarbonized porous silicon optical reflectors, Nanoscale Research Letters 7 (2012) 311.
145. T. Jalkanen, V. Torres-Costa, E. Ma ̈kila ̈, M. Kaasalainen, R. Koda, T. Sakka, Y.H. Ogata, J. Salonen, Selective Optical Response of Hydrolytically Stable Stratified Si Rugate Mirrors to Liquid Infiltration, ACS applied materials & interfaces 6 (2014) 2884-2892.
146. J. Salonen, E. Laine, L. Niinistö, A. Phys, Lett, Thermal carbonization of porous silicon surface by acetylene. Journal of Applied Physics 91 (2002) 456-461.
147. J. Salonen, V.-. Lehto, M. Björkqvist, E. Laine, L. Niinistö, Studies of Thermally Carbonized Porous Silicon Surfaces, Phys stat sol. 182 (2000) 123-126.
148. J. Salonen, V. Lehto, M. Björkqvist, E. Laine, L. Niinistö, Chemical stability studies of thermally carbonized porous silicon, Mat. Res. Soc. Symp. Proc. 638 (2000).
149. E. Ma ̈kila ̈, L.M. Bimbo, M. Kaasalainen, B. Herranz, A.J. Airaksinen, M. Heinonen, E. Kukk, J. Hirvonen, H.A. Santos, J. Salonen, Amine Modification of Thermally Carbonized Porous Silicon with Silane Coupling Chemistry, Langmuir 28 (2012) 14045-14054.
150. J. Salonen, M. Kaasalainen, O.-. Rauhala, L. Lassila, M. Hakamies, T. Jalkanen, R. Hahn, P. Schmuki, E. Makila, (Invited) Thermal Carbonization of Porous Silicon: The Current Status and Recent Applications, ECS transactions 69 (2015) 167-176.
151. S. Dhar, O. Seitz, M.D. Halls, S. Choi, Y.J. Chabal, L.C. Feldman, Chemical Properties of Oxidized Silicon Carbide Surfaces upon Etching in Hydrofluoric Acid, Journal of the American Chemical Society 131 (2009) 16808-16813.
152. M. Sarparanta, E. Ma ̈kila ̈, T. Heikkila ̈, J. Salonen, E. Kukk, V. Lehto, H.A. Santos, J. Hirvonen, A.J. Airaksinen, 18F-Labeled Modified Porous Silicon Particles for Investigation of Drug Delivery Carrier Distribution in Vivo with Positron Emission Tomography, Molecular pharmaceutics 8 (2011) 1799-1806.
153. J. Riikonen, S. Rigolet, C. Marichal, F. Aussenac, J. Lalevée, F. Morlet-Savary, P. Fioux, C. Dietlin, M. Bonne, B. Lebeau, V. Lehto, Endogenous Stable Radicals for Characterization of Thermally Carbonized Porous Silicon by Solid-State Dynamic Nuclear Polarization 13C NMR, Journal of physical chemistry. C 119 (1900) 19272-19278.
154. J. Paski, M. Björkqvist, J. Salonen, V. Lehto, Effects of treatment temperature on thermally-carbonized porous silicon hygroscopicity, Physic stat sol. 2 (2005) 3379-3383.
155. W. Xu, J. Riikonen, T. Nissinen, M. Suvanto, K. Rilla, B. Li, Q. Wang, F. Deng, V. Lehto, Amine Surface Modifications and Fluorescent Labeling of Thermally Stabilized Mesoporous Silicon Nanoparticles, Journal of physical chemistry. C 116 (2012) 22307-22314.
156. E.M. Lewiecki, Bisphosphonates for the treatment of osteoporosis: insights for clinicians, Therapeutic Advances in Chronic Disease 1 (2010) 115-128.
157. M. Sawicki, D. Lecerclé, G. Grillon, B. Le Gall, A. Sérandour, J. Poncy, T. Bailly, R. Burgada, M. Lecouvey, V. Challeix, A. Leydier, S. Pellet-Rostaing, E. Ansoborlo, F. Taran, Bisphosphonate sequestering agents. Synthesis and preliminary evaluation for in vitro and in vivo uranium(VI) chelation, European journal of medicinal chemistry 43 (2008) 2768-2777.
158. A.B. Martínez, R.L. Cabrini, A.M. Ubios, Orally administered ethane-1-hydroxy-1.1-bisphosphonate reduces the lethal effect of oral uranium poisoning. Health Phys. 78 (2000) 668-671.
159. A. Alanne, M. Tuikka, K. Tõnsuaadu, M. Ylisirniö, L. Hämäläinen, P. Turhanen, J. Vepsäläinen, S. Peräniemi, A novel bisphosphonate-based solid phase method for effective

removal of chromium(iii) from aqueous solutions and tannery effluents, RSC advances 3 (2013) 14132.
160. P.A. Turhanen, J.J. Vepsäläinen, S. Peräniemi, Advanced material and approach for metal ions removal from aqueous solutions, Scientific reports 5 (2015) 8992.
161. T.L. Schull, D.A. Knight, Organometallic phosphonic acids: synthesis and coordination chemistry, Coordination chemistry reviews 249 (2005) 1269-1282.
162. E. Gumienna-Kontecka, J. Jezierska, M. Lecouvey, Y. Leroux, H. Kozlowski, Bisphosphonate chelating agents Coordination ability of 1-phenyl-1-hydroxymethylene bisphosphonate towards Cu ions, Journal of Inorganic Biochemistry 89 (2002) 13.
163. A. Alanne, H. Hyvönen, M. Lahtinen, M. Ylisirniö, P. Turhanen, E. Kolehmainen, S. Peräniemi, J. Vepsäläinen, Systematic Study of the Physicochemical Properties of a Homologous Series of Aminobisphosphonates, Molecules 17 (2012) 10928-10945.
164. S. Brunauer, P.H. Emmett, E. Teller, Adsorption of Gases in Multimolecular Layers, Journal of the American Chemical Society 60 (1938) 309-319.
165. E.P. Barrett, L.G. Joyner, P.P. Halenda, The Determination of Pore Volume and Area Distributions in Porous Substances. I. Computations from Nitrogen Isotherms, Journal of the American Chemical Society 73 (1951) 373-380.
166. S.A. Wood, I.M. Samson, The aqueous geochemistry of gallium, germanium, indium and scandium, Ore geology reviews 28 (2006) 57-102.
167. K.D. Demadis, N. Stavgianoudaki, Chapter 14 - Structural Diversity in Metal Phosphonate Frameworks: Impact on Applications (Book, Chapter 14) Metal Phosphonate Chemistry: From Synthesis to Applications. 2012.
168. E. Matczak-Jon, V. Videnova-Adrabińska, Supramolecular chemistry and complexation abilities of diphosphonic acids, Coordination chemistry reviews 249 (2005) 2458-2488.
169. 169. V. Korovin, Y. Shestak, Y. Pogorelov, Comparison of scandium recovery mechanisms by phosphorus containing sorbents, Solvent extraction and extractants supported on porous carrier. Book; Scandium: compounds, productions, and applications (2011) ISBN 978-161761-465-1, pp. 77-100 (Chapter 3).
170. F. Chi, F. Chi, X. Wang, X. Wang, J. Xiong, J. Xiong, S. Hu, S. Hu, Polyvinyl alcohol fibers with functional phosphonic acid group: synthesis and adsorption of uranyl (VI) ions in aqueous solutions, J Radioanal Nucl Chem 296 (2013) 1331-1340.
171. T. Wang, M. Xu, X. Han, S. Yang, D. Hua, Petroleum pitch-based porous aromatic frameworks with phosphonate ligand for efficient separation of uranium from radioactive effluents, Journal of hazardous materials 368 (2019) 214-220.
172. U. Filipkowska, Adsorption and desorption efficiency of black 8 and black 5 onto chitin and chitosan. Polish Chitin Society (Monograph) 2007.
173. J. Koresh, A. Soffer. Application of the Two-site Langmuir isotherm to microporous adsorbents. J. Colloid and Interface Science 92 (1983) 517-524.
174. R. Kuroda, Y. Nakagomi, K. Ishida. The separatoin of scandium by cation exchange in acid ammonium sulfate media. Journal of chromatography 22 (1966) 143-148.
175. 175. V.P. Mehta, S.M. Khopkar, Cation-exchange studies of yttrium (Ill) and its separation from various other elements, Chromatographia 11 (1978).
176. V.P. Mehta, S.M. Khopkar, Cation exchange chromatographic separation of scandium from other elements on Dowex 50W-X8. Separation science and technology 13 (1978) 933-939.
177. T.C. Jorgensen, L.R. Weatherley, Ammonia removal from wastewater by ion exchange in the presence of organic contaminants, Water Research 37 (2003) 1723-1728.
178. P.N. Nomngongo, J.C. Ngila, T.A.M. Msagati, B. Moodley, Kinetics and Equilibrium Studies for the Removal of Cobalt, Manganese, and Silver in Ethanol using Dowex 50W-x8 Cation Exchange Resin, Separation science and technology 49 (2014) 1848-1859.

179. R.I. Walter, Anion exchange studies of Sc(III) and V(IV). Separation of scandium, titanium and vanadium, Journal of Inorganic Nuclear Chemistry 6 (1958) 58-62.
180. K.A. Orlandini, Cation exchange separation of scandium from rare earths in oxalic acid media, Inorganic & nuclear chemistry letters 5 (1969) 325-331.
181. L. Zhang, X. Chang, Y. Zhai, Q. He, X. Huang, Z. Hu, N. Jiang, Selective solid phase extraction of trace Sc(III) from environmental samples using silica gel modified with 4-(2-morinyldiazenyl)- N-(3-(trimethylsilyl)propyl)benzamide, Analytica Chimica Acta 629 (2008) 84-91.
182. Avdibegovic, W. Zhang, J. Xu, M. Regadio, R. Koivula, K. Binnemans. Selective ion-exchange separation of scandium (III) over iron (III) by crystalline $\alpha$-zirconium phosphate platelets under acidic conditions.Separation and Purification Technology 215 (2018) 81-90.
183. B.J. Teppen, D.M. Miller, Hydration Energy Determines Isovalent Cation Exchange Selectivity by Clay Minerals, Soil Science Society of America Journal 70 (2005) 31-40.
184. D. Avdibegovic, M. Regadio, K. Binnemans, Recovery of scandium (III) from diluted aqueous solutions by a supported ionic liquid phase (SILP). RSC advances 7 (2017) 49664.
185. R. Thakkar, U. Chudasama, Synthesis and characterization of zirconium titanium phosphate and its application in separation of metal ions, Journal of hazardous materials 172 (2009) 129-137.
186. M.M. Abou-Mesalam, Sorption kinetics of copper, zinc, cadmium and nickel ions on synthesized silico-antimonate ion exchanger, Colloids and Surfaces A: Physicochemical and Engineering Aspects 225 (2003) 85.
187. D. Smith, Ionic hydration enthalpies, J. Chem. Educ. 54 (1977) 540-542.
188. L. Li, W. Ma, S. Shen, H. Huang, Y. Bai, H. Liu, A Combined Experimental and Theoretical Study on the Extraction of Uranium by Amino-Derived Metal–Organic Frameworks through Post-Synthetic Strategy, ACS applied materials & interfaces 8 (2016) 31032-31041.
189. D. Shao, Y. Li, X. Wang, S. Hu, J. Wen, J. Xiong, A.M. Asiri, H.M. Marwani, Phosphate-Functionalized Polyethylene with High Adsorption of Uranium(VI), ACS omega 2 (2017) 3267-3275.
190. M.G. Mahfouz, A.A. Galhoum, N.A. Gomaa, S.S. Abdel-Rehem, A.A. Atia, T. Vincent, E. Guibal, Uranium extraction using magnetic nano-based particles of diethylenetriamine-functionalized chitosan: Equilibrium and kinetic studies, Chemical engineering journal (Lausanne, Switzerland : 1996) 262 (2015) 198-209.
191. Y. Hu, E. Drouin, D. Larivière, F. Kleitz, F. Fontaine, Highly Efficient and Selective Recovery of Rare Earth Elements Using Mesoporous Silica Functionalized by Preorganized Chelating Ligands, ACS applied materials & interfaces 9 (2017) 38584-38593.
192. M. Balintova, A. Petrilakova, Study of pH Influence on the Selective Precipitation of Heavy Metals from Acid Mine Drainage, Chemical engineering transactions 25 (2011) 345-350.
193. R.M. Freitas, T.A.G. Perilli, A.C.Q. Ladeira, Oxidative Precipitation of Manganese from Acid Mine Drainage by Potassium Permanganate, Journal of chemistry 2013 (2013) 1-8.
194. K. Pyrzyńska, K. Kilian, M. Pęgier, Separation and purification of scandium: From industry to medicine, Separation & Purification Reviews 48 (2019) 65-77.
195. C.W. Abney, R.T. Mayes, T. Saito, S. Dai, Materials for the Recovery of Uranium from Seawater, Chemical Reviews 117 (2017) 13935-14013.
196. X. Guo, D. Wu, S.V. Ushakov, T. Shvareva, H. Xu, A. Navrotsky, Energetics of hydration on uranium oxide and peroxide surfaces, Journal of materials research 34 (2019) 3319-3325.
197. J. Riikonen, J. Rantanen, R. Thapa, N.T. Le, S. Rigolet, P. Fioux, P. Turhanen, N.K. Bodiford, J.R. Kalluri, T. Ikonen, T. Nissinen, B. Lebeau, J. Vepsäläinen, J.L. Coffer, V. Lehto, Rapid synthesis of nanostructured porous silicon carbide from biogenic silica, J. Am. Ceram. Soc. 104 (2020) 766.

198. O. Haluska, A. Rahmani, A. Salami, P. Turhanen, J. Vepsäläinen, R. Lappalainen, V. Lehto, J. Riikonen, Plant-based nanostructured silicon carbide modified with bisphosphonates for metal adsorption, Microporous and mesoporous materials 324 (2021) 111294.

PUBLICATION I

Riikonen A, Nissinen T, Alanne A, Thapa R, Fioux P, Bonne M, Rigolet S, Morlet-Savary F, Aussenac F, Marichal C, Lalevee J, Vepsäläinen J, Lebeau B, Lehto VP

**Stable surface functionalization of carbonized mesoporous silicon**

*Inorganic Chemistry Frontiers*, 7 (3): 631-641 (2019)

https://doi.org/10.1039/C9QI01140D

INORGANIC CHEMISTRY
FRONTIERS

RESEARCH ARTICLE

View Article Online
View Journal



Cite this: DOI: 10.1039/c9qi01140d

# Stable surface functionalization of carbonized mesoporous silicon†

Joakim Riikonen, [a,b,c] Tuomo Nissinen,[a] Aino Alanne,[d] Rinez Thapa,[a] Philippe Fioux,[b,c] Magali Bonne, [b,c] Séverinne Rigolet, [b,c] Fabrice Morlet-Savary,[b,c] Fabien Aussenac,[e] Claire Marichal,[b,c] Jacques Lalevée, [b,c] Jouko Vepsäläinen,[d] Bénédicte Lebeau [b,c] and Vesa-Pekka Lehto *[a]

Received 4th September 2019,
Accepted 22nd November 2019

DOI: 10.1039/c9qi01140d

rsc.li/frontiers-inorganic

Mesoporous silicon (PSi) is an emerging nanomaterial studied in *e.g.* biomedical, sensor and energy applications. In many applications, a major obstacle in its commercial use is the instability of its surfaces, especially when functionalized with organic molecules. In the present work, we introduce a surface functionalization method for PSi, in which carbonized surface of silicon is functionalized with terminal alkenes. A good surface coverage of 0.3 molecules per nm$^2$ was achieved and the material showed excellent aqueous stability at low and neutral pH. It also withstood a highly basic solution for several days. The developed method was used to graft bisphosphonates on the surface and the material was used for metal adsorption. Because of its excellent stability, the adsorbent material lasted up to 50 adsorption/desorption cycles without a significant deterioration of its performance.

## 1. Introduction

Mesoporous silicon (PSi) has many potential applications in *e.g.* drug delivery, sensing, Li-ion batteries and adsorption. It is relatively unstable in its native form because of its high surface area and reactivity of the Si–Si bonds. Therefore, surface of PSi is typically passivated by oxidation, carbonization or hydrosilylation to improve its stability.

Many applications of PSi, such as sensing and separation, require grafting of functional molecules on the surface.[1,2] The stability of these surfaces has been a focus of several studies.[2–6] Among the first functionalization strategies of PSi was grafting of alkenes, or alkynes on PSi by hydrosilylation.[7] Although the highly hydrophobic surfaces passivated by hydrosilylation are shown to be stable for several hours even at pH 13,[8] the grafting of molecules with functional groups, such as carboxylic acids, leads to significantly less stable materials.[6] Good to moderate stability of the hydrosilylated materials in aqueous solutions near neutral pH has been shown only up to few hours[3,9] with the exception of a 2-month stability study conducted by Kilian *et al.*[5] They observed dissolution of PSi in phosphate buffered saline visually after one month but also saw significant changes in the structure in the first few days. However, the amount of the grafted molecules on the surface was not studied directly.

Many surface functionalization strategies rely on grafting organic molecules on oxidized PSi *via* Si–O bonds which are easily hydrolyzed in an aqueous environment and are thus sensitive to degradation.[10] A more stable functionalization can be achieved if only stable Si–C and C–C bonds are exposed on the surface. Sciacca *et al.* and Jalkanen *et al.* studied hydrophobic PSi that was thermally hydrocarbonized at 500 °C and subsequently functionalized with a carboxylic acid.[4,6] Sciacca *et al.* observed an improved structural stability of the material in phosphate buffered saline for 2 h. Jalkanen *et al.* studied the stability in harsher conditions and observed complete dissolution of the material in 1 M KOH in 24 h.

Thermal carbonization of PSi at high temperatures (above 800 °C) has been shown to produce highly stable surfaces consisting of silicon carbide, silicon oxycarbide and carbon.[11,12] So far, functionalization of thermally carbonized PSi (TCPSi) has been performed *via* silanization which grafts functional molecules on the surface *via* Si–O bonds leaving the functional molecules susceptible to hydrolysis.[13]

In the present study, a new functionalization method for TCPSi is introduced in which terminal alkenes are directly grafted on the carbonized silicon surface leading to functionalization which is highly stable in aqueous solutions

[a]Department of Applied Physics, University of Eastern Finland, Yliopistonranta 1F, 70211 Kuopio, Finland. E-mail: vesa-pekka.lehto@uef.fi
[b]Université de Haute Alsace, CNRS, IS2M UMR 7361, F-68100 Mulhouse, France
[c]Université de Strasbourg, France
[d]School of Pharmacy, University of Eastern Finland, Yliopistonranta 1B, 70211 Kuopio, Finland
[e]Bruker Biospin SA, 34, rue de l'industrie, 67166 Wissembourg Cedex, France
†Electronic supplementary information (ESI) available. See DOI: 10.1039/c9qi01140d

for several weeks and resists even high pH solutions for several days.

The developed method is used to functionalize TCPSi with bisphosphonates that are good chelation agents for metals.[14] Several mesoporous materials have been proposed for metal adsorption applications[15–20] but their repeated use has often not been studied supposedly due to their low stability and diminishing performance. If repeated use is studied, it is reported for less than ten ad/desorption cycles and even the most stable materials lose at least 1% of their capacity per cycle.[15–17] The aim of the present study is to provide a material that can be reused several tens of times without significant reduction of its capacity thus essentially reducing the costs in demanding applications.

# 2. Experimental

## 2.1. Production of PSi

PSi was produced by electrochemical etching in 1 : 1 HF (38–40%)/EtOH mixture on p+ Si wafers (0.01–0.02 Ω cm) with 40 mA $cm^{-2}$ current density for 2400 s. HF is highly toxic and a special care should be taken to prevent any contact with the liquid and inhalation of vapor. PSi films were detached from the wafer with a high current pulse and dried at 65 °C for 2 h. The PSi films were milled to microparticles in a planetary ball mill and sieved to 25 μm–75 μm size fraction. PSi was used in different forms, microparticles, freestanding films or films supported on the substrate depending on the demands of measurement in order to obtain high quality data. Films supported on the substrate were produced similarly as above by etching a 5 μm porous layer on the wafer without the high current pulse.

## 2.2. Bisphosphonate synthesis

10-Undecenoic acid, oxalyl chloride and $P(OSiMe_3)_3$ were purchased from Aldrich. $CDCl_3$ (D 99.96%) used as NMR solvent was purchased from Euriso-Top.

The bisphosphonate molecule (*Tetrakis(trimethylsilyl) 1-(trimethylsilyloxy)undec-10-ene-1,1-diylbisphosphonate*) was synthesized according to the method published by Lecouvey *et al.* (ESI Fig. S1†).[21] 10-undecenoic acid (13.56 mmol, 2.50 g) in 20 ml of freshly distilled dichloromethane was placed in dried two necked flask equipped with an argon inlet. Oxalyl chloride (27.10 mmol, 3.44 g) was added dropwise on ice. The reaction mixture was stirred at room temperature for 1 hour, evaporated and the formation of the corresponding acid chloride was observed by NMR. Two equivalents of tris(trimethyl silyl) phosphite (27.10 mmol, 8.09 g) was added dropwise to the acid chloride under argon at 0 °C. Once the addition was complete, the reaction mixture was left under magnetic stirring at room temperature for 2 h. Volatile fractions were then evaporated under reduced pressure. Yellow oily substance with 94% yield was obtained. $^1$H NMR (500.1 MHz, $CDCl_3$) $\delta$ 5.80 (ddt, 1H, $^3J_{HH}$ = 17.2, 10.3 and 6.7 Hz, $CH_2$═C$\underline{H}$–$CH_2$), 4.98 (dd, 1H, $^3J_{HH}$ = 17.2, $^2J_{HH}$ = 2.2, C$\underline{H_2}$═CH), 4.92 (d, 1H, $^3J_{HH}$ = 10.3, $^2J_{HH}$ = 2.2, C$\underline{H_2}$═CH), 2.07–1.99 (m, 2H), 1.96–1.84 (m, 2H), 1.60–1.51 (m, 2H), 1.41–1.33 (m, 2H), 1.33–1.20 (m, 8H), 0.34–0.25 (m, 45H); $^{13}$C NMR (125.8 MHz, $CDCl_3$) $\delta$ 139.0, 114.1, 78.2 (t, $^1J_{CP}$ = 166.2 Hz), 35.6, 33.7, 30.3, 29.4, 29.4, 29.0, 28.9, 23.8 (t, $^2J_{CP}$ = 6.5 Hz), 2.8 (3C), 1.4 (6C), 1.3 (6C); $^{31}$P NMR (202.5 MHz, $CDCl_3$) $\delta$ 1.95 (s). The compound was left in silylated form to achieve good solubility in mesitylene.

## 2.3. Surface modifications

Three independent surface modifications were performed for each sample type. First, hydrogen terminated PSi (HTPSi) was prepared by briefly immersing PSi in 1 : 1HF/EtOH mixture and drying at 65 °C for 2 h.

The carbonization was performed to the HTPSi in a quartz tube under continuous $N_2$ flow of 1 L $min^{-1}$ throughout the process. Samples were first flushed with nitrogen for 30 min then acetylene flow of 1 L $min^{-1}$ was added for 15 min. The sample was then placed into a preheated oven at 500 °C. After 15 min at 500 °C, the acetylene flow was terminated and the tube was removed from the oven and sample were let to cool down to room temperature (in nitrogen flow). At room temperature, acetylene flow (1 L $min^{-1}$) was applied again for 9 min 40 s and the sample was inserted into the oven at 820 °C 20 s after the acetylene flow was terminated. Sample was heated in the oven for 10 min and then cooled down to room temperature (in nitrogen flow).

For surface functionalization of TCPSi, the neat alkene (undecylenic acid or decene) was added on the TCPSi in the quartz tube and the tube was heated at 120 °C for 16 h. Bisphosphonate functionalization was performed with a mesitylene solution[22] of BP (9 wt%, 1 : 1 mass ratio of BP and PSi). The undecylenic acid grafted TCPSi is labeled UnTCPSi, the decene grafted TCPSi DeTCPSi and the bisphosphonate grafted TCPSi BPTCPSi. The structures of all the PSi materials used in the study are presented in ESI Fig. S2.† The UnTCPSi samples were rinsed thrice with 25 ml chloroform to remove excess undecylenic acid and then six times with 25 ml of a 1 : 1 mixture of EtOH and 1 M NaOH in order to remove physisorbed or dimerized undecylenic acid. The particles were then washed with water and 1 M HCl to convert grafted undecylenic acid from Na salt to the acid form and finally rinsed with water to remove HCl and dried at 65 °C. DeTCPSi was washed eight times with 25 ml of chloroform and dried at 65 °C for 1 h. BPTCPSi was washed eight times with 25 ml of chloroform, then with methanol and dried at 65 °C for 1 h.

To prepare undecylenic acid grafted HTPSi (UnHTPSi), HTPSi was immersed in neat undecylenic acid and heated at 120 °C for 16 h. The material was washed eight times with 25 ml of chloroform and dried at 65 °C for 1 h.

## 2.4. Liquid NMR

$^1$H, $^{31}$P and $^{13}$C NMR spectra were measured on a Bruker Avance 500 DRX spectrometer operating at 500.1, 202.5 and 125.8 MHz, respectively. The NMR spectra measured in $CDCl_3$ were calibrated on the solvent residual signals at 7.26 ppm for

 

$^{1}$H and 77.1 ppm for $^{13}$C and 85% $H_3PO_4$ was used as an external standard in the $^{31}$P measurements.

### 2.5. Nitrogen sorption

Prior to the measurements, the samples were degassed in vacuum at 65 °C for 2 h. The nitrogen adsorption and desorption isotherms were measured with Micromeritics Tristar II 3020. Surface area was calculated using BET (Brunauer, Emmett and Teller) theory, pore size distributions were calculated with BJH (Barrett, Joyner and Halenda) theory and pore volume was calculated from a single point at relative pressure of 0.95.

### 2.6. Electron paramagnetic resonance (EPR)

TCPSi microparticles which were not exposed to air were transferred under nitrogen atmosphere into a glove box with Ar atmosphere. In the glove box, the sample was transferred into 6 mm cylindrical quartz tubes and closed. Electron paramagnetic resonance experiments were performed using an X-Band spectrometer (Bruker EMX-plus Biospin). The radicals were observed under Ar atmosphere at room temperature. The experimental procedure has previously been described in detail.[23] The double integral of the EPR spectrum is proportional to the concentration of paramagnetic centers. A calibration was first done using TEMPO to ensure that this procedure was usable in solid state. TEMPO was also used as standard for calibration of the *g*-factor ($g$ = 2.0061). To measure change in paramagnetic species caused by addition of undecylenic acid on the TCPSi particles that had not been exposed to air, undecylenic acid was injected into the quartz tube and the EPR spectrum was measured immediately. In addition to the above measurements TCPSi that had been in contact with air was measured in air atmosphere.

### 2.7. Solid state NMR characterization

$^{1}$H–$^{29}$Si CPMAS NMR experiments were performed at room temperature, with a Bruker Avance II 300 spectrometer operating at $B_0$ = 7.1 T (Larmor frequency: $\omega_0(^{29}\mathrm{Si})$ = 59.61 MHz and $\omega_0(^{1}\mathrm{H})$ = 300.08 MHz) with a Bruker double channel 7 mm probe at a spinning frequency of 4 kHz, with a proton $\pi/2$ pulse duration of 4.1 μs, a contact time of 4 ms and a recycle delay of 5 s according to $T1$ measurements. $^{29}$Si Chemical shifts were referenced to tetramethylsilane (TMS).

$^{31}$P solid-state MAS NMR experiments were performed at room temperature on Bruker Avance II 400 spectrometer operating at $B_0$ = 9.4 T equipped with a Bruker double channel 4 mm probe at a Larmor frequency of 161.99 MHz. The spectrum was recorded with a $\pi/2$ pulse duration of 3 μs and a recycling delay of 5 s at a spinning frequency of 12 kHz. $^{31}$P spin lattice relaxation times ($T_1$) were measured with the saturation-recovery pulse sequence. $^{31}$P spectrum was referenced to $H_3PO_4$ (85% in water).

### 2.8. DNP NMR characterization

Solid State DNP experiments were performed with a Bruker 263 GHz Solid-State NMR DNP spectrometer with a gyrotron microwave source,[24,25] Ascend DNP 400 WB NMR magnet, Avance III NMR console and a low-temperature 3.2 mm triple resonance $^{1}$H/X/Y DNP MAS probe. The NMR 400 MHz Ascend DNP magnet is equipped with a sweep coil for optimization of the frequency match between the NMR and the electron frequencies. The sample temperature reported was 108 K with microwave irradiation. The microwave power was optimized to achieve the highest DNP signal enhancement. $^{1}$H–$^{13}$C cross polarization (CP) MAS experiments were performed with Spinal64[26] $^{1}$H decoupling during acquisition time. During the CP contact time, both $^{1}$H and $^{13}$C R.F. field were set to 60 kHz, the $^{1}$H decoupling R.F. field strength was set to 95 kHz during the acquisition time. The contact time during the CP step was set to 1 ms. The sample spinning frequency was set to 12 kHz. 8192 scans were acquired with a recycle delay of 6 s which corresponds to a total acquisition time of about 13.5 h.

DNP polarization buildup time (TDNP) measurements were performed using saturation-recovery experiments and results were fit in the T1/T2 relaxation module of Topspin software.

Approximately 10 mg of TCPSi microparticles were loaded in a 3.2 mm sapphire rotor. The rotor was sealed with a Teflon top insert and a Zirconia cap. Chemical shifts were referenced to tetramethylsilane (TMS).

### 2.9. XPS analysis

X-ray photoelectron spectroscopy (XPS) spectra were recorded with a VG SCIENTA SES-2002 spectrometer equipped with a concentric hemispherical analyzer. The incident radiation used was generated by a monochromatic Al Kα X-ray source (1486.6 eV) operating at 420 W (14 kV; 30 mA). Photo-emitted electrons were collected at a take-off angle of 90° from the surface substrate, with electron detection in the constant analyser energy mode (FAT). Widescan spectrum signal was recorded with a pass energy of 500 eV and for high resolution spectra (Si 2p, C 1s and Cu 2p) pass energy was set to 100 eV. Approximately 24 mm$^2$ area of TCPSi film on Si substrate was analysed. The base pressure in the analysis chamber during experimentation was *ca.* $10^{-9}$ mbar. The spectrometer energy scale was calibrated using the Ag $3d^{5/2}$, Au $4f^{7/2}$ and Cu $2p^{3/2}$ core level peaks, set respectively at binding energies of 368.2, 84.0 and 932.6 eV. Spectra were subjected to a Shirley baseline and peak fitting was made with mixed Gaussian–Lorentzian components with equal full-width-at-half-maximum (FWHM) using CASAXPS version 2.3.17 software. The surface composition expressed in atom% was determined using integrated peak areas of each component and take into account transmission factor of the spectrometer, mean free path and Scofield sensitivity factors of each atom. All the binding energies (BE) are referenced to the C 1s peak at 284.5 eV and given with a precision of 0.1 eV. The measured samples were porous films on silicon substrate except for the BPTCPSi samples which were measured as microparticles.

### 2.10. FTIR analysis

FTIR measurements were done in transmission mode with freestanding PSi films with Thermo Scientific Nicolet 8700. The spectral range was 500–4000 cm$^{-1}$ and resolution 4 cm$^{-1}$.

### 2.11. Thermogravimetry

Microparticles were measured by TA TGA Q50 under nitrogen atmosphere. The samples were equilibrated at 80 °C for 30 min and then heated up to 700 °C with 20 °C $min^{-1}$ heating rate.

### 2.12. Scanning electron microscopy

Zeiss HD|VP HR-SEM was utilized for investigation of the morphologies of the particles. The particles were attached to standard aluminum SEM sample holders with conductive carbon adhesive. The imaging was performed with acceleration voltage of 5 kV and InLens detector.

### 2.13. Stability study

One hundred mg of UnHTPSi and UnTCPSi microparticles were first wetted with EtOH and then immersed in 45 ml of 1 M HCl, deionized water or 1 M NaOH. The samples were kept at 30 °C. Part of the samples were removed at predefined time points and washed on a filter paper 3× with 50 ml of deionized water, 3× with 50 ml of 1 : 1 mixture of deionized water and ethanol and 4× with 50 ml of EtOH. The particles were then dried at 65 °C. At each time point the liquid in which the particles were immersed was replaced with a fresh one.

### 2.14. Metal adsorption

Metal adsorption capacity towards copper was investigated using ~200 mg BPTCPSi particles primed in 20 ml of 5 M HCl for 1 h at RT. After washing thrice with 20 ml water, the particles were immersed in 20 ml of 200 ppm $Cu^{2+}$ solution (from $CuCl_2$) at pH = 4.02 with constant mixing. The contact time was 24 h at RT. Cu concentration of the solution was measured before and after adsorption using total reflection X-ray fluorescence spectroscopy, tXRF (S2 Picofox, Bruker). The adsorbed amount was calculated from the concentration difference of the solutions. The reusability of the material was studied by repeating 50 adsorption/desorption cycles. 50 mg of BP-TCPSi particles were placed inside a syringe filter and the following solutions were passed through the particles by gravitation in each cycle: 5 ml of 10 ppm $Cu^{2+}$, 5 ml of deionized $H_2O$, 5 ml of 0.1 M HCL and 5 ml of deionized $H_2O$. Cu concentrations of the solution before and after each cycle was measured with PerkinElmer 5100 flame atomic absorption spectrometer (AAS) with a wavelength of 327.4 nm to calculate the adsorbed/desorbed amounts of Cu.

## 3. Results and discussion

Thermal carbonization of PSi was performed under nitrogen atmosphere with acetylene gas in a two-step process at 500 and 820 °C.[11] After carbonization, the material is cooled to room temperature in nitrogen gas. According to a previous observation, the material will react strongly with a sudden exposure to air and emit bright light (see video in ESI†). A TCPSi sample, that had not been exposed to air, was measured with EPR and observed a high number of carbon radicals in the material ($3.4 \times 10^{18}$ $g^{-1}$). We hypothesized that these radical groups could be utilized to functionalize the material by free radical addition. Therefore, undecylenic acid or 1-decene was added on the TCPSi immediately after carbonization before exposing the material to air. The mixture was then heated at 120 °C for 16 h to further enhance the grafting. The undecylenic acid and 1-decene modified TCPSi samples are referred to as UnTCPSi and DeTCPSi, respectively. Bisphosphonate (BP) grafted TCPSi (BPTCPSi) was also prepared in a similar way for metal adsorption experiments (see Materials and methods for details). A reference sample was prepared by grafting undecylenic acid on hydrogen terminated PSi (UnHTPSi) using conventional hydrosilylation by immersing hydrogen terminated PSi (HTPSi) in undecylenic acid at 120 °C for 16 h. All the surface functionalizations were performed in triplicates to assess repeatability of the method.

The amount of grafted molecules on the samples, measured by thermogravimetry (TG), was 2.3 ± 0.3 wt% in UnTCPSi, 4.6 ± 0.3 wt% in DeTCPSi and 2.7 ± 0.8 wt% in UnHTPSi corresponding to grafting densities of 0.3, 0.9 and 0.4 molecules per $nm^2$, respectively (Table 1). Analysis of UnHTPSi was difficult because mass increase was taking place during the measurement presumably because of oxidation of the material by residual oxygen in the instrument. Very little mass loss was observed in UnTCPSi under 350 °C proving that undecylenic acid was covalently grafted on the surface whereas in DeTCPSi mass loss begun already at 200 °C indicating that some physisorbed molecules were also present (Fig. 1). A control sample

**Table 1** Mass of the organic layer on the materials and the results of nitrogen sorption experiments

| | $A^a$ ($m^2$ $g^{-1}$) | $C_{BET}$ [b] | $V^c$ ($cm^3$ $g^{-1}$) | $D^d$ (nm) | $m^e$ (%) | Coverage[f] ($nm^{-2}$) |
|---|---|---|---|---|---|---|
| HTPSi | 242 ± 1 | 28.8 ± 0.3 | 1.33 ± 0.01 | 17.0 ± 0.1 | — | — |
| UnHTPSi | 211 ± 7 | 35.0 ± 0.4 | 0.94 ± 0.08 | 15.2 ± 0.2 | 2.7 ± 0.8 | 0.4 ± 0.2 |
| TCPSi | 240 ± 5 | 73.9 ± 0.6 | 0.98 ± 0.02 | 15.8 ± 0.1 | — | — |
| UnTCPSi | 223 ± 4 | 57 ± 6 | 0.91 ± 0.01 | 15.6 ± 0.2 | 2.3 ± 0.3 | 0.34 ± 0.04 |
| DeTCPSi | 220 ± 20 | 35 ± 3 | 0.9 ± 0.1 | 15.2 ± 0.5 | 4.7 ± 0.3 | 0.90 ± 0.08 |
| BPTCPSi | 224 ± 2 | 50 ± 1 | 0.87 ± 0.01 | 14.5 ± 0.6 | 2.9 ± 0.5 | 0.23 ± 0.04 |

[a] Specific surface area from nitrogen adsorption calculated by BET theory. [b] BET constant. [c] Specific pore volume area calculated from a single point ($p/p_0$ = 0.95) on nitrogen adsorption isotherm. [d] Average pore diameter calculated by BJH theory from nitrogen desorption isotherms. [e] Mass of functional molecules divided by the total mass of the sample as measured by TG. [f] Number of functional molecules per surface area.

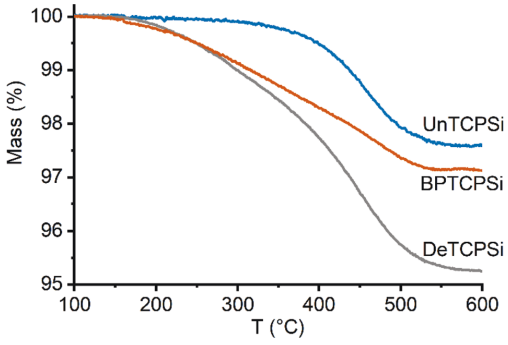


**Fig. 1** TG curves of functionalized TCPSi samples showing mass loss due to decomposition of the functional layer.

was also prepared by exposing a TCPSi sample to air after the carbonization and subsequently immersing it in undecylenic acid at 120 °C for 16 h. In this sample, a significant amount of undecylenic acid was grafted on the TCPSi surface but the mass of the organic layer was 46% smaller than in the sample not exposed to air before functionalization.

The effect of surface functionalization on the pore structure was measured by nitrogen sorption. The surface area, BET constant, pore volume and average pore diameter for HTPSi and TCPSi samples before and after functionalization are shown in Table 1 and the isotherms are shown in ESI S3.† Functionalization caused a decrease in surface area, pore volume and average pore diameter. These values decreased between 10 and 30% after functionalization of HTPSi and between 1 and 12% after functionalization of TCPSi showing that the new functionalization method did not affect the pore structure substantially. Functionalization also affected the BET constant ($C_{BET}$) of the materials. HTPSi had a small $C_{BET}$ value of 28.8 that increased to 34.4 after the functionalization with undecylenic acid. The opposite is observed with TCPSi that had a relatively high $C_{BET}$ of 73.9. After the functionalizations with undecylenic acid or decene, the $C_{BET}$ decreased to 57 and 35, respectively, indicating that the functionalized surface had weaker interactions with the $N_2$ molecule than the non-functionalized surface.

The materials were characterized by X-ray photoelectron spectroscopy (XPS), Fourier transform infrared spectroscopy (FTIR), $^{29}$Si cross polarization magic angle spinning nuclear magnetic resonance spectroscopy (CP-MAS NMR) and $^{13}$C CP-MAS dynamic nuclear polarization (DNP) NMR in order to characterize the chemical groups present on the materials. According to XPS, the samples consisted of Si, C, O and trace level impurities of Na and F (Table 2). As reported earlier, TCPSi consisted mainly of silicon, graphitic carbon, SiC and silicon oxycarbides.[12] No silicon dioxide was detected. An increased amount of COOH was detected for undecylenic acid functionalized samples, UnHTPSi containing more COOH compared with UnTCPSi. It is worth noting that three measurements were performed on each sample revealing a good reproducibility for the TCPSi samples whereas it is not the case for the HTPSi samples indicating higher instability and/or heterogeneity. Relatively high carbon content from 21 to 65 atomic % was due to the surface sensitive nature of the measurements and impurities adsorbed from the air and does not reflect accurately the overall carbon content.

According to the FTIR spectra (Fig. 2), amount of $CH_x$ species increased after grafting. Similar increase in C═O species was observed in undecylenic acid functionalized samples (UnTCPSi and UnHTPSi). Increase in ═CH species present in free undecylenic acid and decene molecules were not observed.

$^{29}$Si CP-MAS NMR spectrum of TCPSi (Fig. 3) shows three prominent features. The broad resonance between −45 and +25 ppm could correspond to several species such as: (i) $M_m$ species [$M_m$ = Si(R,R′,R″)$(OH)_{1-m}(OSi)_m$, $(0 \leq m \leq 1)$ where R, R′ and R″ correspond to C in this particular case] that are

**Table 2** Composition of the samples determined by XPS expressed as atomic %

| | HTPSi (%) | UnHTPSi (%) | TCPSi (%) | UnTCPSi (%) | DeTCPSi (%) | BPTCPSi (%) | BPTCPSi + Cu (%) |
|---|---|---|---|---|---|---|---|
| **Total C** | **21** | **52** | **65** | **63** | **63** | **36** | **36** |
| SiC | 0 | 0 | 20 | 15 | 14 | 19 | 17 |
| C–C | 90 | 83 | 72 | 70 | 76 | 57 | 50 |
| C–OR | 7 | 6 | 5 | 9 | 6 | 11 | 20 |
| C═O | 1 | 1 | 1 | 3 | 2 | 4 | 7 |
| COOH | 2 | 10 | 2 | 3 | 1 | 2 | 2 |
| **Total Si** | **74** | **26** | **23** | **21** | **24** | **38** | **38** |
| $C_3SiO$ | 3 | 7 | 0 | 0 | 0 | 0 | 0 |
| $CSiO_3$ | 0 | 10 | 7 | 10 | 5 | 0 | 0 |
| $SiO_4$ | 0 | 21 | 0 | 0 | 0 | 14 | 23 |
| $C_2SiO_2$ | 0 | 0 | 18 | 17 | 17 | 16 | 19 |
| SiC | 0 | 0 | 53 | 57 | 56 | 19 | 17 |
| Si–Si | 97 | 62 | 22 | 16 | 22 | 51 | 41 |
| **Total O** | **4** | **21** | **11** | **15** | **13** | **23** | **24** |
| **Total F** | **1** | **0** | **1** | **0** | **1** | **0** | **0** |
| **Total Na** | **0** | **0** | **0** | **0** | **0** | **0** | **0** |
| **Total P** | **0** | **0** | **0** | **0** | **0** | **Traces** | **Traces** |
| **Total Cu** | **0** | **0** | **0** | **0** | **0** | **0** | **0.3** |

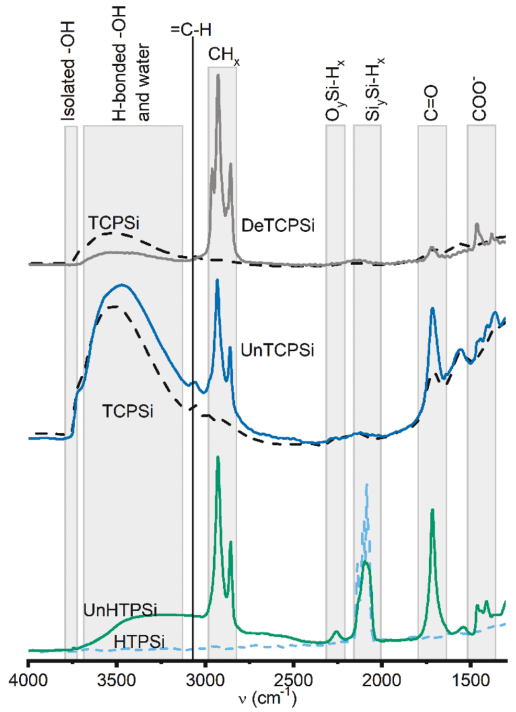


Fig. 2 FTIR spectra of functionalized (solid lines) and unfunctionalized (dashed lines) TCPSi and HTPSi samples.

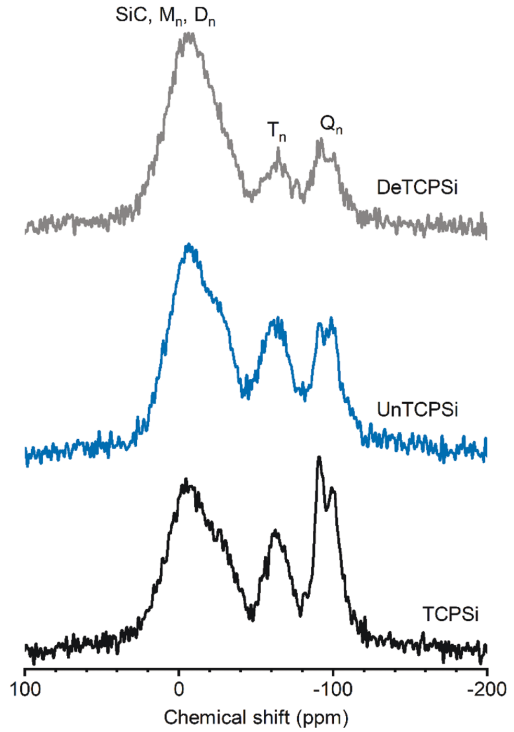


Fig. 3 $^{29}$Si CP-MAS NMR spectra of functionalized and unfunctionalized TCPSi. The intensity of the spectra is normalized according to the height of the highest peak ($M_m$ = Si(R,R′,R″)$(OH)_{1-m}(OSi)_m$, $(0 \le m \le 1)$; $D_n$ = (R,R′)-Si$(OH)_{2-n}(OSi)_n$, $0 \le n \le 2$; $T_n$ = R-Si$(OH)_{3-n}(OSi)_n$, $0 \le n \le 3$; $Q_n$ = Si$(OSi)_n(OH)_{4-n}$, $0 \le n \le 4$).

expected between 0 and 15 ppm, (ii) $D_n$ species [$D_n$ = (R,R′)-Si$(OH)_{2-n}(OSi)_n$, $0 \le n \le 2$] expected in the −25 to −5 ppm range[27] and/or (iii) SiC (from −27 to −10 ppm (ref. 28)). The broad resonance may also be due to oxidized silicon species such as [$Si(Si)_n(OH)_{4-n}$, $n$ = 2–3] expected at −14 and −12 ppm or $Si(Si)_2(OH)(H)$ or Si(Si)(OSi)(OH)(H) expected at −22 and −24 ppm, respectively.[29] These findings are supported by the XPS results in which Si–Si groups, SiC species and $C_2SiO_2$ (D) species are the major components (see Table 2).

The broad resonance between −50 and −80 ppm is assigned to $T_n$ groups [$T_n$ = R-Si$(OH)_{3-n}(OSi)_n$, $0 \le n \le 3$] such as $CSiO_3$ species that were also detected by XPS.

The third broad resonance between −110 and −80 ppm could correspond to $Q_n$ species [$Q_n$ = $Si(OSi)_n(OH)_{4-n}$, $0 \le n \le 4$] and/or hydrogenated silicon species such as $O_3SiH$ (expected at −84 ppm), $Si_3SiH$ (−91 ppm) and $Si_2SiH_2$ (−102 ppm).[30] Presence of $Q_n$ species in NMR spectra despite their absence in XPS spectra can be explained by the fact that the signal corresponding to Si atoms spatially close to hydrogen nuclei such as SiOH species are enhanced in the $^1$H–$^{29}$Si CP-MAS spectrum.

Undecylenic acid and decene functionalized TCPSi show enhanced intensity of the M, D and T species relative to Q/hydrogenated silicon species. This indicates that the surface functionalization occurs on silicon carbides/oxycarbides species because grafting of a decyl carbon chain close to Si atoms will enhance the magnetization transfer from $^1$H to $^{29}$Si. The intensity increase is more significant for the DeTCPSi sample than for the UnTCPSi, in agreement with the higher grafting yield for DeTCPSi. The more pronounced enhancement of the resonance between −20 and +25 ppm with respect to the others suggests grafting of several carbon atoms on one Si atom is favored.

For the UnHTPSi sample, the reaction of SiH with undecyl acid creates a Si–C bond. Indeed, resonances corresponding to T or D species are seen on the $^{29}$Si CP-MAS NMR spectrum of UnHTPSi as expected (ESI S4†).

Measuring $^{13}$C CP-MAS NMR spectra for these samples was challenging due to relatively low amount of carbon in the samples and inherently low sensitivity of the method. As reported earlier, we were able to use dynamic nuclear polarization with the endogenous radicals in the samples to obtain significantly higher quality spectra.[12] Spectra of TCPSi and UnTCPSi are shown in Fig. 4. The resonance corresponding to $sp^2$ carbon from graphitic carbon is observed in both samples between 150 and 110 ppm (ref. 31) as well as the resonance

 

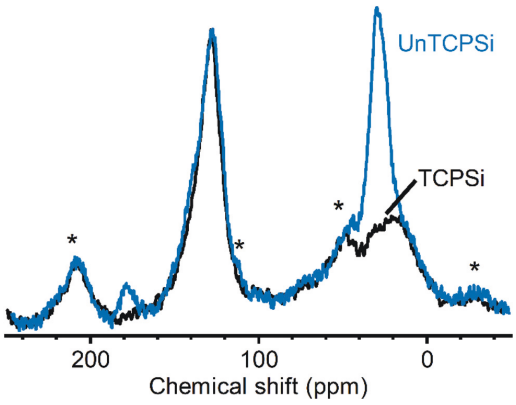


**Fig. 4** $^{13}$C CP-MAS DNP spectra of TCPSi and UnTCPSi. Spinning sidebands are marked with an asterisk.

corresponding to $sp^3$ carbon in SiC and silicon oxycarbide between −10 and 40 ppm.[32,33] As expected, UnTCPSi showed an additional resonance centered at 29 ppm from $CH_2$ groups and at 178 ppm characteristic of COOH groups.

In order to gain insight into the grafting mechanism, EPR measurements were performed for the TCPSi samples stored under inert atmosphere before and immediately after addition of undecylenic acid. The profile fitting revealed that the spectra consisted of two Lorentzian lines with *g*-factors of 2.0034 ± 0.0002 and 2.0043 ± 0.0002 (ESI S5†). There was no statistically significant increase in the total intensity of the resonance with addition of undecylenic acid. This is not surprising since there is no obvious termination reaction for the radical addition. Interestingly, the proportional intensity of the two lines reversed after addition of undecylenic acid on the material. Before the addition of undecylenic acid, the ratio between the peak at lower and higher *g*-values was 0.09 ± 0.02 and after the addition 1.2 ± 0.4. This suggests that there is a transfer of radicals from one species to another. It is challenging to identify the species definitively because of the broad resonances and disordered nature of the material. It has been shown that in $Si_{x-1}C_x$ the spins form a strongly interacting system with *g*-factors decreasing from 2.0055 to 2.0037 as *x* increases from 0 to 1.[34–36] The low *g*-factor component corresponds likely to radicals in the parts of the material with a high carbon content and the high *g*-factor component corresponds to Si rich parts. Therefore, increase in the intensity of the lower *g*-value peak indicates increasing C content in Si rich parts because of the functionalization. Alternatively, the shift towards lower *g*-values may be due to transfer of radicals from Si rich parts to the organic molecule typically having *g*-factor of approximately 2.0023.[37] Similar reversal in the intensities of the relative intensities of the two Lorentzian lines was not observed when undecylenic acid was added on the TCPSi which was not kept under inert conditions.

The $^{29}$Si CP-MAS NMR and EPR results suggest formation of chemical bonds between the surface Si atoms and undecylenic acid molecules. However, neither of these results rule out formation of bonds between surface carbon atoms and undecylenic acid molecules. In fact, reaction with the surface carbon atoms is highly probable because carbonization of PSi results in a carbon rich surface[12] and the radical groups in the SiC composites are more likely to be found on carbon than silicon atoms.[34,36] Furthermore, undecylenic acid molecules can react with other undecylenic molecules which have already reacted with the surface forming molecular chains. This does not seem to take place excessively because the pore size is not significantly reduced after grafting.

The main aim of the new functionalization method is to provide functionalized PSi that is stable in aqueous solutions in a wide pH range. To determine the stability, the UnHTPSi and UnTCPSi microparticles were immersed into 1 M HCl, deionized water and 1 M NaOH at 30 °C. After 1, 3, 6 and 20 days, part of the powder was collected from the liquid, washed to remove any physisorbed molecules and dried. The liquid was changed to a fresh one at each time point. Microparticles were measured with TG to determine the

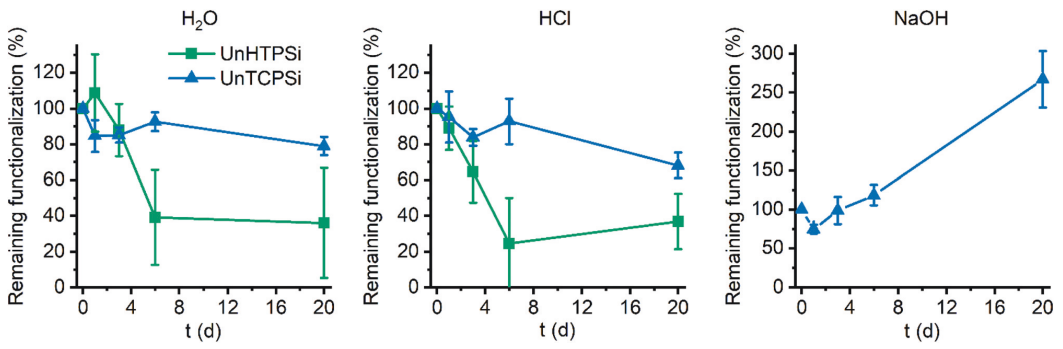


**Fig. 5** Results of stability study in deionized $H_2O$ (left), 1 M HCl (middle) and 1 M NaOH (right).

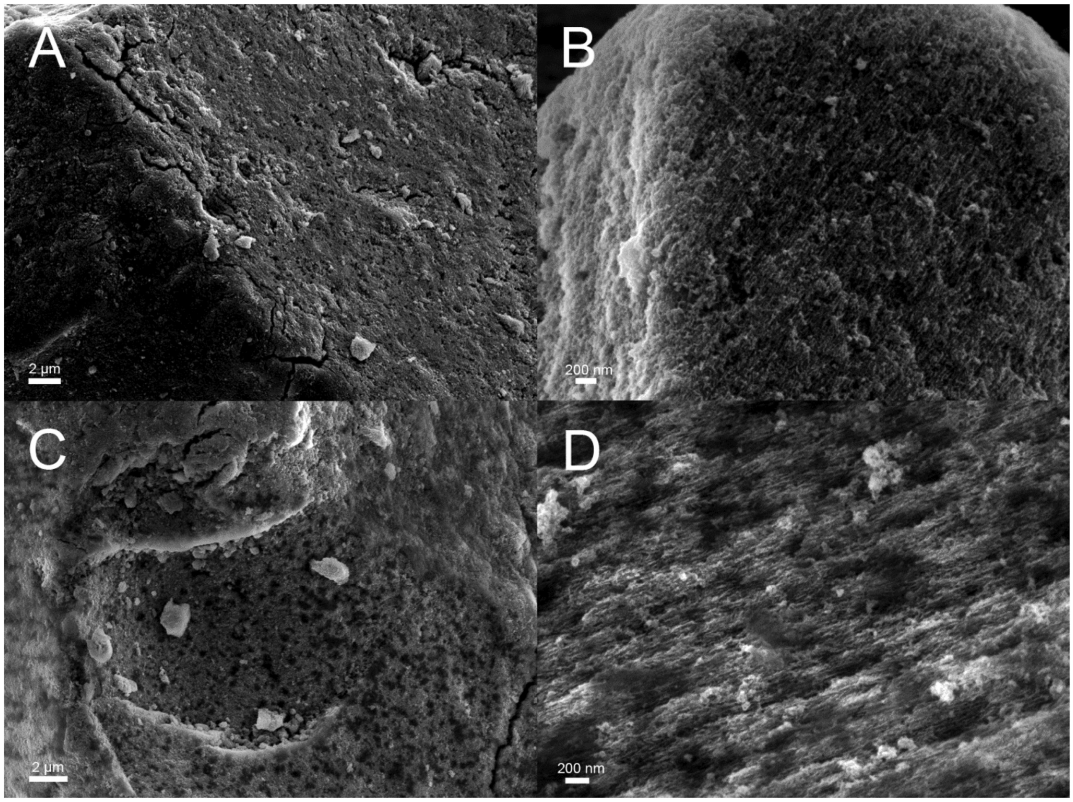


**Fig. 6** Scanning electron microscopy images of UnTCPSi before (A and B) and after (C and D) 20 days incubation in 1 M NaOH solution.

amount of the remaining grafted species in the particles. The results of the stability studies (Fig. 5) show that 68 to 79% of the functional molecules in UnTCPSi remain even after 20 days in 1 M HCl and water, respectively, whereas in UnHTPSi only 24 and 39% of the molecules remains after 6 days in 1 M HCl and water, respectively. In 1 M NaOH solution, UnHTPSi dissolved in just few minutes and no stability data was gathered. However, the functionalization in UnTCPSi remained relatively stable for 6 days. At 20 d time point, a clear increase in the amount of functionalization was observed. This counterintuitive result is due to dissolution of silicon underneath the carbonized and functionalized layer, which decreased the total mass of the sample. Because the organic layer itself was relatively stable, its mass compared to the total mass of the sample increased leading to erroneous values. This conclusion is supported by nitrogen sorption results. The surface area of UnTCPSi sample more than doubled after immersion in 1 M NaOH for 20 days indicating that dissolution of Si below the carbonized layer revealed new surface. The UnTCPSi samples immersed in HCl and water for 20 d showed less than 4% change in specific surface area, pore volume or average pore diameter. Pore structure of UnHTPSi sample experienced significantly larger changes. For example, the specific surface area increased 20 and 40% during 20 d immersion in HCl and water, respectively. SEM

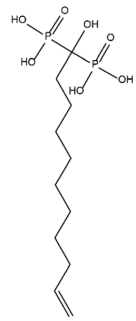


**Fig. 7** Bisphosphonate molecule grafted on BPTCPSi. To prevent a reaction between the bisphosphonate group and the surface of TCPSi, the –OH groups were protected by replacing the hydrogen atoms with trimethylsilyl groups. The OH groups were deprotected by washing the BPTCPSi particles with methanol after grafting.

 

images were taken of the UnTCPSi particles before and after 20 d incubation in NaOH (Fig. 6). The typical fir tree pore structure can still be recognized in the particles even after the 20 days incubation (Fig. 6D), but also some pits were formed in the particles (Fig. 6C and D). It can be concluded, that a highly stable surface functionalization was achieved. However, during a long immersion at very basic conditions the silicon structure under the functionalized surface begun to degrade.

The developed functionalization method was used to graft bisphosphonates (Fig. 7) on the surface of TCPSi (ESI Fig. S2†). The BPTCPSi samples contained 2.9 ± 0.5 wt% of BP molecules (Fig. 1) corresponding to coverage of 0.23 molecules per $nm^2$. Results of the nitrogen sorption and XPS measurements are shown in Tables 1 and 2. $^{29}$Si CP-MAS NMR and Fourier transform infrared spectra of the material are shown in ESI Fig. S6 and S7,† respectively, and the nitrogen sorption isotherm in ESI S3.† The BPTCPSi sample was characterized by $^{31}$P MAS NMR (Fig. 8). The spectrum shows an intense resonance at 20 ppm from the phosphorus atoms of the bisphosphonate. In addition to the main resonance, decomposition of the signal suggests at least three other components at −11, 1 and 11 ppm indicating different protonation states, conformations or possible side products of the grafting reaction.[38] The sharp resonance at 1 ppm corresponds to the silylated bisphosphonate based on liquid state NMR indicating that some silyl groups that were used as protective groups during the functionalization remained in the material.

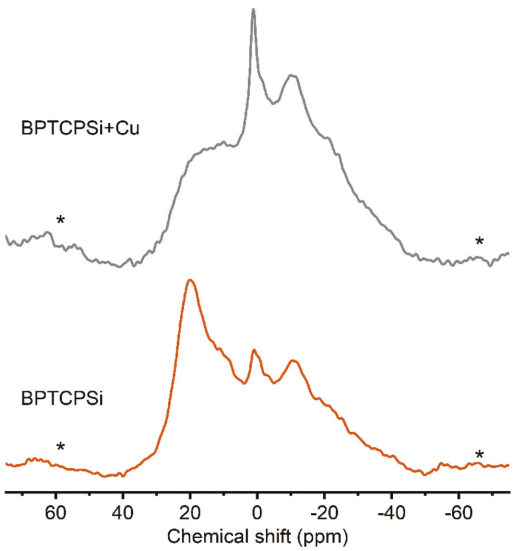


**Fig. 8** $^{31}$P MAS spectra of BPTCPSi before (bottom) and after (top) adsorption of $Cu^{2+}$. The line at 20 ppm corresponds to $^{31}$P nuclei in bisphosphonates. Spinning sidebands are marked with an asterisk.

The performance of the material in metal adsorption applications was tested with $CuCl_2$ solution. The maximum capacity of the material towards chelation of $Cu^{2+}$ was 40 ± 4 μmol $g^{-1}$ corresponding to 0.46 $Cu^{2+}$ ions per bisphosphonate molecule. This is a slightly higher ratio than was reported for solid bisphosphonates (0.35).[14] After the $Cu^{2+}$ adsorption the intensity of the resonance at 20 ppm in the $^{31}$P MAS NMR spectrum decreases significantly (Fig. 7). This suggests interaction between copper and the grafted bisphosphonates as the presence of paramagnetic species such as $Cu^{2+}$ is known to broaden and shift the resonances.[39]

The ability of the material to repeatedly adsorb copper ions from aqueous solution and subsequently to release them into 0.1 M HCl solution was tested by exposing the material to 50 consecutive adsorption–desorption cycles. Between 60 to 80% of the copper ions were adsorbed by BPTCPSi (Fig. 9). Importantly, the results show only small decrease in the performance of the material within the 50 cycles. Similar experiment was also done with unfunctionalized TCPSi. Approximately 90% of $Cu^{2+}$ ions were adsorbed and 30% desorbed (relative to amount of $Cu^{2+}$ ions initially in the solution) in the first cycle (Fig. 9). However, subsequent cycles showed

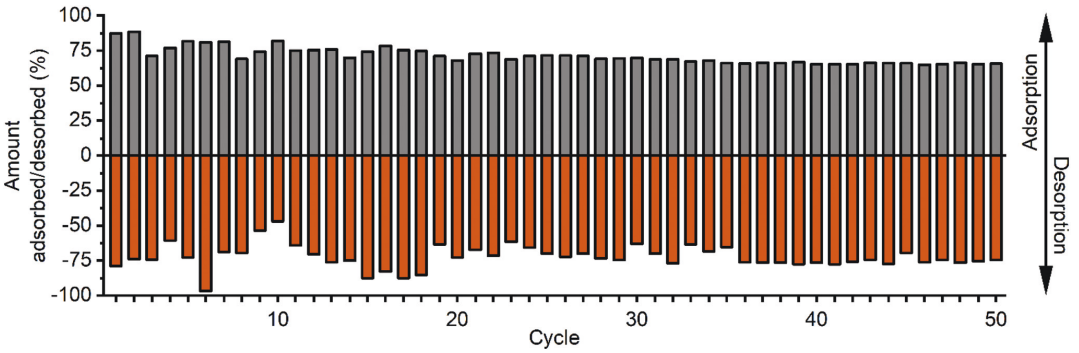


**Fig. 9** Fifty adsorption–desorption cycles of $Cu^{2+}$ ions on TCPSi and BPTCPSi. The amount adsorbed or desorbed is presented relative to the amount of $Cu^{2+}$ available for adsorption initially. The positive values represent adsorption and negative values desorption.

adsorption or desorption values smaller than 20%. The results suggest that there is some irreversible adsorption of $Cu^{2+}$ ions on TCPSi surface as well as small reversible adsorption. However, BP molecules are mainly responsible for the reversible adsorption of $Cu^{2+}$ in BPTCPSi.

## 4. Conclusions

Thermally carbonized porous silicon was functionalized by grafting terminal alkenes directly on the surface. The functionalization was performed with three kinds of molecules; a linear alkane, a carboxylic acid and a bisphosphonate. The resulting material has an unprecedented stability. It can withstand immersion in aqueous solutions at low and neutral pH up to 20 days with loss of less than a third of the functionalized layer. It can also withstand highly basic solutions up to 6 days. This surface functionalization is highly beneficial in applications such as sensing and adsorption that require extended stability of the material in aqueous solutions. Applicability of the bisphosphonate functionalized material was demonstrated in metal adsorption. The material was able to adsorb and desorb copper ions from solution repeatedly for 50 cycles without significant loss of performance.

## Conflicts of interest

J. R. T. N. and V.-P. L. are shareholders of 3AWater Oy which uses and has patent applications regarding the kinds of materials reported in the manuscript.

## Acknowledgements

MSc. Mejor Lama's contribution to the metal adsorption experiments and MSc. Tomi Miettinen's contribution to sample preparation is acknowledged.

This work was supported by the Saastamoinen Foundation, Finnish Cultural foundation, Academy of Finland [project numbers 292601, 288531, 314552] and Tekes [HybREC project].

## References

1 L. Velleman, C. J. Shearer, A. V. Ellis, D. Losic, N. H. Voelcker and J. G. Shapter, Fabrication of self-supporting porous silicon membranes and tuning transport properties by surface functionalization, *Nanoscale*, 2010, **2**, 1756–1761.

2 K. A. Kilian, T. Böcking and J. J. Gooding, The importance of surface chemistry in mesoporous materials: Lessons from porous silicon biosensors, *Chem. Commun.*, 2009, **2009**, 630–640.

3 T. Böcking, K. A. Kilian, K. Gaus and J. J. Gooding, Modifying porous silicon with self-assembled monolayers for biomedical applications: The influence of surface coverage on stability and biomolecule coupling, *Adv. Funct. Mater.*, 2008, **18**, 3827–3833.

4 B. Sciacca, S. D. Alvarez, F. Geobaldo and M. J. Sailor, Bioconjugate functionalization of thermally carbonized porous silicon using a radical coupling reaction, *Dalton Trans.*, 2010, **39**, 10847–10853.

5 K. A. Kilian, T. Böcking, K. Gaus, M. Gal and J. J. Gooding, Si–C linked oligo(ethylene glycol) layers in silicon-based photonic crystals: Optimization for implantable optical materials, *Biomaterials*, 2007, **28**, 3055–3062.

6 T. Jalkanen, E. Mäkilä, T. Sakka, J. Salonen and Y. H. Ogata, Thermally promoted addition of undecylenic acid on thermally hydrocarbonized porous silicon optical reflectors, *Nanoscale Res. Lett.*, 2012, **7**, 1–7.

7 J. M. Buriak and M. J. Allen, Lewis acid mediated functionalization of porous silicon with substituted alkenes and alkynes, *J. Am. Chem. Soc.*, 1998, **120**, 1339–1340.

8 R. Boukherroub, S. Morin, D. D. M. Wayner, F. Bensebaa, G. I. Sproule, J. M. Baribeau and D. J. Lockwood, Ideal passivation of luminescent porous silicon by thermal, noncatalytic reaction with alkenes and aldehydes, *Chem. Mater.*, 2001, **13**, 2002–2011.

9 M. J. Sweetman, F. J. Harding, S. D. Graney and N. H. Voelcker, Effect of oligoethylene glycol moieties in porous silicon surface functionalisation on protein adsorption and cell attachment, *Appl. Surf. Sci.*, 2011, **257**, 6768–6775.

10 H. Ouyang, C. C. Striemer and P. M. Fauchet, Quantitative analysis of the sensitivity of porous silicon optical biosensors, *Appl. Phys. Lett.*, 2006, **88**, 163108.

11 J. Salonen, E. Laine and L. Niinistö, Thermal carbonization of porous silicon surface by acetylene, *J. Appl. Phys.*, 2002, **91**, 456–461.

12 J. Riikonen, S. Rigolet, C. Marichal, F. Aussenac, J. Lalevée, F. Morlet-Savary, P. Fioux, C. Dietlin, M. Bonne, B. Lebeau and V. P. Lehto, Endogenous Stable Radicals for Characterization of Thermally Carbonized Porous Silicon by Solid-State Dynamic Nuclear Polarization 13C NMR, *J. Phys. Chem. C*, 2015, **119**, 19272–19278.

13 W. Xu, J. Riikonen, T. Nissinen, M. Suvanto, K. Rilla, B. Li, Q. Wang, F. Deng and V. P. Lehto, Amine Surface Modifications and Fluorescent Labeling of Thermally Stabilized Mesoporous Silicon Nanoparticles, *J. Phys. Chem. C*, 2012, **116**, 22307–22314.

14 P. A. Turhanen, J. J. Vepsäläinen and S. Peräniemi, Advanced material and approach for metal ions removal from aqueous solutions, *Sci. Rep.*, 2015, **5**, 8992.

15 M. Mureseanu, A. Reiss, I. Stefanescu, E. David, V. Parvulescu, G. Renard and V. Hulea, Modified SBA-15 mesoporous silica for heavy metal ions remediation, *Chemosphere*, 2008, **73**, 1499–1504.

16 Y. Wang, D. Liu, J. Lu and J. Huang, Enhanced adsorption of hexavalent chromium from aqueous solutions on facilely synthesized mesoporous iron–zirconium bimetal oxide, *Colloids Surf., A*, 2015, **481**, 133–142.

 

17 P. Rekha, V. Sharma and P. Mohanty, Synthesis of cyclophosphazene bridged mesoporous organosilicas for CO2 capture and Cr(VI) removal, *Microporous Mesoporous Mater.*, 2016, **219**, 93–102.
18 A. Muoz Garca, A. J. Hunt, V. L. Budarin, H. L. Parker, P. S. Shuttleworth, G. J. Ellis and J. H. Clark, Starch-derived carbonaceous mesoporous materials (Starbon) for the selective adsorption and recovery of critical metals, *Green Chem.*, 2015, **17**, 2146–2149.
19 Z. Wang, L. Chen, X. Du, G. Zou and X. Wang, A pillared process to construct graphitic carbon nitride based functionalized mesoporous materials, *RSC Adv.*, 2016, **6**, 15605–15609.
20 L. Wang, C. Cheng, S. Tapas, J. Lei, M. Matsuoka, J. Zhang and F. Zhang, Carbon dots modified mesoporous organosilica as an adsorbent for the removal of 2,4-dichlorophenol and heavy metal ions, *J. Mater. Chem. A*, 2015, **3**, 13357–13364.
21 M. Lecouvey, I. Mallard, T. Bailly, R. Burgada and Y. Leroux, A mild and efficient one-pot synthesis of 1-hydroxymethylene-1,1-bisphosphonic acids. Preparation of new tripod ligands, *Tetrahedron Lett.*, 2001, **42**, 8475–8478.
22 A. B. Sieval, V. Vleeming, H. Zuilhof and E. J. R. Sudhölter, Improved method for the preparation of organic monolayers of 1-alkenes on hydrogen-terminated silicon surfaces, *Langmuir*, 1999, **15**, 8288–8291.
23 J. Lalevée, F. Dumur, C. R. Mayer, D. Gigmes, G. Nasr, M. A. Tehfe, S. Telitel, F. Morlet-Savary, B. Graff and J. P. Fouassier, Photopolymerization of n -vinylcarbazole using visible-light harvesting iridium complexes as photoinitiators, *Macromolecules*, 2012, **45**, 4134–4141.
24 M. Rosay, L. Tometich, S. Pawsey, R. Bader, R. Schauwecker, M. Blank, P. M. Borchard, S. R. Cauffman, K. L. Felch, R. T. Weber, R. J. Temkin, R. G. Griffin and W. E. Maas, Solid-state dynamic nuclear polarization at 263 GHz: Spectrometer design and experimental results, *Phys. Chem. Chem. Phys.*, 2010, **12**, 5850–5860.
25 M. Blank, P. Borchard, S. Cauffman, K. Felch, M. Rosay and L. Tometich, High-frequency CW gyrotrons for NMR/DNP applications, *IEEE Int. Vac. Electron. Conf.*, 2012, 327–328.
26 B. M. Fung, A. K. Khitrin and K. Ermolaev, An Improved Broadband Decoupling Sequence for Liquid Crystals and Solids, *J. Magn. Reson.*, 2000, **142**, 97–101.
27 B. Alonso and C. Marichal, Solid-state NMR studies of micelle-templated mesoporous solids, *Chem. Soc. Rev.*, 2013, **42**, 3808–3820.
28 L. Gu, D. Ma, S. Yao, X. Liu, X. Han, W. Shen and X. Bao, Template-synthesized porous silicon carbide as an effective host for zeolite catalysts, *Chem. – Eur. J.*, 2009, **15**, 13449–13455.
29 R. A. Faulkner, J. A. DiVerdi, Y. Yang, T. Kobayashi and G. E. Maciel, The surface of nanoparticle silicon as studied by solid-state NMR, *Materials*, 2013, **6**, 18–46.
30 W. K. Chang, M. Y. Liao and K. K. Gleason, Characterization of porous silicon by solid-state nuclear magnetic resonance, *J. Phys. Chem.*, 1996, **100**, 19653–19658.
31 C. Hontoria-Lucas, A. J. López-Peinado, J. D. D. López-González, M. L. Rojas-Cervantes and R. M. Martín-Aranda, Study of oxygen-containing groups in a series of graphite oxides: Physical and chemical characterization, *Carbon*, 1995, **33**, 1585–1592.
32 C. T. Brigden, I. Farnan and P. R. Hania, Multi-nuclear NMR study of polytype and defect distribution in neutron irradiated silicon carbide, *J. Nucl. Mater.*, 2014, **444**, 92–100.
33 S. J. Widgeon, S. Sen, G. Mera, E. Ionescu, R. Riedel and A. Navrotsky, 29Si and 13C Solid-state NMR spectroscopic study of nanometer-scale structure and mass fractal characteristics of amorphous polymer derived silicon oxycarbide ceramics, *Chem. Mater.*, 2010, **22**, 6221–6228.
34 P. J. Gaczi and D. C. Booth, ESR in CVD silicon and silicon-carbon alloys, *Sol. Energy Mater.*, 1981, **4**, 279–289.
35 T. Shimizu, M. Kumeda and Y. Kiriyama, ESR studies on sputtered amorphous SiC, SiGe and GeC films, *Solid State Commun.*, 1981, **37**, 699–703.
36 N. Ishii, M. Kumeda and T. Shimizu, A simple molecular orbital calculation of ESR g-values for amorphous Si1-xCx, Si1-xGex and Ge1-xCx, *Solid State Commun.*, 1982, **41**, 143–146.
37 C. F. Young, E. H. Poindexter and G. J. Gerardi, Electron paramagnetic resonance of porous silicon: Observation and identification of conduction-band electrons, *J. Appl. Phys.*, 1997, **81**, 7468–7470.
38 M. S. Ironside, M. J. Duer, D. G. Reid and S. Byard, Bisphosphonate protonation states, conformations, and dynamics on bone mineral probed by solid-state NMR without isotope enrichment, *Eur. J. Pharm. Biopharm.*, 2010, **76**, 120–126.
39 M. Tang, K. Mao, S. Li, J. Zhuang and K. Diallo, Paramagnetic effects on the NMR spectra of isotropic bicelles with headgroup modified chelator lipids and metal ions, *Phys. Chem. Chem. Phys.*, 2016, **18**, 15524–15527.

*Supplementary Information*

# Stable surface functionalization of carbonized mesoporous silicon

Joakim Riikonen,[a,b] Tuomo Nissinen,[a] Aino Alanne,[c] Rinez Thapa,[a] Philippe Fioux,[b] Magali Bonne,[b] Séverinne Rigolet,[b] Fabrice Morlet-Savary,[b] Fabien Aussenac,[d] Claire Marichal,[b] Jacques Lalevée,[b] Jouko Vepsäläinen,[c] Bénédicte Lebeau[b] and Vesa-Pekka Lehto[a*]

[a] Department of Applied Physics, University of Eastern Finland, Yliopistonranta 1F, 70211 Kuopio, Finland.
[b] Université de Haute Alsace, CNRS, IS2M UMR 7361, F-68100 Mulhouse, France Université de Strasbourg, France
[c] School of Pharmacy, University of Eastern Finland, Yliopistonranta 1B, 70211 Kuopio, Finland.
[d] Bruker Biospin SA, 34, rue de l'industrie, 67166 Wissembourg Cedex, France.

Figure S1. Synthesis scheme of the bisphosphonate molecule ..... 2
Figure S2. The structures of the surfaces of the materials produced in the present work.. ..... 2
Figure S3. Nitrogen sorption isotherms ..... 3
Figure S4. 1H-29Si CP-MAS NMR spectra of UnHTPSi and HTPSi ..... 4
Figure S5. EPR spectrum of TCPSi before and after addition of undecylenic acid ..... 4
Figure S6. 29Si CP-MAS NMR spectra of BPTCPSi ..... 5
Figure S7. FTIR spectra of TCPSi and BPTCPSi ..... 5

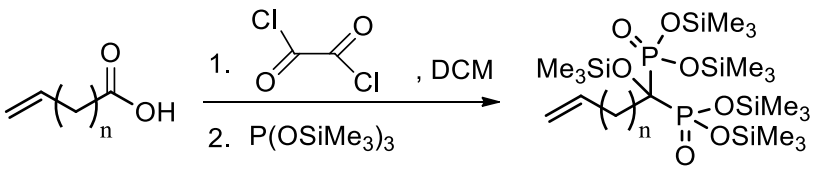


Figure S1. Synthesis scheme of the bisphosphonate molecule.

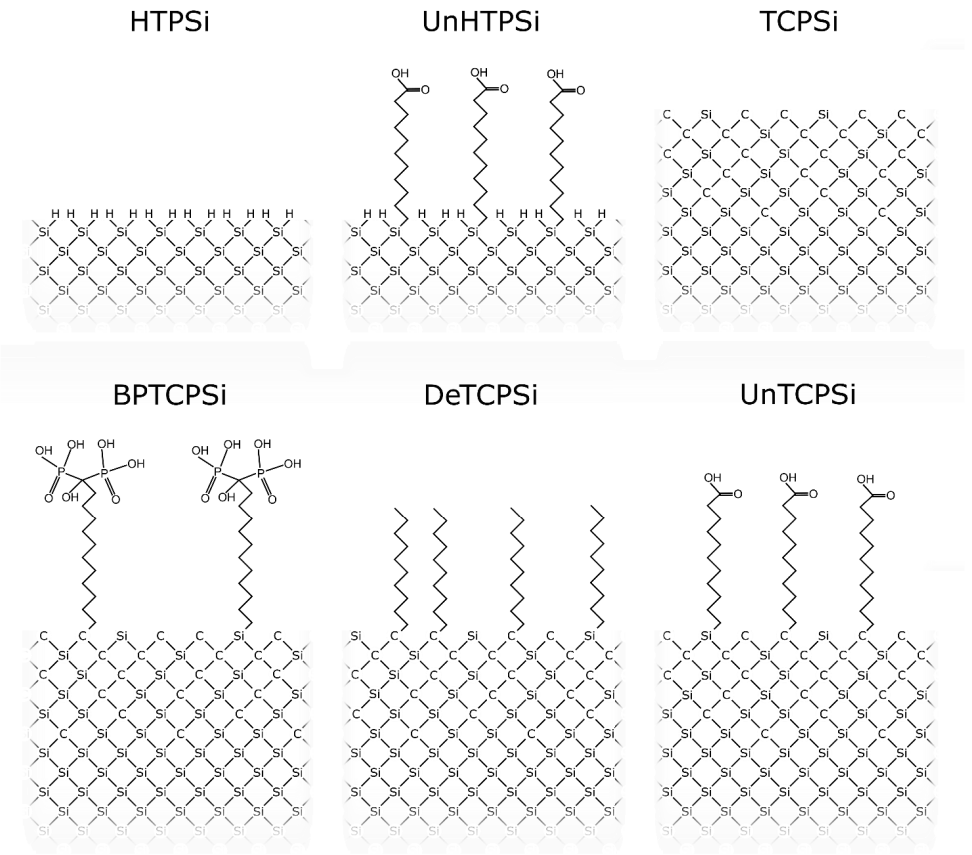


Figure S2. The structures of the surfaces of the materials produced in the present work. HTPSi consists of silicon framework with hydrogen termination on the surface. UnHTPSi is produced by grafting undecylenic acid on HTPSi by hydrosilylation. TCPSi consists of silicon framework with a carbon rich surface layer including silicon carbide silicon oxycarbide and graphitic carbon. BPTCPSi, DeTCPSi and Un TCPSi are produced by grafting bisphosphonates, decene and undecylic acid, respectively on the surface of TCPSi.

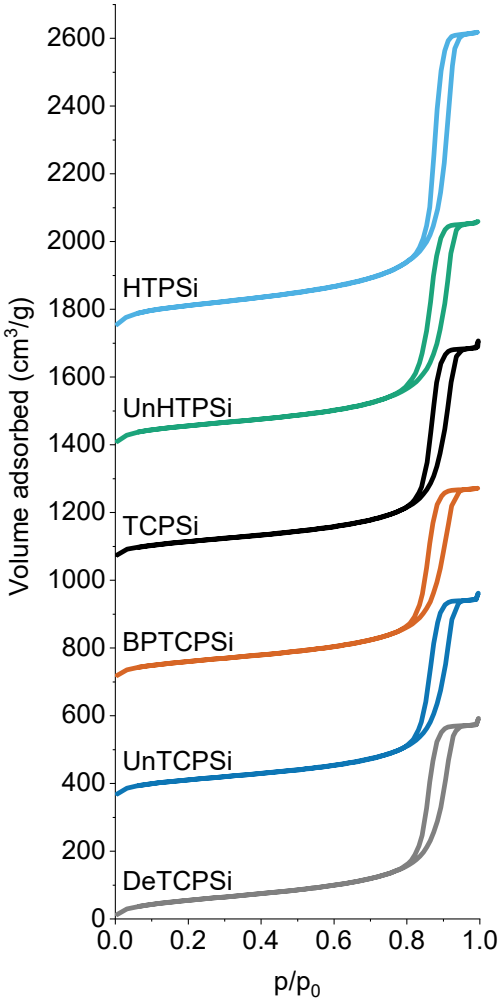


Figure S3. Nitrogen sorption isotherms.

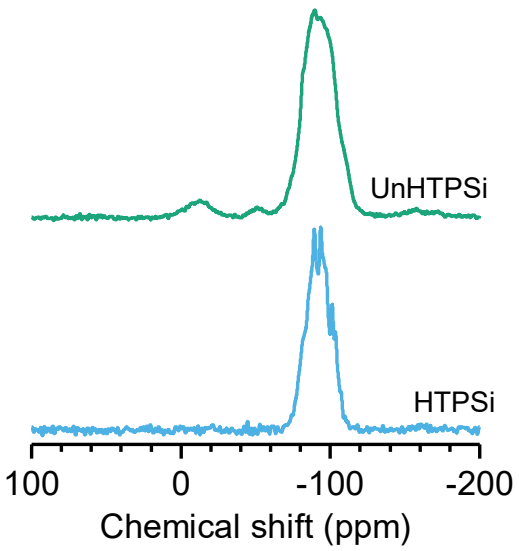


Figure S4. 1H-29Si CP-MAS NMR spectra of UnHTPSi and HTPSi.

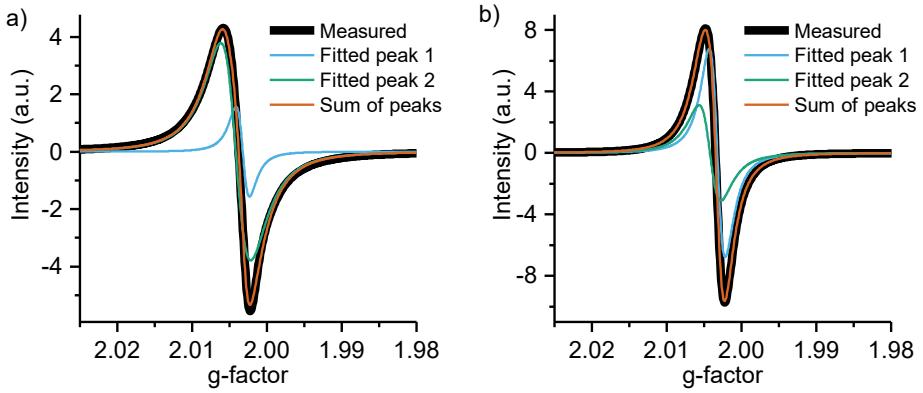


Figure S5. EPR spectrum of TCPSi kept under inert atmosphere a) before addition of undecylenic acid and b) after addition of undecylenic acid with fitted Lorentzian peaks.

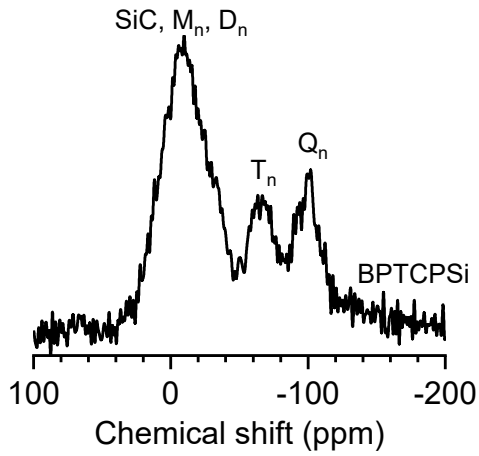


Figure S6. 29Si CP-MAS NMR spectra of BPTCPSi (Mm = Si(R,R',R'')(OH)1−m(OSi)m, (0 ≤ m ≤ 1); Dn = (R,R')-Si(OH)2−n(OSi)n, 0 ≤ n ≤ 2; Tn = R-Si(OH)3−n(OSi)n, 0 ≤ n ≤ 3; Qn = Si(OSi)n(OH)4−n, 0 ≤ n ≤ 4).

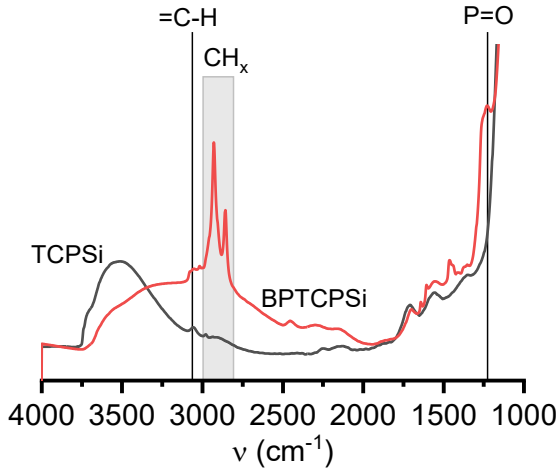


Figure S7. FTIR spectra of TCPSi and BPTCPSi. The stretch mode of P=O is observed at approximately 1250 cm-1 in the BPTCPSi spectrum.

PUBLICATION IV

Thapa R, Rahmani A, Turhanen P, Taskinen A, Nissinen T, Neitola R, Vepsäläinen J, Lehto VP, Riikonen,

**Recovery of uranium with bisphosphonate modified mesoporous silicon**

*Separation and Purfication Technology* 272: 118913 (2021)

https://doi.org/10.1016/j.seppur.2021.118913

Separation and Purification Technology 272 (2021) 118913

Contents lists available at ScienceDirect

Separation and Purification Technology

journal homepage: www.elsevier.com/locate/seppur

# Recovery of uranium with bisphosphonate modified mesoporous silicon

Rinez Thapa [a], Arezoo Rahmani [a], Petri Turhanen [b], Antti Taskinen [c], Tuomo Nissinen [a], Raisa Neitola [c], Jouko Vepsäläinen [b], Vesa-Pekka Lehto [a,*], Joakim Riikonen [a]

[a] Department of Applied Physics, University of Eastern Finland, P.O.Box 1627, Yliopistonranta 1, FI-70211 Kuopio, Finland
[b] School of Pharmacy, University of Eastern Finland, P.O.Box 1627, Yliopistonranta 1, FI-70211 Kuopio, Finland
[c] Geological Survey of Finland (GTK), Tutkijankatu 1, FI-83500 Outokumpu, Finland

ARTICLE INFO

*Keywords:*
Uranium
Adsorption
Bisphosphonate
Mesoporous
Silicon

ABSTRACT

Anthropogenic activities such as mining and ore beneficiation generate large amounts of uranium-contaminated wastewater. The metal is radioactive and toxic; therefore, it needs to be removed to protect the environment and human health. Adsorption is a viable method to remove uranium from wastewater because of the low energy consumption and ability to remove even low concentrations of uranium. However, most adsorbents are not effective to selectively adsorb uranium and their stability is typically degraded in repeated adsorption/desorption cycles. Herein, we employed a novel nanostructured adsorbent to selectively remove uranium from a tailing obtained from processing of real ore sample by Knelson concentration method. The adsorbent consisted of bisphosphonate ligands grafted on highly stable carbonized surfaces of mesoporous silicon. The porous structure of the adsorbent enhanced its permeability allowing it to be used in a column setup where metal solutions were flown through the adsorbent. The adsorbent was capable of repeatedly adsorbing and desorbing uranium without significant reduction in the performance. Importantly, the adsorbent showed essentially higher selectivity towards uranium than towards other less harmful metal ions, and the material could be regenerated with an acid. Desorption was carried out with sulfuric acid resulting in 15-fold enrichment of uranium compared to the initial solution, while other metals did not concentrate efficiently. The adsorbent was capable of selectively capturing uranium from a solution with various other metals and the adsorbed uranium was rapidly desorbed and quantified with a reasonable purity, indicating the adsorbent as a potential candidate for industrial applications.

## 1. Introduction

Even though naturally occurring uranium is not highly radioactive, it is chemically toxic causing dysfunction of the skeleton and the kidneys if ingested [1–3]. Hexavalent U(VI), which is typically present in water as uranyl ion $UO_2^{2+}$, forms soluble compounds that prevail in some radioactive wastewater [4,5]. Large volumes of such wastewaters are generated from nuclear industries, mining, and hydrometallurgical processing of uraniferous ores. Development of new technologies to remove U from the wastewater is crucial to secure the public health and the environmental safety without jeopardizing industrial output.

Conventional techniques such as precipitation, reverse osmosis, and solvent extraction have been utilized in U extraction. The precipitation and reverse osmosis are not able to extract U selectively because of the co-extraction of dissolved metals [3,6]. In solvent extraction, phosphorous based extractants, for instance, tri-n-butylphosphote is frequently used because of its good stability and selectivity towards U owing to its ability to form stable coordination complexes with uranyl ions [7–9]. However, solvent loss and release of volatile compounds are the shortcomings of the solvent extraction technique [5,6]. Moreover, these methods generate additional wastes that require further treatment and are not feasible with low metal concentrations [6].

To overcome the above-mentioned challenges, adsorption is proficient technology, in which metal ions are directly accumulated onto solid-phase adsorbents [4,5,10–13]. Since the wastewaters are typically acidic and contain low concentration of U among other, more concentrated metals [12–14], the adsorbent must be highly selective at low pH to capture U predominantly in order to acquire high purity products for the safe U disposal and wastewater management. Moreover, the adsorbent needs to have excellent stability during repeated use without deterioration in the adsorption/desorption performance for it to be sustainable and economically feasible.

* Corresponding author.
*E-mail address:* vesa-pekka.lehto@uef.fi (V.-P. Lehto).

https://doi.org/10.1016/j.seppur.2021.118913
Received 29 January 2021; Received in revised form 27 April 2021; Accepted 4 May 2021
Available online 13 May 2021

In recent years, mesoporous silica have shown potential as efficient adsorbents [12–19]. The rigid mesoporous framework offers a large surface area facilitating conjugation of ligands that are selective towards U. In particular, phosphorous based ligands have been demonstrated to extract U effectively from aqueous solutions because of their high affinity towards U species [12–17]. Furthermore, the porous structure of the mesoporous silicas enhances water-permeability enabling its use in a flow-through process to recover U from continuous wastewater streams. Nevertheless, in terms of long-term use, the stability of mesoporous silica is hampered in aqueous environments because of dissolution of the few nanometer thin pore walls [18,20,21].

Besides the mesoporous framework, the functional ligands also need to be stable in repeated use. As ideal ligands for metal adsorption, bisphosphonates (BP) with two phosphonate [$PO(OH)_2$] moieties bonded together with geminal carbon atom (P-C-P) are highly stable molecules, which have been demonstrated to extract a variety of metals from aqueous solutions [22–24].

In our previous studies, we synthesized highly stable thermally carbonized mesoporous silicon (TCPSi) as supporting material [24], upon which BP molecules were grafted via a terminal double bond [22,24]. Herein, we synthesized BP-TCPSi microparticles and employed them in a flow-through filter to extract U from a continuous wastewater stream. The stability of BP-TCPSi, its selectivity towards U and its efficacy in desorption for safe and economic disposal of U were investigated.

## 2. Experimental section

### 2.1. Materials

Silicon wafers (Okmetic Oy), hydrofluoric acid (HF 38–40%, Merck), ethanol (EtOH 99.5%, Altia Oyj) was used in electrochemical etching to produce porous silicon (PSi). The synthesis of the bisphosphonate has been described elsewhere [24]. Mesitylene (99% extra pure, ACROS Organics™) was supplied by Fisher Scientific, Finland. Uranium ICP standard (1000 mg/L in 2–5% $HNO_3$, AccuStandard® Inc.) was used to prepare U solutions. Sulfuric acid ($H_2SO_4$, 95–97%) and hydrochloric acid (HCl, 37%) were purchased from Merck, Finland. Wastewater sample containing U (9 mg/L) was obtained from a laboratory scale mineral processing test on a natural uranium-bearing ore sample. The experiment was performed at GTK Mintec in Outokumpu, Finland and the process consisted of crushing, grinding, flotation and Knelson gravity concentration. The pulp obtained from Knelson concentrator was filtrated using vacuum filtration and the filtered Knelson tails (KT, pH 3.3) was used in metal adsorption experiments.

### 2.2. Synthesis of BP-TCPSi and its characteristics

PSi films were produced from Si wafers (p-type, 15 cm in diameter, 0.01–0.02 Ωcm resistivity) through electrochemical etching. The electrolyte contained 50% HF and 50% EtOH. The applied current density during the etching was 30 mA/cm$^2$ for 40 min. The films were detached from the substrate with high current pulses (160 mA/cm$^2$ for 1 s followed by 255 mA/cm$^2$ for 2 s). The films were dried at 65 °C for 1 h and then communized with ball mill (Fritsch Pulverisette 7) at rotation speed of 100 rpm for 3 min. The milled particles were sieved through 25 and 75 μm sieves to obtain the final microparticle fraction [25].

Thermal carbonization of PSi (TCPSi) was conducted in a tube oven as described elsewhere as follows [24]. Microparticles were incubated with the fresh electrolyte (50% HF and 50% EtOH) for 10 min. After sedimentation, the particles were separated from the supernatant and dried at 65 °C for 45 min. Particles were placed inside a quartz tube. $N_2$ gas was used to flush the tube at the rate of 1 L/min for 30 min and later with acetylene at 1 L/min for 15 min. With continuous flow of both gases, the quartz tube was placed in a tube oven at 500 °C for 14 min 30 sec. Acetylene flow was stopped and after additional 30 s with $N_2$ flow at 500 °C, the sample was taken out and cooled for 30 min at RT. After the cooling, acetylene flow was again applied for 9 min 40 s and terminated while the $N_2$ flow was continued for further 20 s at the room temperature. Then, the quartz tube was put back into the oven and the sample was heated at 820 °C for 10 min under the $N_2$ atmosphere. After the heating, the quartz tube was kept under $N_2$ flow at room temperature for 40 min.

For functionalization of TCPSI, BP molecules (Fig. 1) were mixed with TCPSi in ratio of 1:2 w/w under the continuous $N_2$ flow. The BP (250 mg) were pre-degassed (bubbling with $N_2$) in 10 mL mesitylene solution and mixed with the freshly prepared TCPSi (500 mg) in a quartz tube. The tube opening was closed with a Teflon cap. The sample was then incubated at 120 °C for 19 h. The synthesized BP-TCPSi particles were cooled to RT (30 min), washed with 200 mL MeOH using suction filtration (polypropylene, 10 μm pore size) and dried at 65 °C for 1 h.

As the reference material, unfunctionalized TCPSi was produced with mesitylene treatment as described above but without adding BP into the solution. The synthesized BP-TCPSi and TCPSi samples were characterized as follows. Laser diffraction (Mastersizer 2000, Malvern Instruments, UK) was used to measure the particle size of the samples in EtOH. Scanning electron microscopy (SEM, Zeiss Sigma HP VD) coupled with energy dispersive X-ray spectroscopy (Thermo Noran NS7 double-EDS, ThermoFisher) was used to study the morphology and elemental compositions of the samples. SEM samples were prepared on aluminum stub and the images were taken with SE2 or InLenS Detector and the applied voltage was 5 kV. The voltage of 15 kV was used for the EDS analysis. Thermogravimetric analysis (TGA, NETZSCH TG 209 *F1 Libra*®) was used to determine the conjugated BP amount applying the parameters as follows: equilibration at 80 °C for 30 min and heating to 700 °C at the rate of 20 °C/min under nitrogen flow (200 mL/min). Surface area, pore diameter and pore volume of the particles were measured using gas adsorption (Micromeritics Tristar II 3020) using $N_2$ but before the measurement the samples were dried in vacuum for 1 h at 65 °C (VacPrep 061, Micromeritics) in order to remove the moisture.

### 2.3. Batch adsorption experiments

Adsorption kinetics and adsorption isotherms were studied at pH 3 by mixing 10 mg BP-TCPSi with 10 mL of solution with desired U concentrations prepared from an artificial U standard. The pH of the U solutions was adjusted with $HNO_3$/NaOH. Samples were shaken at 80 rpm. Before starting the adsorption tests, the BP-TCPSi was primed by

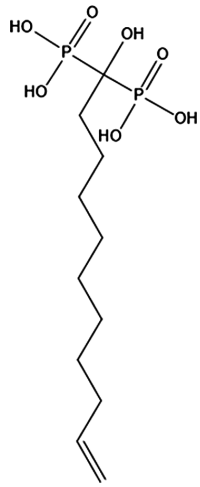


**Fig. 1.** Structure of the bisphosphonate molecule.

incubating in 10 mL of 5 M HCl for 1 h followed by washing thrice with 10 mL milliQ water.

The adsorption kinetics was examined using initial U concentration of 10 mg/L at varying contact times from 5 min to 48 h. At each predetermined time point, 200 μL of the supernatant was taken out to measure the U concentration. The adsorption isotherm was measured after 24 h of mixing in varying initial concentration of U from 4 to 20 mg/L. The particles were centrifuged (6000 rpm, 1 min), and supernatant was taken for inductively coupled plasma mass spectrometer, ICP-MS (NexION 350D, Perkin Elmer) measurements for the determination of the concentrations of the metals. In the ICP-MS measurements, rinse solution was 2.5% $HNO_3$ and the internal standards were 100 μg/L Sc and 100 μg/L Lu. The amount of adsorbed U per gram of BP-TCPSi was calculated from the U concentrations before and after the mixing.

### 2.4. Flow-through setup

BP-TCPSi (~20 mg) powder was packed in borosilicate glass column (Omnifit® Labware, 2.5 × 0.3 cm). Desired liquid was pushed through the material using plastic syringe attached to a syringe pump (Al-1600, New Era Pump Systems Inc., Supplementary Fig. S1). The adsorbent was primed with 5 mL of 5 M HCl at 0.2 mL/min followed by washing with 10 mL milliQ water at 1 mL/min. For the adsorption step, 10 mL of the minewater sample (KT) was filtered at 0.25 mL/min, whereas the desorption was carried out by using 0.5 mL of 1 M $H_2SO_4$ at 1.25 mL/min. The absolute volumes of the filtrated liquids were measured by weighing and the metal concentrations were determined by ICP-MS. After every adsorption and desorption step, the particles were washed with water.

## 3. Results and discussion

### 3.1. Material characterization

Particle size distributions of TCPSi and BP-TCPSi were measured with laser diffraction (Fig. S2) and the median particle sizes were determined to be 72 μm and 73 μm, respectively. The SEM images show the irregular structure and rough surface of the microparticles (Fig. 2). The $N_2$ sorption isotherms were of type IV, which is typical for mesoporous materials (Fig. 3A). The pore-size distributions had peaks in the range between 7 and 20 nm, which indicated the material to have mesoporous structures (Fig. 3B). The surface area, pore diameter, and pore volume of BP-TCPSi were slightly reduced as a result of the conjugation of the BP molecules (Table 1). The conjugated BP amount in BP-TCPSi was calculated by comparing the TG curves of the functionalized and unfunctionalized TCPSi samples (Fig. 3C). The mass loss associated with decomposition of BP was 1.71 ± 0.03% w/w, which is equivalent to 52 ± 1 μmol BP per gram of the sample with the surface coverage of 0.141 ± 0.003 molecules/$nm^2$. The functionalization was additionally confirmed by the EDS analysis where the phosphorous peak was detected at 2.01 keV with BP-TCPSi but not with TCPSi (Fig. S3).

### 3.2. Batch setup adsorption

Artificial U solution was used in batch experiments to study the adsorption of U with BP-TCPSi at various pH. The results indicate the adsorbed amount to increase with increasing pH (Fig. S4). Since the pH of the KT was 3.3, adsorption kinetics and the adsorption isotherm were studied at pH 3. Adsorption kinetics was examined to find out the time needed for complete adsorption. The adsorption kinetics curve (Fig. 4A) showed rapid U uptake at the beginning and was very slow after 10 h. Increase in the adsorbed U amounts from 24 h to 48 h was negligible. Based on this finding, 24 h time was used in the adsorption isotherm measurements to allow long enough time to reach the equilibrium at every concentration.

The adsorption isotherm data was fitted with different isotherm models (Fig. 4B) and the parameters derived from the fittings are listed in Table 2. Langmuir model did not fit the data well ($R^2 = 0.88$) indicating that the adsorption did not take please solely by monolayer chemisorption on identical binding sites. Freundlich model gave a better fit ($R^2 = 0.95$) but does not represent the plateau in adsorption at high equilibrium concentrations adequately. To overcome the limitation of the Langmuir and Freundlich model, Sips model is typically used to predict the degree of heterogeneity of the adsorption sites [26–28]. The Sips model showed good fit with the experimental data ($R^2 = 0.97$) suggesting that the adsorbent consisted of heterogenous binding sites since $n_s < 1$ (Table 2) [26–28]. The adsorption capacity value generated by the Sips model ($q_{ms} = 60 \pm 7$ μmol/g) is slightly higher than the total amount of BP ligands grafted on the BP-TCPSi sample (52 ± 1 μmol/g). On the other hand, adsorption of U with unfunctionalized TCPSi sample under similar experimental setup was negligible, 2 ± 1 μmol/g with initial concentration, $C_i = 10$ mg/L and $C_e = 9$ mg/L. Therefore, the U adsorption on BP-TCPSi must be principally associated with the BP moieties. However, the shape of the isotherm implies that non-identical binding sites exist in the material. To model adsorption on two distinct sites, the experimental data was fitted with double Langmuir model, which consists of two Langmuir isotherms. The double Langmuir model showed good fit with the experimental data ($R^2 = 0.97$) and the combined maximum capacity ($Q_{max} = q_{m1} + q_{m2} = 52 \pm 3$ μmol/g) was in line with the total amount of BP grafted on the material (52 ± 1 μmol/g). Therefore, it seems plausible that the adsorption of U is associated with BP ligands but with two separate binding mechanism with different affinities ($K_{L1}$ and $K_{L2}$). Nonetheless, the exact mechanisms of the binding of U on the BP-TCPSi remains unclear.

In literature, several adsorbents functionalized with phosphonate moieties have been reported to have considerable adsorption capacity for U, for instance with polyvinyl alcohol fibers modified with phosphonic acid (135 μmol/g at pH 4.5) [29], mesoporous organosilica-phosphonate hybrids (220 μmol/g at pH 4) [15], phosphonate grafted on mesoporous carbon (630 μmol/g at pH 4) [11], phosphate functionalized polyethylene (730 μmol/g at pH 8) [30], and diphosphonic acid functionalized on nanofiber silica (540 μmol/g at pH 7.5) [31].

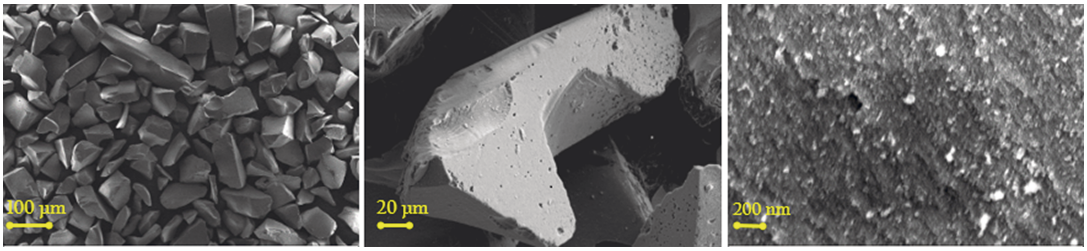


**Fig. 2.** SEM images at various length scales showing morphology of BP-TCPSi particles.

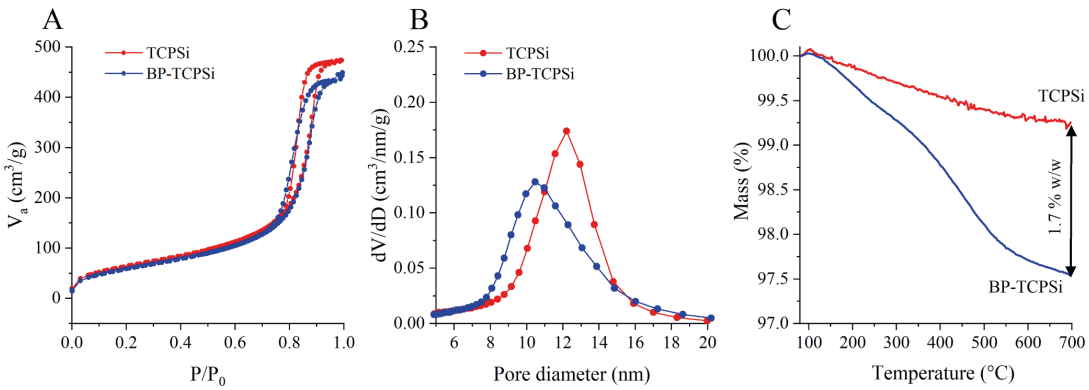


**Fig. 3.** $N_2$ physisorption isotherms **(A)**, pore size distributions **(B)** and TG curves **(C)** of TCPSi and BP-TCPSi samples.

**Table 1**
Results from $N_2$ physisorption of BP-TCPSi in comparison with TCPSi (mean ± σ, n = 3).

| Material | Surface area (m$^2$/g)[a] | Pore volume (cm$^3$/g)[b] | Pore diameter (nm)[c] |
|---|---|---|---|
| TCPSi | 238 ± 1 | 0.8 ± 0.1 | 12.3 ± 0.2 |
| BP-TCPSi | 221 ± 1 | 0.7 ± 0.1 | 10.5 ± 0.1 |

[a] BET surface area calculated from the adsorption isotherm.
[b] Specific pore volume calculated from desorption isotherm at $p/p_0 = 0.9$.
[c] Average pore diameter calculated with BJH theory using desorption branch of isotherm.

### 3.3. Flow-through setup

The KT sample was used to study the adsorption, desorption, and selectivity of BP-TCPSi towards U. The original pH of the KT was 3.3. The initial concentration of various metals in KT sample were analysed with ICP-MS (Fig S5). The initial concentrations of the main constituents were: Mg 452 μM, Al 40 μM, U 38 μM, Mn 17 μM, Cu 13 μM. The metals with concentrations below 5 μM are not evaluated in the present results.

#### 3.3.1. Breakthrough curves

The breakthrough curves of the metals with BP-TCPSi were evaluated as function of the filtration volume. As shown in Fig. 5, the U ions retained longer in the column than the other metals indicating superior selectivity of the adsorbent towards U. For instance, the volume required to dispense 5% ($C_f/C_i$ at 0.05) of U in the raffinate was approximately 10 mL equal to 285 bed volumes, while other metals were dispensed in significant quantities already in the first 2 mL (57 bed volumes).

#### 3.3.2. Reusability, selectivity, and desorption studies

The stability of BP-TCPSi was tested by using it in ten consecutive adsorption/desorption cycles in a flow through setup. As shown in Fig. 6A, the BP-TCPSi was highly stable to repeatedly adsorb U from the KT sample followed by desorption with sulphuric acid. The average adsorption efficiency was 91 ± 6% and the average desorption efficiency was 97 ± 9% from the 10 cycles examined in the flow-through setup. In our earlier study, the material has been shown to be reusable for as many as 50 cycles without significant reduction in the adsorption/desorption performance [22].

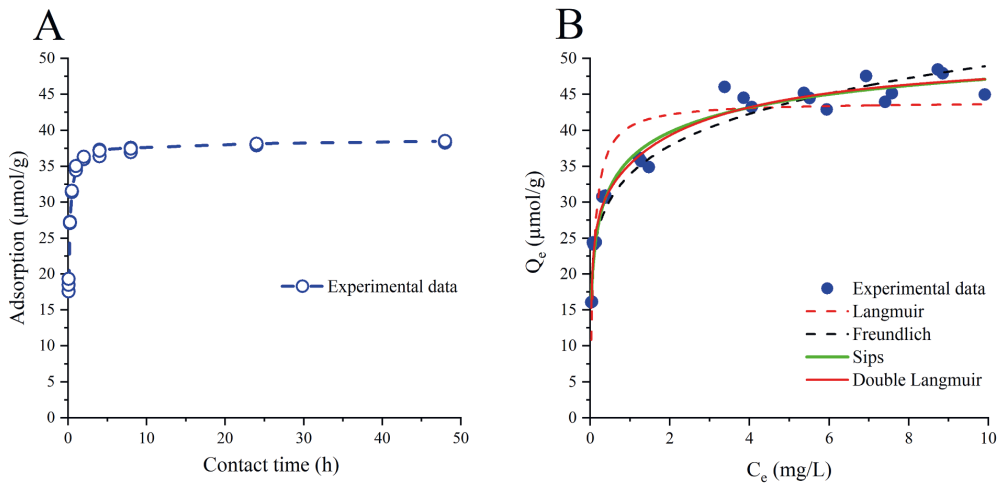


**Fig. 4.** Adsorption kinetics **(A)** and adsorption isotherm **(B)** of U with BP-TCPSi at pH 3. The isotherm is plotted with the amount of adsorbed U ($Q_e$) as function of equilibrium concentration ($C_e$) in the supernatant.

**Table 2**
Isotherm parameters derived from adsorption isotherm models and their equations.

| | | | | | |
|---|---|---|---|---|---|
| ***Langmuir*** $Q_e = \frac{q_m K_L C_e}{1 + K_L C_e}$ | $R^2$ | $q_m$ (μmol/g) | $K_L$ (L/mg) | | |
| | 0.88 | 45 ± 2 | 9 ± 3 | | |
| ***Freundlich*** $Q_e = K_F C_e^{1/n}$ | $R^2$ | $K_F$ (μmol/g) | n | | |
| | 0.95 | 34 ± 1 | 6 ± 1 | | |
| ***Sips*** $Q_e = \frac{q_{ms} K_S C_e^{n_s}}{1 + K_S C_e^{n_s}}$ | $R^2$ | $q_{ms}$ (μmol/g) | $K_S$ (L/mg) | $n_s$ | |
| | 0.97 | 60 ± 7 | 2 ± 1 | 0.4 ± 0.1 | |
| ***Double Langmuir*** $Q_e = \frac{q_{m1} K_{L1} C_e}{1 + K_{L1} C_e} + \frac{q_{m2} K_{L2} C_e}{1 + K_{L2} C_e}$ | $R^2$ | $q_{m1}$ (μmol/g) | $q_{m2}$ (μmol/g) | $K_{L1}$ (L/mg) | $K_{L2}$ (L/mg) |
| | 0.97 | 30 ± 2 | 22 ± 2 | 40 ± 10 | 0.5 ± 0.2 |

where,
$R^2$ is the non-linear regression coefficients of the fitted curves.
$q_m$, $K_F$, $q_{ms}$, $q_{m1}$, and $q_{m2}$ represent the adsorption capacity.
$K_L$, $K_S$, $K_{L1}$, and $K_{L2}$ are the constants representing the binding affinity.
n and $n_s$ are the constants representing adsorption intensity or surface heterogeneity.

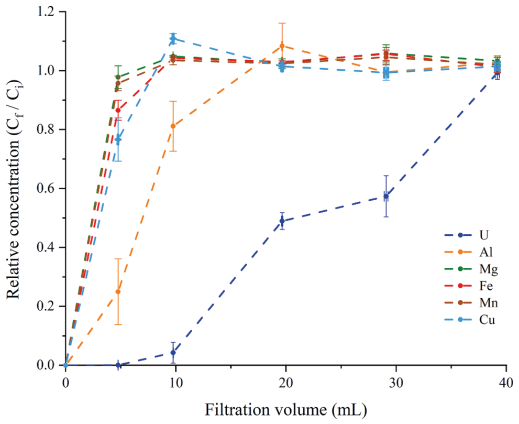


**Fig 5.** Breakthrough curves for adsorption of metals as function of filtration volume. The KT sample was fed into a column with 20 mg BP-TCPSi at flow rate of 0.25 mL/min until the metal concentrations after filtration ($C_f$) was equivalent to the initial concentrations ($C_i$). The error bars represent the standard deviation (mean ± σ, n = 3).

The distribution coefficient, $K_d$ was used to interpret the selectivity of BP-TCPSi towards U in comparison with the other metals. The $K_d$ values were calculated using Eq. (1)

$$K_d = \frac{(C_i - C_f)}{C_f} \times \frac{V}{m} \quad (1)$$

where, $C_i$ and $C_f$ are the metal concentrations before and after the adsorption, respectively, $m$ is the mass of adsorbent and $V$ is the volume of metal solution.

Regardless of the high concentrations of interfering metals, such as Mg and Fe, the $K_d$ values of U were higher in all 10 cycles in comparison with other metals (Fig. 6B). Notably, the $K_d$ values of U decreased from ca. 22000 to 5000 mL/g in the first four cycles. The decrease is because the adsorption of U was not 100% efficient in every cycle resulting small amount of U to prevail in the filtrate after the adsorption ($C_f$ = 0.2 – 1.2 mg/L) (Fig. S6). Since the $K_d$ value is inversely proportional to the $C_f$ values, a small increase in $C_f$ values corresponded to a large drop in the $K_d$ values. However, the $K_d$ (U) value remain steady after the 4th cycle, which was still substantially higher in comparison to the $K_d$ values for other metals. Nonetheless, the $K_d$ (U) values are comparable with other adsorbents reported in literature, for instance, carboxyl functionalized metal organic framework [32], superparamagnetic phosphonate grafted mesoporous carbon [11], and ion-imprinted mesoporous silica [13].

To further compare the selective adsorption of BP-TCPSi for U in relation to the other metals, the selectivity coefficients (β) values were determined, which were calculated using equation (2)

$$\beta = \frac{K_d(U)}{K_d(M)} \quad (2)$$

where $K_d$ (U) and $K_d$ (M) are the distribution coefficients of uranyl ion and an interfering ion in the solution, respectively.

The β values were > 20 in every cycle against all the interfering metals emphasizing that BP-TCPSi can selectively capture U even at low concentrations (Supplementary material, Table S1). In the literature, there are comparable β values for U from the range of interfering metal ions such as with dihydroimidazole functionalized SBA-15 adsorbent (β > 10 at pH 3.6) [18] and multi-layered vanadium carbide nanosheets (β > 10 at pH 4.5) [33].

The present results show an excellent selectivity of BP-TCPSi towards the uranyl ion, which as a strong Lewis acid has a high affinity with P = O and $PO_3^{2-}$ functional groups [11,29,30,34]. Furthermore, larger radius (5f orbitals) of uranyl ion bind more strongly with the donor ligands in comparison to other metals with smaller ionic radius [11,34]. On the other hand, adsorption of the metals with unfunctionalized TCPSi were negligible (≤ 1 μmol/g) (Fig. S7), emphasizing that the BP functionalization was necessary for efficient metal adsorption.

Although various adsorbents that are reasonably selective towards U have been studied, their stabilities are rarely reported adequately and the reusability studies are done only in batch setup [11–13,15,18,30,32,35–39]. Typically, the adsorbents have reduced adsorption performance in repeated use because the functional ligands are not stable during the regeneration phase [15,18,30,32,35]. In case of BP-TCPSi, the BP ligands are directly grafted on carbonized silicon surfaces via terminal alkenes leading to exception stability of the functional layer [22,24]. To detect possible leaching of the BP molecules from BP-TCPSi during the stability experiment, TG measurements were carried out with fresh and the cycled BP-TCPSi. The difference in the TG mass loss of BP-TCPSi before and after the experiment was not significant (p-value > 0.5), indicating that BP ligands were intact on the sample after the 10 cycles (Fig. S8).

Desorption was carried out with 1 M $H_2SO_4$ and the U was rapidly desorbed in 0.5 mL of $H_2SO_4$ corresponding to 14 bed volumes (0.035 mL). As shown in Fig. 6A, apart from the 1st cycle, U desorbed completely although the volume of the eluent was relatively small. Therefore, the concentration of U in the final filtrate (150 ± 20 mg/L) was enriched by at least a 15-fold in comparison to the initial concentration (9 mg/L) (Fig. 6C). Besides U, the concentration of the interfering metals in the filtrate were relatively low such as Fe (13 ± 3 mg/L) and Al (2 ± 1 mg/L) and other metals at levels below 1 mg/L.

The BP-TCPSi fulfils important requirements of a potent adsorbent i.e., material was able to selectively capture U, efficiently desorb the metal, and was stable in repeated use. Moreover, BP-TCPSi was used as filters in an easy-to-use flow-through system, in which large volumes of the eluent can be continuously flown through porous structure of BP-TCPSi. The flow-through system opens a new avenue to simplify the adsorption technology, for instance, by directly coupling it with analytical devices for online separation/determination of metals.

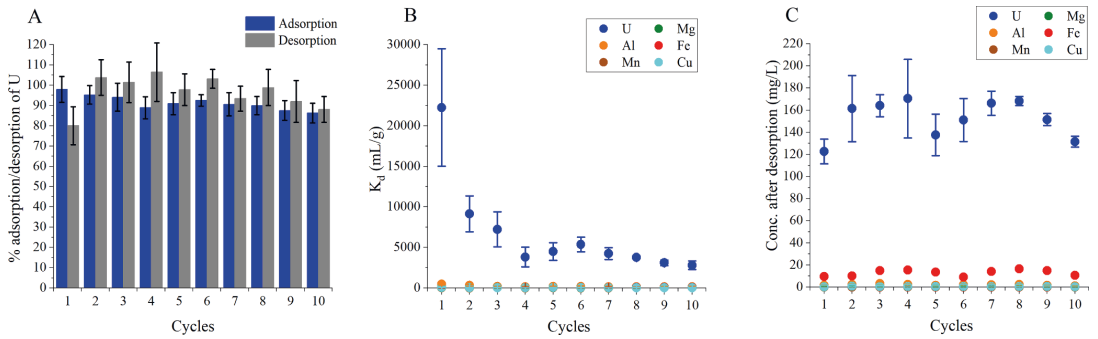


**Fig. 6.** Reusability of BP-TCPSi in U extraction for 10 adsorption/desorption cycles **(A)**, distribution coefficients ($K_d$) of metals **(B)**, and metal concentrations in the filtrate after desorption with 0.5 mL of 1 M $H_2SO_4$ **(C)**. Error bars represent standard deviation (n = 4).

## 4. Conclusions

Nanostructured thermally carbonized porous silicon with functional BP molecules on the surface (BP-TCPSi) was employed to extract uranium from a minewater sample obtained from a beneficiation process of uranium-bearing ore sample. Adsorption isotherm was best described with a model consisting of two Langmuir isotherms indicating the adsorption of U with BP-TCPSi to occur at two non-identical binding sites. The combined maximum adsorption capacity of the two sites was determined to be 52 ± 3 μmol/g. The adsorbent showed substantial distribution coefficient values ($K_d$ as high as 22000 mL/g) for uranium as well as high selectivity coefficient values ($\beta > 20$), indicating the material to have excellent selectivity towards uranium despite larger concentrations of other metal ions. Essentially, the uranium extracted by BP-TCPSi was rapidly desorbed in a small volume corresponding to 14 bed volumes using 1 M sulfuric acid. Concentration of uranium after the desorption (150 ± 20 mg/L) was 15 times higher than the initial concentration while the concentrations of other metals were reduced effectively. Concentrating the uranium in a low volume of liquid allows a safer and more economical disposal of the uranium containing waste. Removal of the radioactive and highly toxic metal protects the water resources, improves environmental safety, and secures human health. Furthermore, the BP-TCPSi showed great stability for repeated adsorption/desorption cycles, which is crucial for industrial scale operations in terms of the cost-effectiveness and feasibility. The adsorbent was successfully used in a flow-through process, which greatly simplifies processing large volumes of wastewater that need to be treated in an industrial setting.

## CRediT authorship contribution statement

**Rinez Thapa:** Conceptualization, Methodology, Investigation, Writing - original draft, Visualization, Funding acquisition. **Arezoo Rahmani:** Methodology. **Petri Turhanen:** Resources. **Antti Taskinen:** Methodology, Resources. **Tuomo Nissinen:** Methodology. **Raisa Neitola:** Resources. **Jouko Vepsäläinen:** Resources. **Vesa-Pekka Lehto:** Conceptualization, Resources, Writing - review & editing, Supervision, Project administration, Funding acquisition. **Joakim Riikonen:** Conceptualization, Methodology, Investigation, Visualization, Writing - review & editing, Supervision, Project administration, Funding acquisition.

## Declaration of Competing Interest

J.R., T.N. and V-P.L. are shareholders of 3AWater Oy, which has Intellectual Property Rights (IPR) related to the material reported in the manuscript.

## Acknowledgement

The work was funded by the Finnish Cultural Foundation, the Academy of Finland (292601 and 292599) and the Foundation for Research of Natural Resources in Finland (1794/16, 1801/17 and 2018003).

## Appendix A. Supplementary material

Supplementary data to this article can be found online at https://doi.org/10.1016/j.seppur.2021.118913.

## References

[1] P. Kurttio, A. Auvinen, L. Salonen, H. Saha, J. Pekkanen, I. Mäkeläinen, S. B. Väisänen, I.M. Penttilä, H. Komulainen, Renal Effects of Uranium in Drinking Water, Environ. Health. Perspect. 110 (2002) 337–342, 10.1289%2Fehp.02110337.

[2] M.L. Zamora, B.L. Tracy, J.M. Zielinski, D.P. Meyerhof, M.A. Moss, Chronic ingestion of uranium in drinking water: a study of kidney bioeffects in humans, Toxicol. Sci. 43 (1998) 68–77, https://doi.org/10.1093/toxsci/43.1.68.

[3] I.A. Katsoyiannis, A.I. Zouboulis, Removal of uranium from contaminated drinking water: a mini review of available treatment methods, Desalination Water Treat. 51 (2013) 2915–2925, https://doi.org/10.1080/19443994.2012.748300.

[4] F.F. Li, W.R. Cui, W. Jiang, C.R. Zhang, R.P. Liang, J.D. Qiu, Stable $sp^2$ carbon-conjugated covalent organic framework for detection and efficient adsorption of uranium from radioactive wastewater, J. Hazard. Mater. 392 (2020), 122333, https://doi.org/10.1016/j.jhazmat.2020.122333.

[5] J. Wang, S. Zhuang, Extraction and adsorption of U(VI) from aqueous solution using affinity ligand-based technologies: an overview, Rev. Environ. Sci. Biotechnol. 18 (2019) 437–452, https://doi.org/10.1007/s11157-019-09507-y.

[6] S.E. Kentish, G.W. Stevens, Innovations in separations technology for the recycling and re-use of liquid waste streams, Chem. Eng. J. 84 (2001) 149–159, https://doi.org/10.1016/S1385-8947(01)00199-1.

[7] M.K. Nazal, M.A. Albayyari, F.I. Khalili, E. Asoudani, Synergistic effect of tri-n-butyl phosphate (TBP) or tri-n-octyl phosphine oxide (TOPO) with didodecylphosphoric acid (HDDPA) on extraction of uranium(VI) and thorium(IV) ions, J. Radioanal. Nucl. Chem. 312 (2017) 133–139, https://doi.org/10.1007/s10967-017-5204-3.

[8] A.P. Paiva, P. Malik, Recent advances on the chemistry of solvent extraction applied to the reprocessing of spent nuclear fuels and radioactive wastes, J. Radioanal. Nucl. Chem. 261 (2004) 485–496, https://doi.org/10.1023/B:JRNC.0000034890.23325.b5.

[9] C.M. Wai, Y.J. Liao, W. Liao, G. Tian, R.S. Addleman, D. Quach, S.P. Pasilis, Uranium dioxide in ionic liquid with a tri-n-butylphosphate-HNO 3 complex-dissolution and coordination environment, Dalton T. 40 (2011) 5039, https://doi.org/10.1039/C0DT01518K.

[10] J. Wang, C. Chen, Biosorbents for heavy metals removal and their future, Biotechnol. Adv. 27 (2009) 195–226, https://doi.org/10.1016/j.biotechadv.2008.11.002.

[11] S.M. Husnain, H.J. Kim, W. Um, Y. Chang, Y. Chang, Superparamagnetic Adsorbent Based on Phosphonate Grafted Mesoporous Carbon for Uranium Removal, Ind. Eng. Chem. Res. 56 (2017) 9821–9830, https://doi.org/10.1021/acs.iecr.7b01737.

[12] T.M. Budnyak, A. Gładysz-Płaska, A.V. Strizhak, D. Sternik, I.V. Komarov, M. Majdan, V.A. Tertykh, Imidazole-2yl-Phosphonic Acid Derivative Grafted onto Mesoporous Silica Surface as a Novel Highly Effective Sorbent for Uranium (VI) Ion Extraction, ACS Appl. Mater. Interf. 10 (2018) 6681–6693, https://doi.org/10.1021/acsami.7b17594.

[13] S. Yang, J. Qian, L. Kuang, D. Hua, Ion-Imprinted Mesoporous Silica for Selective Removal of Uranium from Highly Acidic and Radioactive Effluent, ACS App. Mat. Interf. 9 (2017) 29337–29344, https://doi.org/10.1021/acsami.7b09419.
[14] W. Zhang, G. Ye, J. Chen, Novel mesoporous silicas bearing phosphine oxide ligands with different alkyl chains for the binding of uranium in strong HNO3 media, J. Mater. Chem. A 1 (2013) 12706–12709, https://doi.org/10.1039/C3TA13028B.
[15] P.J. Lebed, J. Savoie, J. Florek, F. Bilodeau, D. Larivière, F. Kleitz, Large Pore Mesostructured Organosilica-Phosphonate Hybrids as Highly Efficient and Regenerable Sorbents for Uranium Sequestration, Chem. Mater. 24 (2012) 4166–4176, https://doi.org/10.1021/cm3023709.
[16] H. Sarafraz, G. Alahyarizadeh, A. Minuchehr, H. Modaberi, A. Naserbegi, Economic and Efficient phosphonic functional groups mesoporous silica for uranium selective adsorption from aqueous solutions, Sci Rep 9 (2019) 9686–9710, https://doi.org/10.1038/s41598-019-46090-2.
[17] X. Wang, J. Lan, Y. Zhao, Z. Li, L. Yuan, Y. Wang, Z. Chai, W. Shi, Y. Feng, Y. Liu, Mesoporous silica SBA-15 functionalized with phosphonate and amino groups for uranium uptake, Sci. China Chem 55 (2012) 1705–1711, https://doi.org/10.1007/s11426-012-4625-7.
[18] L. Yuan, Y. Liu, W. Shi, Z. Li, J. Lan, Y. Feng, Y. Zhao, Y. Yuan, Z. Chai, A novel mesoporous material for uranium extraction, dihydroimidazole functionalized SBA-15, J. Mater. Chem. 22 (2012) 17019, https://doi.org/10.1039/C2JM31766D.
[19] D. Li, S. Egodawatte, D.I. Kaplan, S.C. Larsen, S.M. Serkiz, J.C. Seaman, K. G. Scheckel, J. Lin, Y. Pan, Extraction of Uranium from Seawater Simulant by Functionalized Magnetic Mesoporous Silica Nanoparticles: Capacity and Molecular Mechanisms, Environ. Sci. Technol. 51 (2017) 14330–14341, 10.1021%2Facs.est.7b03778.
[20] C.W. Abney, R.T. Mayes, T. Saito, S. Dai, Materials for the Recovery of Uranium from Seawater, Chem. Rev. 117 (2017) 13935–14013, https://doi.org/10.1021/acs.chemrev.7b00355.
[21] S. Husnain, W. Um, W. Woojin-Lee, Y. Chang, Magnetite-based adsorbents for sequestration of radionuclides: a review, RSC Adv. 8 (2018) 2521–2540, https://doi.org/10.1039/C7RA12299C.
[22] R. Thapa, T. Nissinen, P. Turhanen, J. Määttä, J. Vepsäläinen, V. Lehto, J. Riikonen, Bisphosphonate modified mesoporous silicon for scandium adsorption, Micropor. Mesopor. Mat. 296 (2020), 109980, https://doi.org/10.1016/j.micromeso.2019.109980.
[23] P.A. Turhanen, J.J. Vepsäläinen, S. Peräniemi, Advanced material and approach for metal ions removal from aqueous solutions, Sci Rep 5 (2015) 8992, https://doi.org/10.1038/srep08992.
[24] J. Riikonen, T. Nissinen, A. Alanne, R. Thapa, P. Fioux, M. Bonne, S. Rigolet, F. Morlet-Savary, F. Aussenac, C. Marichal, J. Lalevée, J. Vepsäläinen, B. Lebeau, V. Lehto, Stable surface functionalization of carbonized mesoporous silicon, Inorg. Chem. Front. 7 (2020) 631–641, https://doi.org/10.1039/C9QI01140D.
[25] J. Riikonen, M. Salomäki, J. van Wonderen, M. Kemell, W. Xu, O. Korhonen, M. Ritala, F. MacMillan, J. Salonen, V. Lehto, Surface Chemistry, Reactivity, and Pore Structure of Porous Silicon Oxidized by Various Methods, Langmuir 28 (2012) 10573–10583, https://doi.org/10.1021/la301642w.
[26] J. Wang, X. Guo, Adsorption isotherm models: classification, physical meaning, application and solving method, Chemosphere 258 (2020), 127279, https://doi.org/10.1016/j.chemosphere.2020.127279.
[27] K.Y. Foo, B.H. Hameed, Insights into the modeling of adsorption isotherm systems, Chem. Eng. J. 156 (2010) 2–10, https://doi.org/10.1016/j.cej.2009.09.013.
[28] M. A. Al-Ghouti, D.A. Da'ana, Guidelines for the use and interpretation of adsorption isotherm models: A review. J. Hazard. Mater. 393 (2020), 122383. https://doi.org/10.1016/j.jhazmat.2020.122383.
[29] F. Chi, F. Chi, X. Wang, X. Wang, J. Xiong, J. Xiong, S. Hu, S. Hu, Polyvinyl alcohol fibers with functional phosphonic acid group: synthesis and adsorption of uranyl (VI) ions in aqueous solutions, J. Radioanal. Nucl. Chem. 296 (2013) 1331–1340, https://doi.org/10.1007/s10967-012-2303-z.
[30] D. Shao, Y. Li, X. Wang, S. Hu, J. Wen, J. Xiong, A.M. Asiri, H.M. Marwani, Phosphate-Functionalized Polyethylene with High Adsorption of Uranium(VI), ACS Omega 2 (2017) 3267–3275, https://doi.org/10.1021/acsomega.7b00375.
[31] W. Chouyyok, J.W. Pittman, M.G. Warner, K.M. Nell, D.C. Clubb, G.A. Gill, R. S. Addleman, Surface functionalized nanostructured ceramic sorbents for the effective collection and recovery of uranium from seawater, Dalton T. 45 (2016) 11312–11325, https://doi.org/10.1039/C6DT01318J.
[32] L. Li, W. Ma, S. Shen, H. Huang, Y. Bai, H. Liu, A Combined Experimental and Theoretical Study on the Extraction of Uranium by Amino-Derived Metal-Organic Frameworks through Post-Synthetic Strategy, ACS App Mat. Interf. 8 (2016) 31032–31041, https://doi.org/10.1021/acsami.6b11332.
[33] L. Wang, L. Yuan, K. Chen, Y. Zhang, Q. Deng, S. Du, Q. Huang, L. Zheng, J. Zhang, Z. Chai, M.W. Barsoum, X. Wang, W. Shi, Loading Actinides in Multilayered Structures for Nuclear Waste Treatment: The First Case Study of Uranium Capture with Vanadium Carbide MXene, ACS App. Mat. Interf. 8 (2016) 16396–16403, https://doi.org/10.1021/acsami.6b02989.
[34] B. Bai, Y. Fang, Q. Gan, Y. Yang, L. Yuan, W. Feng, Phosphorous-Based Pillar[5]arenes for Uranyl Extraction, Chin. J. Chem. (2015) 1–7, https://doi.org/10.1002/cjoc.201400899.
[35] T.S. Anirudhan, P.G. Radhakrishnan, Improved performance of a biomaterial-based cation exchanger for the adsorption of uranium(VI) from water and nuclear industry wastewater, J. Environ. Radioact. 100 (2009) 250–257, https://doi.org/10.1016/j.jenvrad.2008.12.006.
[36] S. Xie, X. Liu, B. Zhang, H. Ma, C. Ling, M. Yu, L. Li, J. Li, Electrospun nanofibrous adsorbents for uranium extraction from seawater, J. Mater. Chem. A 3 (2015) 2552–2558, https://doi.org/10.1039/C4TA06120A.
[37] L.C.B. Stopa, M. Yamaura, Uranium removal by chitosan impregnated with magnetite nanoparticles: adsorption and desorption, Int. J. Nucl. Energy Sci. Technol. 5 (2010) 283–289, https://doi.org/10.1504/IJNEST.2010.035538.
[38] M.G. Mahfouz, A.A. Galhoum, N.A. Gomaa, S.S. Abdel-Rehem, A.A. Atia, T. Vincent, E. Guibal, Uranium extraction using magnetic nano-based particles of diethylenetriamine-functionalized chitosan: Equilibrium and kinetic studies, Chem. Eng. J. 262 (2015) 198–209, https://doi.org/10.1016/j.cej.2014.09.061.
[39] L. Yuan, Y. Liu, W. Shi, Y. Lv, J. Lan, Y. Zhao, Z. Chai, High performance of phosphonate-functionalized mesoporous silica for U(vi) sorption from aqueous solution, Dalton T 40 (2011) 7446–7453, https://doi.org/10.1039/c1dt10085h.

Supplementary Information

# Recovery of uranium with bisphosphonate modified mesoporous silicon

Rinez Thapa[a], Arezoo Rahmani[a], Petri Turhanen[b], Antti Taskinen[c], Tuomo Nissinen[a], Raisa Neitola[c], Jouko Vepsäläinen[b], Vesa-Pekka Lehto[a*] and Joakim Riikonen[a]

[a] *Department of Applied Physics, University of Eastern Finland, P.O.Box 1627, Yliopistonranta 1, FI-70211 Kuopio, Finland.*

[b] *School of Pharmacy, University of Eastern Finland, P.O.Box 1627, Yliopistonranta 1, FI-70211 Kuopio, Finland.*

[c] *Geological Survey of Finland (GTK), Tutkijankatu 1, FI-83500 Outokumpu, Finland.*

**Corresponding author: vesa-pekka.lehto@uef.fi*

## Declaration of competing interests

J.R., T.N. and V-P.L. are shareholders of 3AWater Oy, which has Intellectual Property Rights (IPR) related to the material reported in the manuscript.

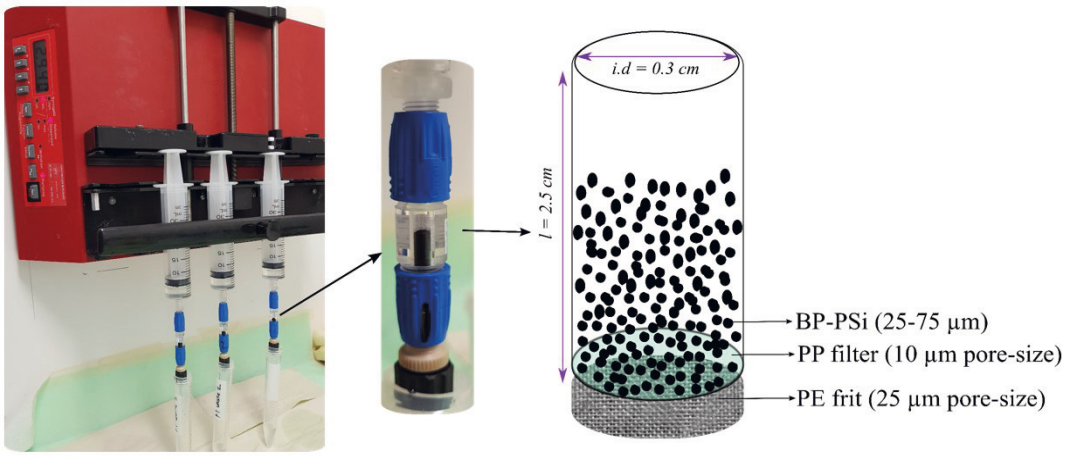


**Fig. S1.** Flow-through setup used in this study.

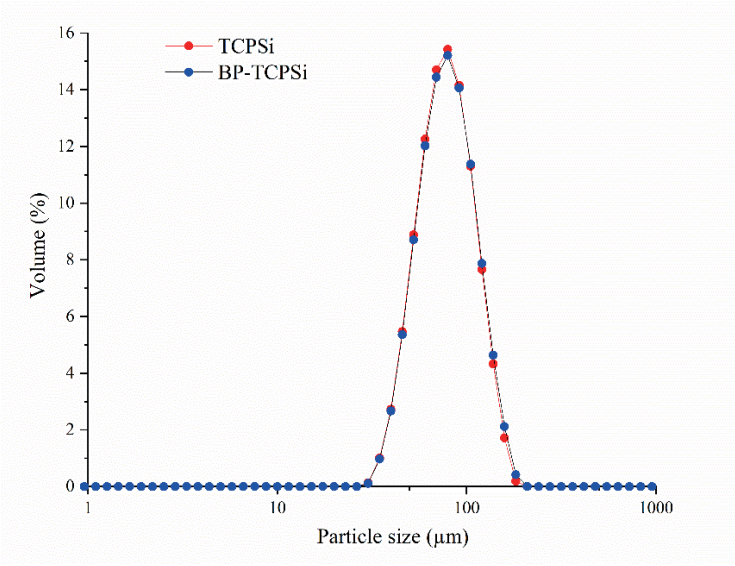


**Fig. S2.** Particle size distributions of BP-TCPSi and unfunctionalized TCPSi measured by laser diffraction.

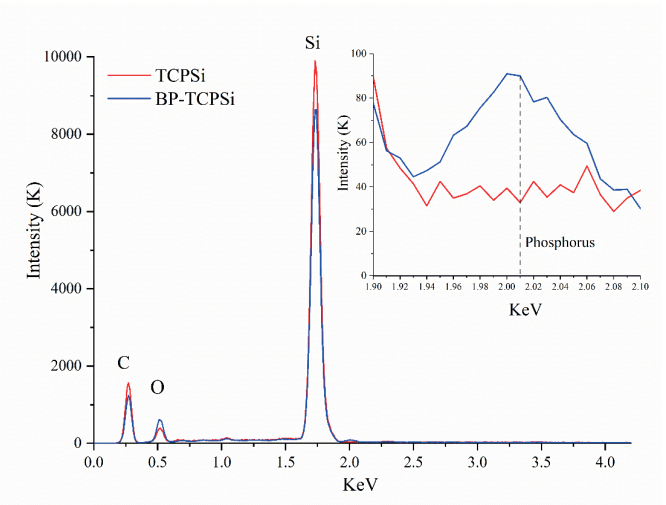


**Fig. S3.** EDS spectra showing phosphorus peak in BP-TCPSi sample but not with unfunctionalized TCPSi.

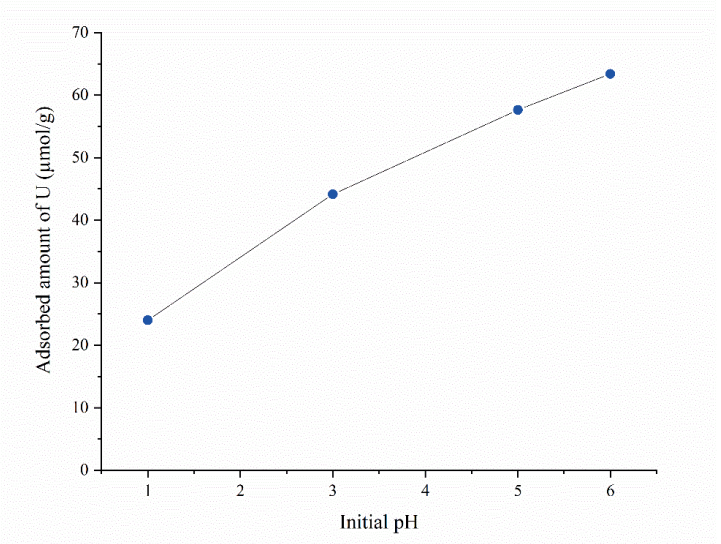


**Fig S4.** Adsorbed amount of U with BP-TCPSi as function of pH. Experimental condition: 10 mg BP-TCPSi agitated with 10 mL of 16 mg/L U for 24 h at room temperature.

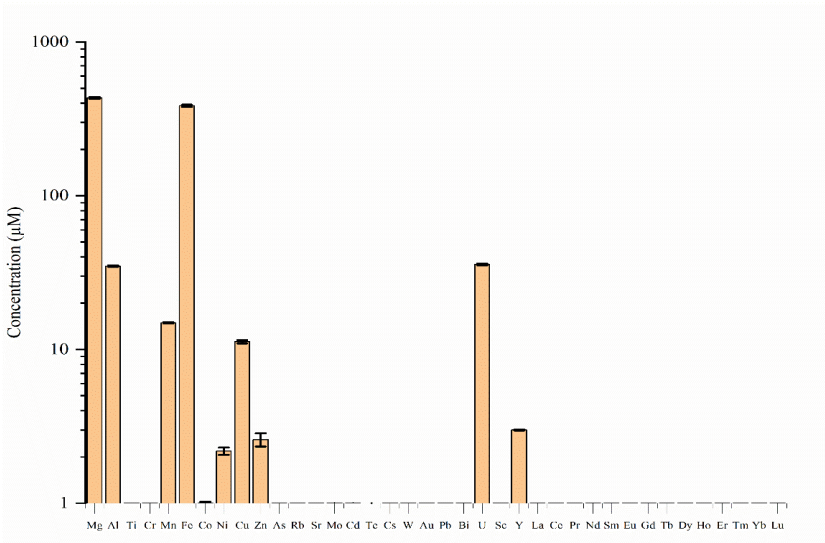


**Fig. S5**. Molar concentration of metals in the processed minewater (Knelson tails, KT) measured by ICP-MS. The error bars represent the standard deviation (n = 3).

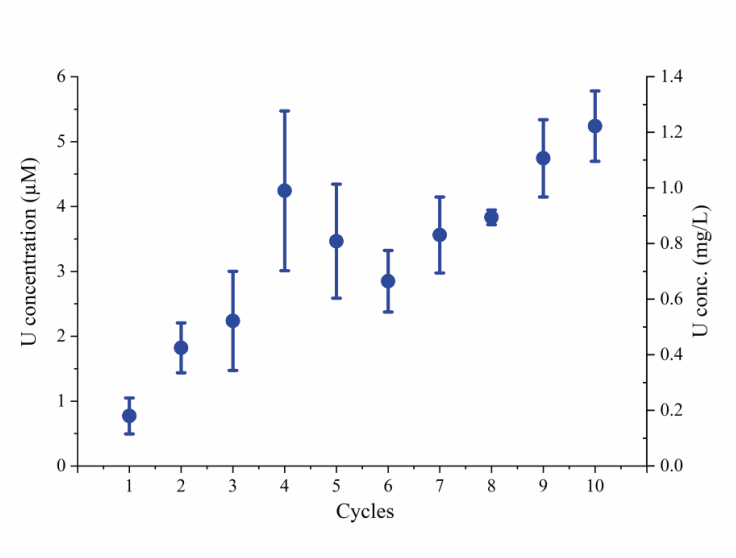


**Fig. S6.** Uranium concentration in the filtrates after adsorption in the ten consecutive adsorption desorption cycles.

**Table S1.** Selectivity coefficient (β) values (averages, n = 4) of BP-TCPSi for U relative to other metal ions (M) in the KT for the 10 consecutive adsorption desorption cycles.

| Cycle | Selectivity coefficient, $\beta = K_d$ (U) / $K_d$ (M) | | | | |
|---|---|---|---|---|---|
| | **Mg** | **Fe** | **Al** | **Mn** | **Cu** |
| **Cycle 1** | 700 ± 300 | 300 ± 100 | 50 ± 20 | 900 ± 400 | 300 ± 100 |
| **Cycle 2** | 500 ± 300 | 200 ± 50 | 30 ± 10 | 600 ± 200 | – [a] |
| **Cycle 3** | 400 ± 100 | 100 ± 50 | 40 ± 10 | 400 ± 100 | 200 ± 100 |
| **Cycle 4** | – [a] | 100 ± 50 | 30 ± 10 | – [a] | 100 ± 50 |
| **Cycle 5** | 200 ± 50 | 60 ± 20 | 20 ± 10 | 200 ± 50 | 80 ± 20 |
| **Cycle 6** | – [a] | 100 ± 50 | 30 ± 10 | – [a] | 100 ± 50 |
| **Cycle 7** | 200 ± 100 | 100 ± 50 | 30 ± 20 | – [a] | 90 ± 20 |
| **Cycle 8** | 200 ± 50 | 60 ± 10 | 30 ± 10 | 200 ± 30 | 70 ± 10 |
| **Cycle 9** | 100 ± 20 | 50 ± 10 | 20 ± 10 | 100 ± 50 | 60 ± 10 |
| **Cycle 10** | 90 ± 20 | 50 ± 10 | 20 ± 10 | 90 ± 30 | 50 ± 10 |

[a] β values could not be reliably determined because of very low adsorbed amounts.

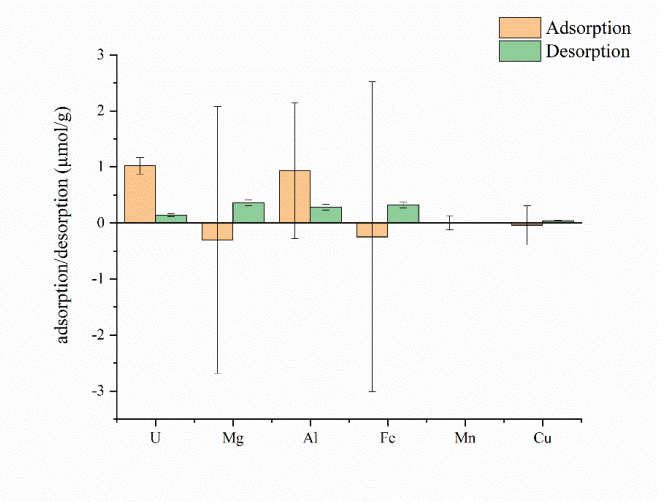


**Fig. S7.** Adsorption/desorption of metals with unfunctionalized TCPSi in the flow-through setup. Adsorption was performed with 10 mL of processed minewater (Knelson tails, KT) at pH 3.3 with 20 mg TCPSi. The flow rate was 0.25 mL/min. Desorption was performed using 0.5 mL of 1 M $H_2SO_4$ with the flow rate of 1.25 mL/min.

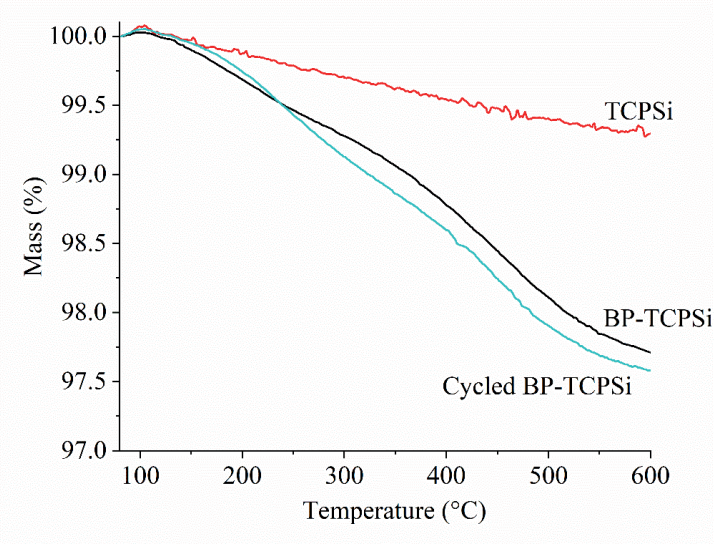


**Fig. S8.** TGA curves of TCPSi and BP-TCPSi before adsorption as well as BP-TCPSi after the 10 adsorption/desorption cycles (Cycled BP-TCPSi).

**RINEZ THAPA**

Adsorption is resource efficient technology to recover specific metals even at low concentration from dissolved metal solution. In this work, a novel functionalized nanoporous silicon-based adsorbent was developed. The adsorbent exhibited good selectivity towards scandium and uranium from multi-metal solution and was effectively reusable up to 50 adsorption/desorption cycles. The porous framework of the adsorbent facilitated its use in column setup that can be employed in an industrial setting.

UNIVERSITY OF
EASTERN FINLAND

**uef.fi**

**PUBLICATIONS OF**
**THE UNIVERSITY OF EASTERN FINLAND**
Dissertations in Forestry and Natural Sciences

ISBN 978-952-61-4330-9
ISSN 1798-5668